TECHNISCHE UNIVERSITÄT WIEN

THESIS

A Mass Conserving Mixed Stress-Strain rate Finite Element Method for Non-Newtonian Fluid Simulations

submitted to the Faculty of Electrical Engineering and Information Technology
at the Vienna University of Technology
by

Jan Ellmenreich BSc
Matriculation number: 01526208

in accordance with the requirements of the degree of

Master of Science

in

Computational Science and Engineering

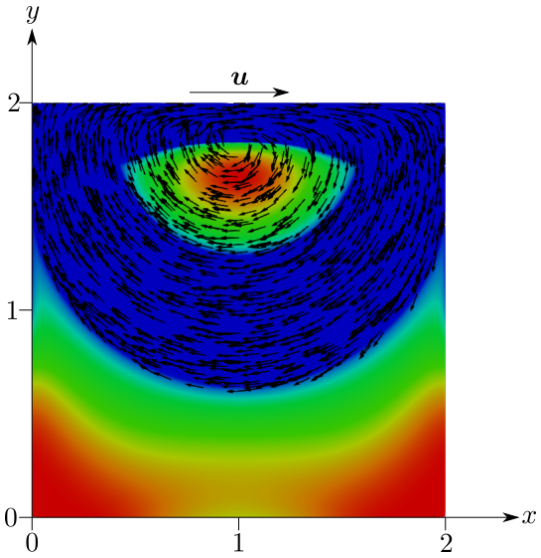

BOARD MEMBERS

Prof. Dr. Joachim Schöberl	SUPERVISOR
Institute of Analysis and Scientific Computing, TU Wien	
Dr. Philip Lukas Lederer	CO-SUPERVISOR
Institute of Analysis and Scientific Computing, TU Wien	

Die approbierte gedruckte Originalversion dieser Diplomarbeit ist an der TU Wien Bibliothek verfügbar
The approved original version of this thesis is available in print at TU Wien Bibliothek.
TU Bibliothek Your knowledge hub WIEN

Author's e-mail:
jan.ellmenreich@outlook.com

Github repository:
JanEllmenreich/ngsolve-nonnewtonian

Cover:
Non-Newtonian (*Bingham*) cavity flow

Last update:
Vienna, December 7, 2021

Jan Ellmenreich

Die approbierte gedruckte Originalversion dieser Diplomarbeit ist an der TU Wien Bibliothek verfügbar
The approved original version of this thesis is available in print at TU Wien Bibliothek.
TU Bibliothek Your knowledge hub WIEN

Die approbierte gedruckte Originalversion dieser Diplomarbeit ist an der TU Wien Bibliothek verfügbar
The approved original version of this thesis is available in print at TU Wien Bibliothek.

Abstract

Many non-Newtonian models assume a non-linear relation between the deviatoric stress tensor $\boldsymbol{\tau}$ and the rate-of-strain tensor $\boldsymbol{\varepsilon}(\boldsymbol{u})$, which is not necessarily given in explicit form. Therefore the requirement on a finite element method is the capability to capture the behaviour of the non-linear constitutive relation.
Inspired by the work of [GLS19, GLS20] and assuming incompressible, stationary, isothermal, laminar flow, we present a new mixed finite element method by introducing a variable for the rate-of-strain tensor $\boldsymbol{\varepsilon}$, such that the embedding of a general implicit constitutive relation of the form $\mathcal{G}(\boldsymbol{\tau}, \boldsymbol{\varepsilon}) := 0$ is very natural. Thus making it suitable for the simulation of a broader range of non-Newtonian fluids.
We prove solvability of the new discrete variational formulation in a two-dimensional Newtonian setting by showing continuity of the bilinear forms, coercivity on the kernel and the discrete *Ladyzhenskaya–Babuška–Brezzi* condition. By construction our newly introduced mixed finite element approximates the velocity $\boldsymbol{u}$ in an exactly divergence free matter. This fact results in a property known as pressure robustness.
Ultimately, we perform some non-Newtonian numerical experiments in a two-dimensional channel and illustrate the achieved L^2-errors in comparison to various other standard mixed finite elements.

Die approbierte gedruckte Originalversion dieser Diplomarbeit ist an der TU Wien Bibliothek verfügbar
The approved original version of this thesis is available in print at TU Wien Bibliothek.
TU Bibliothek Your knowledge hub WIEN

Kurzfassung

Zahlreiche Nichtnewtonsche Modelle gehen von einer nichtlinearen Beziehung zwischen dem Spannungsdeviator $\boldsymbol{\tau}$ und dem Verzerrungsgeschwindigkeitstensor $\boldsymbol{\varepsilon}(\boldsymbol{u})$ aus, die nicht unbedingt in expliziter Form vorliegt. Aus diesem Grund ist eine Anforderung an die Finite-Elemente-Methode das Verhalten des nichtlinearen Materialgesetzes zu erfassen.
Angelehnt an die Publikationen [GLS19, GLS20] und unter der Annahme einer inkompressiblen, stationären, isothermen, laminaren Strömung, stellen wir, durch Einführung einer Variable für den Verzerrungsgeschwindigkeitstensor $\boldsymbol{\varepsilon}$, eine neue gemischte Finite-Elemente-Methode vor, so dass die Einbindung eines jeglichen Materialgesetzes in impliziter Form $\mathcal{G}(\boldsymbol{\tau}, \boldsymbol{\varepsilon}) := 0$ sehr einfach realisierbar ist. Damit ist die Methode geeignet für die Simulation eines breiten Spektrums an Nichtnewtonschen Fluiden.
Lösbarkeit der neuen diskreten Schwachen Formulierung beweisen wir im Fall einer zweidimensionalen Newtonschen Strömung, indem wir Stetigkeit der Bilinearformen, Elliptizität im Kern und die diskrete *Ladyzhenskaya-Babuška-Brezzi*-Bedingung zeigen. Konstruktionsbedingt approximiert das neu eingeführte gemischte Finite-Element die Geschwindigkeit $\boldsymbol{u}$ auf einer exakt divergenzfreien Weise. Diese Tatsache führt zu einer Eigenschaft, die als Druckrobustheit bekannt ist.
Schließlich führen wir einige Nichtnewtonsche numerische Experimente in einem zweidimensionalen Kanal durch und veranschaulichen die erzielten L^2-Fehler im Vergleich zu anderen üblichen gemischten Finite-Elemente.

Die approbierte gedruckte Originalversion dieser Diplomarbeit ist an der TU Wien Bibliothek verfügbar
The approved original version of this thesis is available in print at TU Wien Bibliothek.
TU Bibliothek Your knowledge hub WIEN

Acknowledgments

First and foremost, I would like to express my sincere thanks to my advisor Dr. Philip Lederer, who has constantly supported me with new inputs, advice and motivation in times like these. Without his patience during endless online meetings, the completion of this thesis would certainly not have been possible. Moreover, his unique didactics and enthusiasm allowed my scientific interest to grow even more.
Secondly, I very much would like to thank my family and friends, especially my parents, who have supported me unconditionally in every way during my studies and life. Special thanks to my girlfriend for her emotional support and encouragement, and to my brother for his scientific advice.

Danksagung

An erster Stelle möchte ich mich bei meinem Betreuer Dr. Philip Lederer bedanken, der mich in Zeiten wie diesen immer wieder mit neuen Inputs, Ratschlägen und Motivation unterstützt hat. Ohne seine Geduld bei endlosen Online-Meetings wäre die Vollendung dieser Arbeit sicherlich nicht möglich gewesen. Zudem hat seine einzigartige Didaktik und seine Begeisterung mein wissenschaftliches Interesse umso mehr gesteigert.
Des Weiteren möchte ich mich ganz herzlich bei meiner Familie und meinen Freunden bedanken, insbesondere bei meinen Eltern, die mich während meines Studiums und in meinem Leben in jeder Hinsicht bedingungslos unterstützt haben. Mein besonderer Dank gilt meiner Freundin für ihre emotionale Unterstützung und Ermutigung, und meinem Bruder für seinen wissenschaftlichen Rat.

Die approbierte gedruckte Originalversion dieser Diplomarbeit ist an der TU Wien Bibliothek verfügbar
The approved original version of this thesis is available in print at TU Wien Bibliothek.
TU Bibliothek Your knowledge hub WIEN

Statuatory Declaration

I hereby declare that I have written this thesis in accordance with the Code of Conduct - Rules for Ensuring Good Scientific Practice, in particular without the inadmissible help of third parties and without the use of any aids other than those indicated. Data and concepts taken directly or indirectly from other sources are clearly indicated with reference to the source. The work has not been submitted in the same or a similar form in other examination procedures either in Austria or abroad.

Vienna, December 7, 2021

Jan Ellmenreich

Eidesstattliche Erklärung

Hiermit erkläre ich, dass ich die vorliegende Arbeit gemäß dem Code of Conduct – Regeln zur Sicherung guter wissenschaftlicher Praxis, insbesondere ohne unzulässige Hilfe Dritter und ohne Benutzung anderer als der angegebenen Hilfsmittel, angefertigt wurde. Die aus anderen Quellen direkt oder indirekt übernommenen Daten und Konzepte sind unter Angabe der Quelle gekennzeichnet. Die Arbeit wurde bisher weder im In- noch im Ausland in gleicher oder in ähnlicher Form in anderen Prüfungsverfahren vorgelegt.

Wien, am 7. Dezember, 2021

Jan Ellmenreich

Die approbierte gedruckte Originalversion dieser Diplomarbeit ist an der TU Wien Bibliothek verfügbar
The approved original version of this thesis is available in print at TU Wien Bibliothek.
TU Bibliothek Your knowledge hub WIEN

Contents

Die approbierte gedruckte Originalversion dieser Diplomarbeit ist an der TU Wien Bibliothek verfügbar
The approved original version of this thesis is available in print at TU Wien Bibliothek.
TU Bibliothek Your knowledge hub WIEN

Die approbierte gedruckte Originalversion dieser Diplomarbeit ist an der TU Wien Bibliothek verfügbar
The approved original version of this thesis is available in print at TU Wien Bibliothek.
TU Bibliothek Your knowledge hub WIEN

List of Figures

Die approbierte gedruckte Originalversion dieser Diplomarbeit ist an der TU Wien Bibliothek verfügbar
The approved original version of this thesis is available in print at TU Wien Bibliothek.
TU Bibliothek Your knowledge hub WIEN

List of Tables

Die approbierte gedruckte Originalversion dieser Diplomarbeit ist an der TU Wien Bibliothek verfügbar
The approved original version of this thesis is available in print at TU Wien Bibliothek.
TU Bibliothek Your knowledge hub WIEN

1

Introduction

In many fields, but especially in industrial processes, non-Newtonian fluids are encountered. Whether for dairy products, cosmetics, drilling muds or waxy crude oils [CR08], the simulation of such fluids can be very demanding. Primarily because these are described by non-linear mathematical models and thus require a method capable of capturing this behaviour, and secondarily because the arising non-linear system requires iterative solution techniques. In this thesis we present a new mass conserving finite element method suited for the approximation of a generalized non-Newtonian fluid flow.
To restrict the range of application, for the time being we only consider incompressible, stationary, isothermal, laminar fluid flows. By these assumptions the conservation of momentum, mass and angular momentum are given by

$$-\operatorname{div}(\boldsymbol{\tau}) + \nabla p = \boldsymbol{f} \qquad \text{in } \Omega, \tag{1.1a}$$
$$\operatorname{div}(\boldsymbol{u}) = 0 \qquad \text{in } \Omega, \tag{1.1b}$$
$$\boldsymbol{\tau} = \boldsymbol{\tau}^{\mathrm{T}} \qquad \text{in } \Omega, \tag{1.1c}$$
$$\boldsymbol{u} = 0 \qquad \text{on } \partial\Omega, \tag{1.1d}$$

where $\boldsymbol{\tau}, \boldsymbol{u}, p, \boldsymbol{f}$ are the deviatoric stress tensor, the velocity, the mechanical pressure, an external force respectively, and $\Omega \subset \mathbb{R}^d$ the computational domain in two $d = 2$ or three dimensions $d = 3$. For convenience, we assumed homogeneous boundary conditions, even though this is not essential. To close upper system of equations, a further relation is required, namely the connection between the kinematic and the kinetic quantities, which is usually referred to as constitutive relation.
In 1843 and 1845 *Saint-Venant* and *Stokes* respectively, derived for an incompressible, Newtonian fluid the well-known constitutive relation [Bat00]

$$\boldsymbol{\tau} = 2\mu\boldsymbol{\varepsilon}(\boldsymbol{u}), \tag{1.2}$$

where μ is the dynamic viscosity and $\boldsymbol{\varepsilon}(\boldsymbol{u})$ the symmetric velocity gradient. The system of equations (1.1)-(1.2) is also known as *Stokes* equations and the existence of weak solutions of the corresponding saddle-point problem is well analysed in literature [BBF13, Bre74, AMS+04]. Although solvability is not inherited from the continuous setting, many stable finite elements have been found solving the discrete variational formulation

Find $\boldsymbol{u}_h, p_h \in V_h, Q_h$ such that

$$2\mu \int_\Omega \boldsymbol{\varepsilon}(\boldsymbol{u}_h) : \boldsymbol{\varepsilon}(\overline{\boldsymbol{u}}_h)\, dx - \int_\Omega \operatorname{div}(\overline{\boldsymbol{u}}_h) p_h\, dx = \int_\Omega \rho \boldsymbol{f} \cdot \overline{\boldsymbol{u}}_h\, dx \qquad \forall \overline{\boldsymbol{u}}_h \in V_h,$$
$$- \int_\Omega \operatorname{div}(\boldsymbol{u}_h)\overline{p}_h\, dx = 0 \qquad \forall \overline{p}_h \in Q_h.$$

Die approbierte gedruckte Originalversion dieser Diplomarbeit ist an der TU Wien Bibliothek verfügbar
The approved original version of this thesis is available in print at TU Wien Bibliothek.
TU Bibliothek Your knowledge hub WIEN

For example the famous two-field *Taylor-Hood* ($\mathcal{TH}$, 4.1.1) element [TH73] and the *Scott-Vogelius* ($\mathcal{SV}$, 4.1.3) element [SV85].
A recently developed four-field mass conserving mixed stress ($\mathcal{MCS}$, 4.3.1) element [GLS19, GLS20] approximates in a slightly nonconforming matter a similar variational formulation, namely

Find $\boldsymbol{\tau}_h, p_h, \boldsymbol{u}_h, \boldsymbol{\omega}_h \in \Sigma_h^{\oplus} \times Q_h \times U_h \times W_h$ such that

$$\begin{aligned}
\frac{1}{2\mu}\int_\Omega \boldsymbol{\tau}_h : \overline{\boldsymbol{\tau}}_h \, dx + \langle \operatorname{div}(\overline{\boldsymbol{\tau}}_h), \boldsymbol{u}_h\rangle + \int_\Omega \boldsymbol{\omega}_h : \overline{\boldsymbol{\tau}}_h \, dx &= 0 && \forall \overline{\boldsymbol{\tau}}_h \in \Sigma_h^{\oplus},\\
\langle \operatorname{div}(\boldsymbol{\tau}_h), \overline{\boldsymbol{u}}_h\rangle + \int_\Omega \overline{\boldsymbol{\omega}}_h : \boldsymbol{\tau}_h \, dx + \int_\Omega \operatorname{div}(\overline{\boldsymbol{u}}_h) p_h \, dx &= -\int_\Omega \rho \boldsymbol{f} \cdot \overline{\boldsymbol{u}}_h \, dx && \forall \overline{\boldsymbol{u}}_h, \overline{\boldsymbol{\omega}}_h \in V_h \times W_h,\\
\int_\Omega \operatorname{div}(\boldsymbol{u}_h)\overline{p}_h \, dx &= 0 && \forall \overline{p}_h \in Q_h,
\end{aligned}$$

where $\boldsymbol{\omega}$ is the skew-symmetric velocity gradient, also known as rate-of-rotation tensor.
While the above mentioned finite elements are suitable for simulating Newtonian flows, they are not for general non-Newtonian flows, whose constitutive law is non-linear in $\boldsymbol{\tau}$ and $\boldsymbol{\varepsilon}(\boldsymbol{u})$. On one hand the two-field discretisations do not approximate the deviatoric stress tensor $\boldsymbol{\tau}$, thus require an explicit constitutive relation. On the other hand the mass conserving mixed stress ($\mathcal{MCS}$) method requires by derivation of the weak formulation the proportionality in the constitutive relation between the deviatoric stress tensor $\boldsymbol{\tau}$ and the rate-of-strain tensor $\boldsymbol{\varepsilon}(\boldsymbol{u})$. Additionally, by the choice of the finite element space $\boldsymbol{u}_h \in V_h \subset H_0(\operatorname{div}, \Omega)$, the symmetric velocity gradient $\boldsymbol{\varepsilon}(\boldsymbol{u}_h)$, needed in many non-Newtonian models, is not well defined on Ω. For this reasons upper mentioned finite elements are not suited to approximate generalized non-Newtonian fluids, whose constitutive relation is given in implicit form

$$\mathcal{G}(\boldsymbol{\tau}, \boldsymbol{\varepsilon}(\boldsymbol{u})) := 0, \tag{1.3}$$

provided the non-linear weak formulation has an unique solution.
Rajagopal laid the cornerstone of generalized implicit constitutive relations in his papers [Raj03, Raj06]. He provided a new framework for the formulation of sophisticated constitutive relations in harmony with the second law of thermodynamics. For example the famous viscoplastic non-Newtonian *Bingham* model [GW11]

$$\begin{cases} \boldsymbol{\tau} = 2\mu\boldsymbol{\varepsilon}(\boldsymbol{u}) + \dfrac{\tau_y}{|\boldsymbol{\varepsilon}(\boldsymbol{u})|}\boldsymbol{\varepsilon}(\boldsymbol{u}) & \text{if } |\boldsymbol{\tau}| > \tau_y, \\ \boldsymbol{\varepsilon}(\boldsymbol{u}) = \boldsymbol{0} & \text{if } |\boldsymbol{\tau}| \le \tau_y, \end{cases} \tag{1.4}$$

can be completely written in terms of a continuous implicit relation [GO20]

$$\mathcal{G}(\boldsymbol{\tau}, \boldsymbol{\varepsilon}(\boldsymbol{u})) = 2\mu\left(\tau_y + (|\boldsymbol{\tau}| - \tau_y)^+\right)\boldsymbol{\varepsilon}(\boldsymbol{u}) - (|\boldsymbol{\tau}| - \tau_y)^+ \boldsymbol{\tau} = 0,$$

where $(|\boldsymbol{\tau}| - \tau_y)^+ := \max(|\boldsymbol{\tau}| - \tau_y, 0)$.
The embedding of such a generalized implicit constitutive relation is very natural for a discrete three-field formulation, where the entire implicit constitutive relation gets tested by functions $\overline{\boldsymbol{\tau}} \in \Sigma_h$, independently of its structure.

Die approbierte gedruckte Originalversion dieser Diplomarbeit ist an der TU Wien Bibliothek verfügbar
The approved original version of this thesis is available in print at TU Wien Bibliothek.
TU Bibliothek Your knowledge hub WIEN

Find $\boldsymbol{\tau}_h, p_h, \boldsymbol{u}_h \in \Sigma_h \times Q_h \times U_h$ such that

$$\begin{aligned}
\int_\Omega \mathcal{G}(\boldsymbol{\tau}_h, \boldsymbol{\varepsilon}(\boldsymbol{u}_h)) : \overline{\boldsymbol{\tau}}_h \, dx = 0 \qquad & \forall \overline{\boldsymbol{\tau}}_h \in \Sigma_h, \\
\int_\Omega \boldsymbol{\tau}_h : \boldsymbol{\varepsilon}(\overline{\boldsymbol{u}}_h) \, dx - \int_\Omega \operatorname{div}(\overline{\boldsymbol{u}}_h) p_h \, dx = \int_\Omega \rho \boldsymbol{f} \cdot \overline{\boldsymbol{u}}_h \, dx \qquad & \forall \overline{\boldsymbol{u}}_h \in V_h, \\
- \int_\Omega \operatorname{div}(\boldsymbol{u}_h) \overline{p}_h \, dx = 0 \qquad & \forall \overline{p}_h \in Q_h.
\end{aligned}$$

By the discrete stability analysis of the linear Newtonian case, namely

$$\mathcal{G}(\boldsymbol{\tau}_h, \boldsymbol{\varepsilon}(\boldsymbol{u}_h)) := \boldsymbol{\varepsilon}(\boldsymbol{u}_h) - \frac{1}{2\mu} \boldsymbol{\tau}_h = 0,$$

every two-field conforming finite element augmented with piecewise discontinuous symmetric matrix-valued polynomials is an appropriate approximation to the three-field discrete variational formulation (see ($\mathcal{TH}$-$\mathcal{S}$, 4.2.1) and ($\mathcal{SV}$-$\mathcal{S}$, 4.2.2)).
In this thesis we extend the ($\mathcal{MCS}$) discrete variational formulation [GLS19, GLS20] in a similar way, such that the embedding of a generalized implicit constitutive relation is self-evident. As the mass conserving mixed stress ($\mathcal{MCS}$) method already approximates the deviatoric stress tensor $\boldsymbol{\tau}$, we introduce a new variable for the rate-of-rotation tensor $\boldsymbol{\varepsilon}$, such that the discrete variational formulation becomes

Find $\boldsymbol{u}_h, \boldsymbol{\omega}_h, \boldsymbol{\varepsilon}_h, \boldsymbol{\tau}_h, p_h, \in U_h \times W_h \times \Xi_h \times \Sigma_h^{\oplus} \times Q_h$ such that

$$\begin{aligned}
\int_\Omega \mathcal{G}(\boldsymbol{\tau}_h, \boldsymbol{\varepsilon}_h) : \overline{\boldsymbol{\varepsilon}}_h \, dx = 0 \qquad & \forall \overline{\boldsymbol{\varepsilon}}_h \in \Xi_h, \\
\int_\Omega \boldsymbol{\varepsilon}_h : \overline{\boldsymbol{\tau}}_h \, dx + \langle \operatorname{div}(\overline{\boldsymbol{\tau}}_h), \boldsymbol{u}_h \rangle + \int_\Omega \boldsymbol{\omega}_h : \overline{\boldsymbol{\tau}}_h \, dx = 0 \qquad & \forall \overline{\boldsymbol{\tau}}_h \in \Sigma_h^{\oplus}, \\
\langle \operatorname{div}(\boldsymbol{\tau}_h), \overline{\boldsymbol{u}}_h \rangle + \int_\Omega \overline{\boldsymbol{\omega}}_h : \boldsymbol{\tau}_h \, dx + \int_\Omega \operatorname{div}(\overline{\boldsymbol{u}}_h) p_h \, dx = - \int_\Omega \rho \boldsymbol{f} \cdot \overline{\boldsymbol{u}}_h \, dx \qquad & \forall \overline{\boldsymbol{u}}_h, \overline{\boldsymbol{\omega}}_h \in V_h \times W_h, \\
\int_\Omega \operatorname{div}(\boldsymbol{u}_h) \overline{p}_h \, dx = 0 \qquad & \forall \overline{p}_h \in Q_h.
\end{aligned}$$

We show solvability of the discrete problem for the linear Newtonian case

$$\mathcal{G}(\boldsymbol{\tau}_h, \boldsymbol{\varepsilon}_h) := -2\mu \boldsymbol{\varepsilon}_h + \boldsymbol{\tau}_h = 0,$$

by proving kernel ellipticity and the discrete LBB condition.
Similarly to the ($\mathcal{MCS}$) method, by construction $\operatorname{div}(V_h) \subset Q_h$ the new finite element method is exactly divergence free

$$\int_\Omega \operatorname{div}(\boldsymbol{u}_h) \overline{p}_h \, dx = \int_\Omega \operatorname{div}(\boldsymbol{u}_h) \operatorname{div}(\boldsymbol{u}_h) \, dx = 0 \quad \forall \overline{p}_h \in Q_h \qquad \Rightarrow \qquad \operatorname{div}(\boldsymbol{u}_h) = 0,$$

thus pressure robust. For this reason we give it the designation ***m**ass **c**onserving mixed **s**tress-**s**train rate method* ($\mathcal{MCS}$-$\mathcal{S}$). On the basis of three non-Newtonian numerical experiments in an usual setting, namely a two-dimensional channel flow [GW11, GO20, HMST17, GO21], we illustrate the achieved $L^2(\Omega)$-finite element errors in comparison to standard finite elements.

Die approbierte gedruckte Originalversion dieser Diplomarbeit ist an der TU Wien Bibliothek verfügbar
The approved original version of this thesis is available in print at TU Wien Bibliothek.
TU Bibliothek Your knowledge hub WIEN

Although the method approximates 5 quantities, namely $\boldsymbol{u}_h, \boldsymbol{\omega}_h, \boldsymbol{\varepsilon}_h, \boldsymbol{\tau}_h, p_h$, most of them are defined element locally. From a computational perspective we have the same amount of coupling degrees of freedom as conventional finite element methods [Led19].

Thesis layout

1. In Chapter 2 we introduce the governing equations describing the motion of a fluid. Moreover, we discuss the definition of Newtonian fluids, before roughly classifying non-Newtonian fluids and providing some examples of application. Ultimately, well-known non-Newtonian constitutive relations are presented.
2. Chapter 3 is dedicated to the introduction of different variational formulations of Stokes equations.
3. In Chapter 4 we discuss various finite elements approximating the variational formulations listed in Chapter 3, together with a short note on the discrete stability. In particular we present our new mass conserving mixed stress-strain rate ($\mathcal{MCS}$-$\mathcal{S}$) finite element method and perform all the necessary proofs to show solvability of the discrete variational formulation.
4. Chapter 5 is intended to show the achieved results for a series of non-Newtonian numerical experiments in a well-known setting, namely a flow in a two-dimensional channel.
5. Ultimately, Chapter 6 summarises and reproduces the significant conclusions of this thesis, along with an outline for future work.

Notation

$\int dx$	Integral over domain $dx \subset \mathbb{R}^d$
$\int ds$	Integral over boundary $ds \subset \mathbb{R}^{d-1}$
a	lower case latin/greek letters denote a scalar value
$\boldsymbol{a}$	lower case bold latin letters denote a vector
$\boldsymbol{\alpha}$	lower case bold greek letters denote a matrix/tensor
$\boldsymbol{I}$	identity matrix
$\mathrm{tr}(\boldsymbol{\alpha}) = \sum_{i=0}^{d}(\boldsymbol{\alpha})_{ii}$	trace of a matrix
$\boldsymbol{\alpha} : \boldsymbol{\beta} = \mathrm{tr}(\boldsymbol{\alpha}\boldsymbol{\beta}^{\mathrm{T}})$	*Frobenius* inner product
$\mathrm{sym}(\boldsymbol{\alpha}) = \frac{1}{2}(\boldsymbol{\alpha} + \boldsymbol{\alpha}^{\mathrm{T}})$	symmetric part of matrix
$\mathrm{skw}(\boldsymbol{\alpha}) = \frac{1}{2}(\boldsymbol{\alpha} - \boldsymbol{\alpha}^{\mathrm{T}})$	skew-symmetric part of matrix
$\mathrm{dev}(\boldsymbol{\alpha}) = \boldsymbol{\alpha} - \frac{1}{d}\mathrm{tr}(\boldsymbol{\alpha})\boldsymbol{I}$	skew-symmetric part of matrix
$\lvert\boldsymbol{\alpha}\rvert^2 = \frac{1}{2}\boldsymbol{\alpha} : \boldsymbol{\alpha}$	Euclidean Norm of matrix
$a_n = \boldsymbol{a} \cdot \boldsymbol{n}$	normal component of vector
$\boldsymbol{a}_t = \boldsymbol{a} - a_n\boldsymbol{n}$	tangential component of vector
$\alpha_{nn} = \boldsymbol{n}^{\mathrm{T}}\boldsymbol{\alpha}\boldsymbol{n}$	normal-normal component of matrix
$\boldsymbol{\alpha}_{nt} = \boldsymbol{\alpha}\boldsymbol{n} - \alpha_{nn}\boldsymbol{n}$	normal-tangential component of matrix
$a \preceq b$	$a \leq cb$ with $c \geq 0$ and independent of mesh size h
$a \sim b$	$a \preceq b$ and $a \succeq b$

Die approbierte gedruckte Originalversion dieser Diplomarbeit ist an der TU Wien Bibliothek verfügbar
The approved original version of this thesis is available in print at TU Wien Bibliothek.
TU Bibliothek Your knowledge hub WIEN

2

Rheology

In this chapter we shortly introduce the *Navier-Stokes* equations needed to describe the motion of a general fluid. Further we make some assumptions on the flow in order to derive the *Stokes* equations, which will be used throughout this thesis. Ultimately, an extensive physical and mathematical modelling insight is given in the constitutive relations linking the stresses and strain rates.

2.1 Governing equations

Etymologically, the term *fluid* has become common because under certain thermodynamic conditions (e.g. in proximity to the critical point) no clear differentiation between a liquid and a gaseous state of aggregation is possible [Her16, Section 1.1]. Unlike a solid, a fluid does not deform into a steady state configuration under the influence of a constant force, but rather flows, which can be viewed as a continuous deformation. This flow property is mostly described in continuum mechanics from an Eulerian point of view, i.e. a in space fixed observer

$$\boldsymbol{u} := \boldsymbol{u}(\mathbf{x}, t).$$

As long as a substance is seen as a continuum, i.e. homogeneous distribution and large enough flow scales compared to the molecular scales [Pop12, Section 2.1], the motion of a fluid is described by the well-known *Navier-Stokes* equations [GO20]

$$\frac{\partial \rho}{\partial t} + \operatorname{div}(\rho \boldsymbol{u}) = 0, \tag{2.1a}$$

$$\frac{\partial (\rho \boldsymbol{u})}{\partial t} + \operatorname{div}(\rho \boldsymbol{u} \otimes \boldsymbol{u}) = \operatorname{div}(\boldsymbol{\sigma}) + \rho \boldsymbol{f}, \tag{2.1b}$$

$$\boldsymbol{\sigma} = \boldsymbol{\sigma}^T, \tag{2.1c}$$

$$\frac{\partial (\rho(e + \frac{1}{2}\boldsymbol{u} \cdot \boldsymbol{u}))}{\partial t} + \operatorname{div}(\rho \boldsymbol{u}(e + \tfrac{1}{2}\boldsymbol{u} \cdot \boldsymbol{u})) = \operatorname{div}(\boldsymbol{\sigma}\boldsymbol{u} - \boldsymbol{q}) + \rho \boldsymbol{f} \cdot \boldsymbol{u}. \tag{2.1d}$$

The set of equations (2.1a) to (2.1d) are according to listing order the balance of mass, momentum, angular momentum and energy. To determine whether a process is feasible or not, the conservation of energy (2.1d) is not sufficient. We must also consider the second law of thermodynamics [GO20]

$$\boldsymbol{\sigma} : \boldsymbol{\varepsilon}(\boldsymbol{u}) + p_{th} \operatorname{div}(\boldsymbol{u}) - \frac{1}{T} \boldsymbol{q} \cdot \nabla T \geq 0, \tag{2.2}$$

Die approbierte gedruckte Originalversion dieser Diplomarbeit ist an der TU Wien Bibliothek verfügbar
The approved original version of this thesis is available in print at TU Wien Bibliothek.
TU Bibliothek Your knowledge hub WIEN

where $\boldsymbol{\varepsilon}(\boldsymbol{u})$ is given as

$$\boldsymbol{\varepsilon}(\boldsymbol{u}) = \frac{1}{2}\left(\nabla \boldsymbol{u} + (\nabla \boldsymbol{u})^{\mathrm{T}}\right). \tag{2.3}$$

The quantities used in (2.1) and (2.2) are

ρ ... Density	$\boldsymbol{u}$ ... Velocity field	$\boldsymbol{\sigma}$ ... *Cauchy* stress tensor
$\boldsymbol{f}$ ... Body forces	e ... Internal energy	$\boldsymbol{q}$ ... Heat flux
$\boldsymbol{\varepsilon}(\boldsymbol{u})$ ... Rate-of-strain tensor	p_{th} ... Thermodynamic pressure	T ... Temperature

In this work we will focus on steady ($\frac{\partial \cdot}{\partial t} = 0$), incompressible ($\rho = \text{const.}$), isothermal ($T = \text{const.}$) and laminar (*Reynolds* number $\mathrm{Re} \ll 1$) flows.
Note: Incompressibility is a property of the flow and not of the substance, as no fluid is truly incompressible. For a *Mach* number $\mathrm{Ma} < 0.3$ it is safe to assume a constant density [And17, Section 1.10].
With these assumptions the balance of energy (2.1d) decouples from the system of equations (2.1a) to (2.1d). We obtain *Stokes* equations

$$\operatorname{div}(\boldsymbol{u}) = 0, \tag{2.4a}$$

$$-\operatorname{div}(\boldsymbol{\sigma}) = \rho \boldsymbol{f}, \tag{2.4b}$$

$$\boldsymbol{\sigma} = \boldsymbol{\sigma}^{T}, \tag{2.4c}$$

and the inequality

$$\boldsymbol{\sigma} : \boldsymbol{\varepsilon}(\boldsymbol{u}) \geq 0. \tag{2.5}$$

To close the above system of equations we need a constitutive relation which links the *Cauchy* stress tensor $\boldsymbol{\sigma}$ to a deformation variable. In general one splits the *Cauchy* stress tensor $\boldsymbol{\sigma}$ in an isotropic/spherical part and a deviatoric part

$$\boldsymbol{\sigma} = \frac{1}{3}\operatorname{tr}(\boldsymbol{\sigma})\boldsymbol{I} + \boldsymbol{\tau}.$$

The "*mean normal stress*"

$$\boldsymbol{\sigma} = \frac{1}{3}\operatorname{tr}(\boldsymbol{\sigma})\boldsymbol{I},$$

is usually referred as the mechanical pressure

$$p = -\frac{1}{3}\operatorname{tr}(\boldsymbol{\sigma}),$$

or from a mathematical perspective, as the *Lagrange* multiplier, which enforces the incompressibility constraint (2.4a). By no means are the above mentioned definitions equivalent in an universal setting for generalised fluids. For a deeper discussion about the equivalence of the "*mean normal stress*", "*mechanical pressure*", "*Lagrange multiplier*" and "*thermodynamic pressure*" we refer to *Rajagopal* [Raj15].
In this work we focus on constitutive relations, where non-linearities arise in the deviatoric stress tensor $\boldsymbol{\tau}$ with $\operatorname{tr}(\boldsymbol{\tau}) = 0$, hence it is appropriate to adress to p as a *Lagrange* multiplier. Thus we define the *Cauchy* stress tensor as

$$\boldsymbol{\sigma} = -p\boldsymbol{I} + \boldsymbol{\tau}.$$

Die approbierte gedruckte Originalversion dieser Diplomarbeit ist an der TU Wien Bibliothek verfügbar
The approved original version of this thesis is available in print at TU Wien Bibliothek.
TU Bibliothek Your knowledge hub WIEN

2.2 Newtonian fluids

As for many other PDEs, the underlying assumption for the *Navier-Stokes* equations is that part of the fluxes are proportional to the primal quantities gradient. For heat conduction problems we have *Fourier's* law which links the heat flux q to the temperature gradient ∇T, while in solid mechanics we have *Hooke's* law which relates the *Cauchy* stress tensor $\widetilde{\boldsymbol{\sigma}}$[1] to the symmetric displacement gradient (strain tensor $\widetilde{\boldsymbol{\varepsilon}}$). Similarly it follows for fluids, where following relation can be derived for the deviatoric stress tensor [Bat00, Section 3.3]

$$\boldsymbol{\tau} = 2\mu\boldsymbol{\varepsilon}(\boldsymbol{u}) + \lambda \mathrm{div}(\boldsymbol{u})\boldsymbol{I}.$$

For incompressible flows the *Cauchy* stress tensor then becomes

$$\boldsymbol{\sigma} = -p\boldsymbol{I} + 2\mu\boldsymbol{\varepsilon}(\boldsymbol{u}).$$

We see that inequality 2.5 is automatically fulfilled

$$\boldsymbol{\sigma} : \boldsymbol{\varepsilon}(\boldsymbol{u}) = (-p\boldsymbol{I} + 2\mu\boldsymbol{\varepsilon}(\boldsymbol{u})) : \boldsymbol{\varepsilon}(\boldsymbol{u}) = 2\mu \left|\boldsymbol{\varepsilon}(\boldsymbol{u})\right|^2 \geq 0.$$

The constant material property μ is referred to as dynamic viscosity and is characterizing for Newtonian fluids, as it establishes the linear relationship between stresses and strain rates. Although the dynamic viscosity is independent of the strain rates and stresses, it can be both temperature and pressure dependent $\mu(T, p)$. Some dynamic viscosities for common Newtonian fluids are listed in Table 2.1, while in Figure 2.1 the Newtonian behaviour of water and petrol can be observed.

Fluid	Hydrogen	Air	Petrol	Water	Lubricating oil	Corn syrup
μ [Pa · s]	10^{-5}	$2 \cdot 10^{-5}$	$3 \cdot 10^{-4}$	10^{-3}	10^{-1}	10^{3}

TABLE 2.1 – Dynamic viscosities for common fluids at standard conditions [Bar00, Section 5.3]

An additional condition for a fluid to be classified as Newtonian is the constraint for the normal components of the deviatoric stress tensor [CR08, Section 1.2]:

$$\boldsymbol{\tau}_{ii} = 0. \tag{2.6}$$

A fluid which shows a constant viscosity behaviour, but does not fulfil condition (2.6) is e.g. the constant viscosity Boger fluid [CR08, Section 1.2].

2.3 Non-Newtonian fluids

Pure fluids are rare. Mostly they consist of a mixture of substances with different molecular sizes. As long as homogeneity is given and the continuum hypothesis holds, they can be considered as single-phase flows with an averaged dynamic viscosity. In general the stress - strain rate relation is no longer linear, but linked by the non-linear dynamic viscosity $\mu(\boldsymbol{\varepsilon}(\boldsymbol{u}), \boldsymbol{\tau})$. Examples are encountered in everyday life, but especially in many industrial processes [GW11, CR08]. A glimpse of these substances is given in Table 2.2.

[1] The Tilde $\sim$ has been used to avoid a clash of notation

Die approbierte gedruckte Originalversion dieser Diplomarbeit ist an der TU Wien Bibliothek verfügbar
The approved original version of this thesis is available in print at TU Wien Bibliothek.
TU Bibliothek Your knowledge hub WIEN

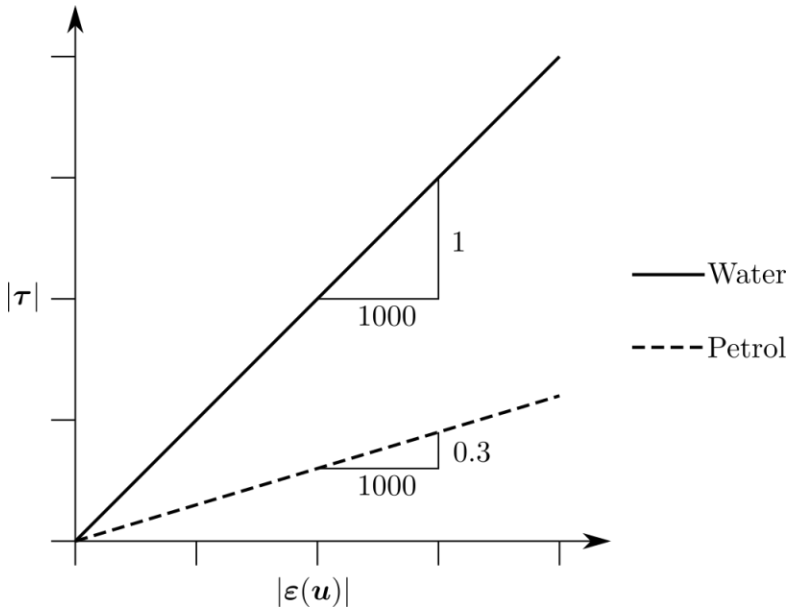

FIGURE 2.1 – Newtonian Stress-strain rate behaviour for water and petrol at standard conditions

■ Adhesives (wall paper paste, carpet adhesive)	■ Foodstuffs (fruit/vegetable purees and concentrates, sauces, salad dressings, mayonnaise, jams and marmalades, ice-cream, soups, ...)
■ Ales (beer, liqueurs)	■ Greases and lubricating oils
■ Animal waste slurries from cattle farms	■ Mine tailings and mineral suspensions
■ Biological fluids	■ Molten lava and magmas
■ Bitumen	■ Paints, polishes and varnishes
■ Cement paste and slurries	■ Paper pulp suspensions
■ Chalk slurries	■ Peat and lignite slurries
■ Chocolates	■ Polymer melts and solutions, reinforced plastic, rubber
■ Coal slurries	■ Printing colours and ink
■ Cosmetics and personal care products (nail polish, lotions and creams, lipsticks, shampoos, shaving foams, toothpaste)	■ Pharmaceutical products (creams, foams, suspensions)
■ Dairy products and dairy waste streams (cheese, butter, yogurts, fresh cream, whey)	■ Sewage sludge
■ Drilling muds	■ Wet beach sand
■ Fire fighting foams	■ Waxy crude oils

TABLE 2.2 – Examples of fluids showing non-Newtonian behaviour [CR08, Section 1.2]

Two applications come to our mind:

1. **Painting**
   Paint clearly shows a so called thixotropic behaviour, which is synonymous to a time-dependent shear-thinning behaviour. The longer you brush the paint e.g. on

Die approbierte gedruckte Originalversion dieser Diplomarbeit ist an der TU Wien Bibliothek verfügbar
The approved original version of this thesis is available in print at TU Wien Bibliothek.
TU Bibliothek Your knowledge hub WIEN

a wall, the more it liquefies until a certain limit. This relates to a time-dependent decrease in viscosity. On the other hand, when left at rest, paint becomes thicker again, preventing it from dripping down the wall.

2. **Drilling**
   In drilling operations cuttings have to be transported from the borehole to the surface. For this issues special fluids have been conceived so that they are suitable for drilling operations. The requirements on those fluids are to exhibit enough drag to transport cuttings to the surface and to prevent their sedimentation at rest. Such drilling muds can be categorized as viscoplastic fluids, since they show the presence of a yield stress below which there is no movement of the fluid [GW11].

Roughly, non-Newtonian fluids can be categorized in three subgroups [CR08, Section 1.2]

(I) time-independent fluids, also known as "generalized Newtonian fluids" (GNF),
(II) time-dependent fluids,
(III) visco-elastic fluids,

although it is possible for real materials to show characteristics of each subgroup.
In regard to the previously made assumptions, in this work we focus solely on time-independent fluids. This category is further subdivided in

(i) pseudoplastic fluid,
(ii) dilatant fluid,
(iii) viscoplastic

Figure 2.2 depicts the difference in the stress-strain rate curve between the above listed fluids and a Newtonian fluid.

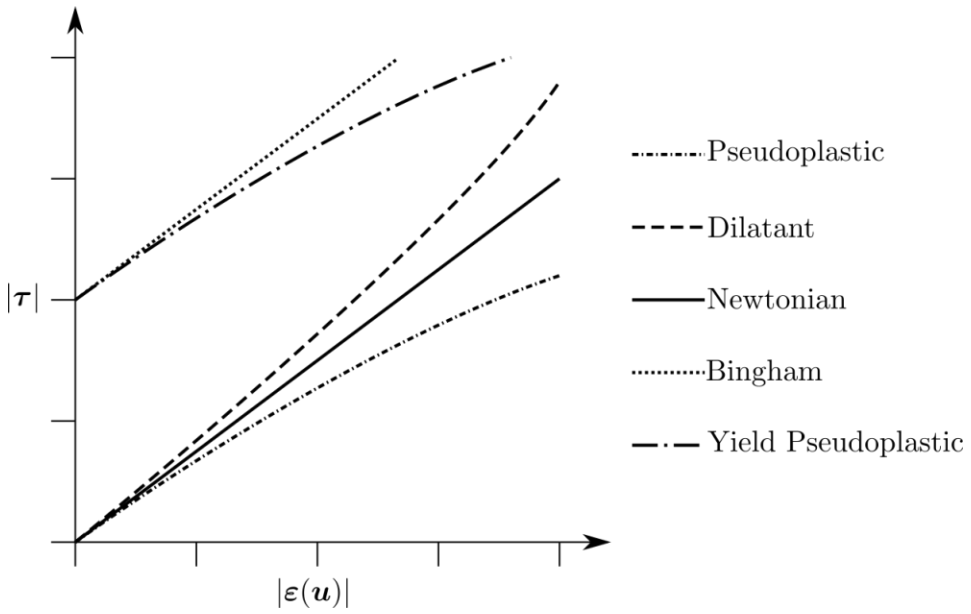

FIGURE 2.2 – Stress - strain rate relation for time-independent fluids

Die approbierte gedruckte Originalversion dieser Diplomarbeit ist an der TU Wien Bibliothek verfügbar
The approved original version of this thesis is available in print at TU Wien Bibliothek.
TU Bibliothek Your knowledge hub WIEN

2.3.1 Pseudoplastic fluid

Pseudoplastic or shear-thinning behaviour is one of the most encountered when dealing with time-independent non-Newtonian fluids. These mixtures are characterised by decreasing viscosity with an increase in shear rate, which causes them to liquefy and exert less drag. An explanation for this effect is given when looking at the micro-structures of the fluid. At rest and in thermodynamic equilibrium the micro-structures assume a state of random disorder when *Brownian* motion dominates [Bar89b, Section 7.1]. By application of a force the micro-structures arrange or deform in the direction of the flow, hence exert a lower drag force. Macroscopically, this leads to a reduction in viscosity [CR08, Section 1.7]. A schematic visualisation of the rearranging and deforming of such micro-structures can be seen in Figure 2.3 on a single droplet.

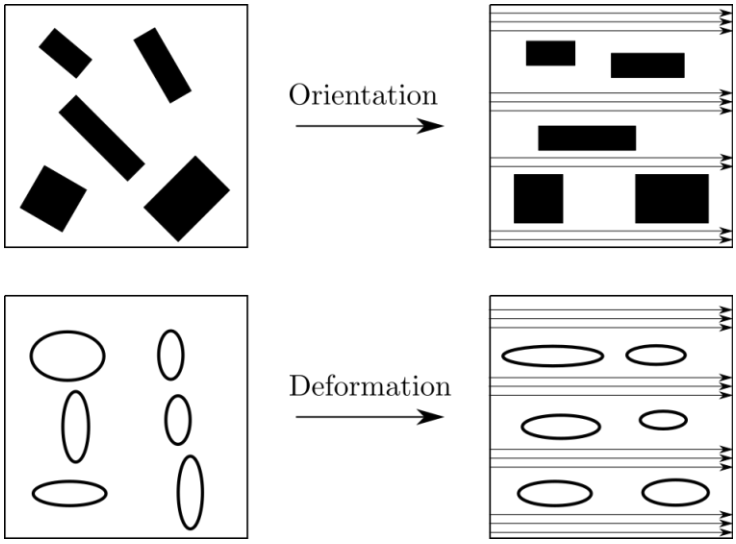

FIGURE 2.3 – Orientation and deformation of micro-structures at rest and in flow [CR08, Section 1.7]

There are other effects that cause shear-thinning behaviour, such as stretching and disintegration of micro-structures, disentangled molecules. For more details we refer to [CR08, Bar89b].
The dynamic viscosity μ is usually constant at low and high shear rates, denoted by μ_0 and μ_∞ respectively [Bar00, Section 9.1]. This property can be explained by the fact that microstructures are resistant to their own deformation at low shear rates, while at high shear rates they reach a point of maximum extent where no longer drag reduction occurs. An illustrative representation can be seen in Figure 2.4.

Mathematical models

In literature [CR08, Bar00, Bar89a, GO20] one can find various models developed over the last century. Some of them are based on curve fitting experimental data gained by measurements, while others are based on statistical mechanics [CR08, Section 1.3].
Probably, the simplest model is the power-law model, usually known as the *Ostwald-de Waele* constitutive relation [GO20, Equation 1.7], as it is based on two parameters

$$\boldsymbol{\tau} = 2K\dot{\gamma}^{r-2}\boldsymbol{\varepsilon}(\boldsymbol{u}) \qquad K > 0, 2 > r > 1, \tag{2.7}$$

Die approbierte gedruckte Originalversion dieser Diplomarbeit ist an der TU Wien Bibliothek verfügbar
The approved original version of this thesis is available in print at TU Wien Bibliothek.
TU Bibliothek Your knowledge hub WIEN

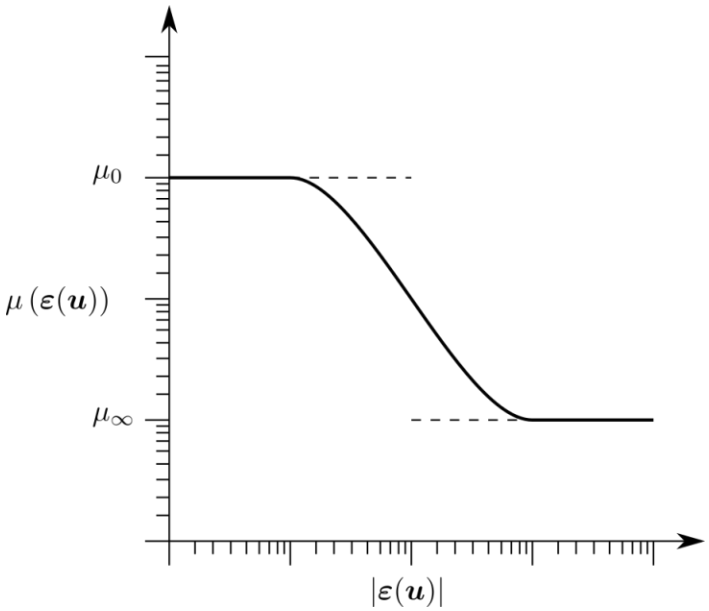

FIGURE 2.4 – Characteristic viscosity curve of a pseudoplastic fluid

where the generalized shear rate $\dot{\gamma}$ is defined as [GW11, Section 3.1]

$$\dot{\gamma} = 2|\boldsymbol{\varepsilon}(\boldsymbol{u})|. \tag{2.8}$$

Typical values for the consistency value K and the power-law index[2] r are given in Table 2.3.

Material	K [Pa · s]	n	r	$\lvert\boldsymbol{\varepsilon}(\boldsymbol{u})\rvert$ [1/s]
Ball-point pen ink	10	0.85	1.85	$10^0 - 10^3$
Fabric conditioner	10	0.6	1.6	$10^0 - 10^2$
Polymer melt	10000	0.6	1.6	$10^2 - 10^4$
Molten chocolate	50	0.5	1.5	$10^{-1} - 10^1$
Synovial fluid	0.5	0.4	1.4	$10^{-1} - 10^2$
Toothpaste	300	0.3	1.3	$10^0 - 10^3$
Skin cream	250	0.1	1.1	$10^0 - 10^2$
Lubricating grease	1000	0.1	1.1	$10^{-1} - 10^2$

TABLE 2.3 – Consistency K and power-law index r values for a selection of substances [Bar89a, Table 2.3]

More sophisticated models take into account the two limiting viscosities μ_0 and μ_∞. For example the *Carreau-Yasuda* constitutive relation [GO20, Equation 1.8]

$$\boldsymbol{\tau} = 2\left[\mu_\infty + (\mu_0 - \mu_\infty)\left(1 + \Gamma\dot{\gamma}\right)^{\frac{r-2}{2}}\right]\boldsymbol{\varepsilon}(\boldsymbol{u}) \qquad \mu_0, \mu_\infty, \Gamma \geq 0,\ 2 > r > 1,$$

or the *Sisko* constitutive relation [GO20, Equation 1.9]

$$\boldsymbol{\tau} = 2\left(\mu_\infty + \alpha\dot{\gamma}^{r-2}\right)\boldsymbol{\varepsilon}(\boldsymbol{u}) \qquad \mu_\infty, \alpha \geq 0,\ 2 > r > 1.$$

[2] In rheology and engineering books the letter "n" is typically used to denote the power-law index, while in mathematics the letter "r" can be found for the power-law index. We use latter definition. The relation between those indices is given by $r = n + 1$

Die approbierte gedruckte Originalversion dieser Diplomarbeit ist an der TU Wien Bibliothek verfügbar
The approved original version of this thesis is available in print at TU Wien Bibliothek.
TU Bibliothek Your knowledge hub WIEN

Above mentioned models are only applicable to a certain shear rate range. An illustrative sketch is shown in Figure 2.5.

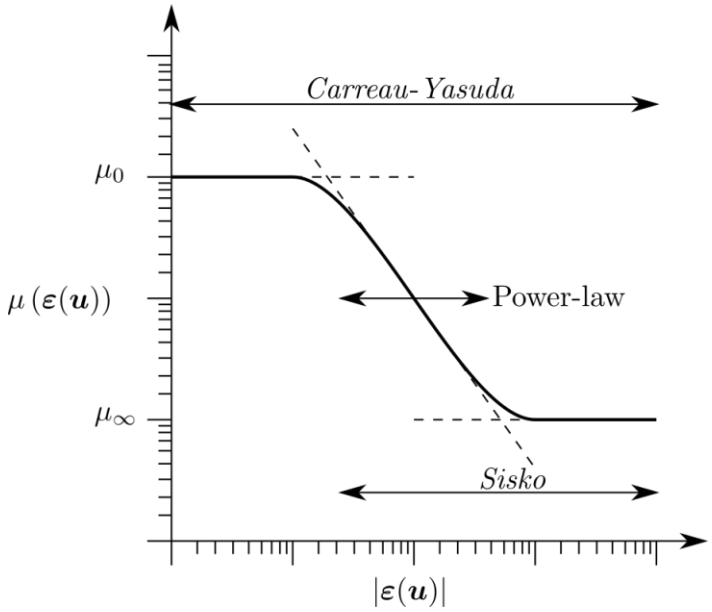

FIGURE 2.5 – Scope of the non-Newtonian pseudoplastic models [Bar00, Section 9.1]

2.3.2 Dilatant fluid

The main characteristic of dilatant fluids compared to pseudoplastic ones is the increase in apparent viscosity at higher shear rates. For this reason they are also called shear-thickening fluids. A possible explanation of such behaviour is again provided by taking into consideration the micro-structures present in the substance. While the fluid has a lubricating effect on the micro-structures at low shear rates, higher shear rates can cause the micro-structures to expand and the fluid can no longer fill the void space. Eventually, the direct contact of the micro-structures and thus friction occurs, which drastically increases the viscosity by increasing rate of strain [CR08, Section 1.3]. An illustration of the occurring solid-solid contact is given in Figure 2.6

Mathematical models

Some dilatant fluids may exhibit pseudoplastic behaviour at low shear rates, which makes the mathematical modelling of such fluids more difficult. However, the power-law model

$$\boldsymbol{\tau} = 2K\dot{\gamma}^{r-2}\boldsymbol{\varepsilon}(\boldsymbol{u}) \qquad\qquad K > 0, r > 2,$$

can be used for the shear-thickening range. For a power-law index $r > 2$ it is trivial that the apparent viscosity increases.

2.3.3 Viscoplastic fluid

Viscoplastic fluids are characterised by an internal stiffness that prevents a shear rate from occurring. However, when a stress threshold is reached, the so-called yield stress τ_y, they

Die approbierte gedruckte Originalversion dieser Diplomarbeit ist an der TU Wien Bibliothek verfügbar
The approved original version of this thesis is available in print at TU Wien Bibliothek.
TU Bibliothek Your knowledge hub WIEN

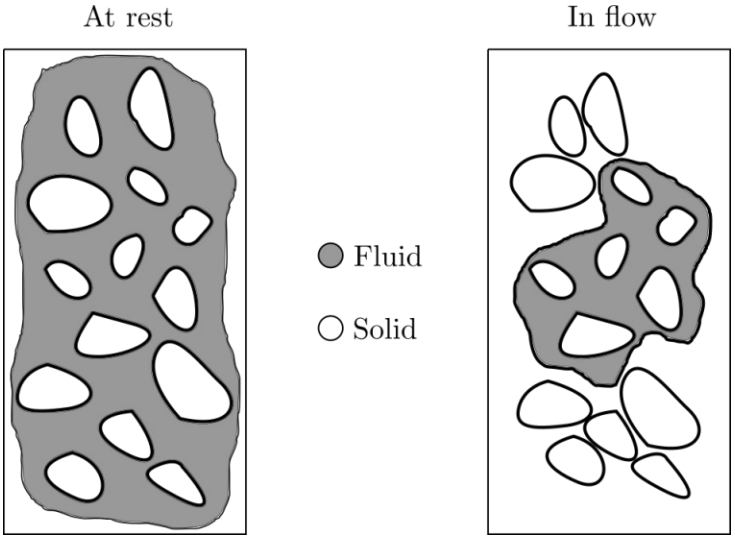

FIGURE 2.6 – Schematic representation of a dilatant fluid at rest and in motion [CR08, Section 1.3]

begin to flow like viscous fluids. The effects of such zero shear rate regions, also known as *unyielded regions*, manifest in a rigid body motion, a solid elastic deformation or a very viscous flow [GW11, Section 1]. Flow regions where the yield stress τ_y is exceeded, also known as *yielded regions*, exhibit either a *Bingham* or a pseudoplastic behaviour as shown in Figure 2.2.

From a microscopic point of view, the micro-structures in the fluid offer sufficient resistance for them not to yield to external forces $|\boldsymbol{\tau}| \leq \tau_y$. When the yield stress is reached $|\boldsymbol{\tau}| > \tau_y$, these structures collapse and the fluid behaves viscously. For some substances this process can be reversible. [CR08, Section 1.3].

Historically, due to the low sensitivity of rheometers, making measurements at low shear rates unreliable, the yield stress τ_y was introduced after extrapolation of the stress-strain rate curve to the zero strain rate axis [GW11, Section 1]. Opinions differ as to whether such a yield stress τ_y is real, nonetheless such approximation is helpful to model substances, which do not strain.

Typical values of yield stresses are given in Table 2.4.

Substances	Yield stress τ_y [Pa]
Ketchup and drilling muds	~ 15
Spaghetti sauce	~ 25
Mustard and apple sauce	~ 60
Mayonnaise	~ 90
Tomato paste	~ 125

TABLE 2.4 – Yield stress values for common substances [Bar00, Section 11.3]

Die approbierte gedruckte Originalversion dieser Diplomarbeit ist an der TU Wien Bibliothek verfügbar
The approved original version of this thesis is available in print at TU Wien Bibliothek.
TU Bibliothek Your knowledge hub WIEN

Mathematical models

The simplest model is certainly the *Bingham* constitutive relation [GW11, Section 3.1]

$$\begin{cases} \boldsymbol{\tau} = 2\mu\boldsymbol{\varepsilon}(\boldsymbol{u}) + \dfrac{\tau_y}{|\boldsymbol{\varepsilon}(\boldsymbol{u})|}\boldsymbol{\varepsilon}(\boldsymbol{u}) & \text{if } |\boldsymbol{\tau}| > \tau_y, \\ \boldsymbol{\varepsilon}(\boldsymbol{u}) = \mathbf{0} & \text{if } |\boldsymbol{\tau}| \leq \tau_y. \end{cases} \tag{2.9}$$

Similar to the power-law model, the constitutive relation (2.9) is based on two parameters: The dynamic viscosity μ and the yield stress τ_y. It is clear from (2.9) that the curve being described in the yielded region is linear. To model non-linear behaviour in the yielded region e.g. shear-thinning/pseudoplastic, a more sophisticated model is needed. One example is the *Herschel-Bulkley* model [GW11, Section 3.1]

$$\begin{cases} \boldsymbol{\tau} = 2K\dot{\gamma}^{r-2}\boldsymbol{\varepsilon}(\boldsymbol{u}) + \dfrac{\tau_y}{|\boldsymbol{\varepsilon}(\boldsymbol{u})|}\boldsymbol{\varepsilon}(\boldsymbol{u}) & \text{if } |\boldsymbol{\tau}| > \tau_y, \\ \boldsymbol{\varepsilon}(\boldsymbol{u}) = 0 & \text{if } |\boldsymbol{\tau}| \leq \tau_y. \end{cases}$$

By taking a closer look, the model is a combination between the power-law model (2.7) and the *Bingham* model (2.9). The generalized shear rate is again given by (2.8).

Die approbierte gedruckte Originalversion dieser Diplomarbeit ist an der TU Wien Bibliothek verfügbar
The approved original version of this thesis is available in print at TU Wien Bibliothek.
TU Bibliothek Your knowledge hub WIEN

3

Newtonian Variational Formulations of Stokes Equations

In this chapter we introduce different variational formulations of *Stokes* equations. In the first place we introduce some used notation, theorems and propositions used throughout this thesis. Secondly, we derive various mixed variational formulations and discuss some stability aspects in a Newtonian setting.

Framework

Let $\Omega \subset \mathbb{R}^d$, where $d = 2, 3$ be an open bounded subset with Lipschitz boundary $\Gamma = \partial\Omega$. Further define the subspaces $\Gamma_D \subseteq \Gamma$ and $\Gamma_N \subseteq \Gamma$ such that $\Gamma_D \cup \Gamma_N = \Gamma$.
The function space $\mathcal{C}^k(\Omega, \mathbb{R})$ contains all real-valued k-times differentiable functions on Ω and accordingly

$$\begin{aligned}
\mathcal{D}(\Omega, \mathbb{R}) &:= \mathcal{C}_0^\infty(\Omega, \mathbb{R}), \\
\mathcal{D}(\Omega, \mathbb{R}^d) &:= \left\{ \boldsymbol{\psi} : \Omega \to \mathbb{R}^d \,|\, \psi_i \in \mathcal{D}(\Omega, \mathbb{R}) \right\}, \\
\mathcal{D}(\Omega, \mathbb{R}^{d\times d}) &:= \left\{ \boldsymbol{\psi} : \Omega \to \mathbb{R}^{d\times d} \,|\, \psi_{ij} \in \mathcal{D}(\Omega, \mathbb{R}) \right\},
\end{aligned}$$

as the space of infinitely differentiable, compactly supported, real-valued scalar($\mathbb{R}$)-, vector($\mathbb{R}^d$)- and matrix($\mathbb{R}^{d\times d}$)-valued functions on Ω. The space of distributions is denoted by $\mathcal{D}'(\Omega)$.
Gradient and divergence operators are defined as

$$\begin{aligned}
(\nabla\psi)_i &= \frac{\partial\psi}{\partial x_i} && \psi \in \mathcal{D}'(\Omega, \mathbb{R}), \\
(\nabla\boldsymbol{\psi})_{ij} &= \frac{\partial\psi_i}{\partial x_j} && \boldsymbol{\psi} \in \mathcal{D}'(\Omega, \mathbb{R}^d), \\
\operatorname{div}(\boldsymbol{\psi}) &= \sum_{i=1}^{d} \frac{\partial(\boldsymbol{\psi})_i}{\partial x_i} && \boldsymbol{\psi} \in \mathcal{D}'(\Omega, \mathbb{R}^d), \\
(\operatorname{div}(\boldsymbol{\psi}))_i &= \sum_{j=1}^{d} \frac{\partial(\boldsymbol{\psi})_{ij}}{\partial x_j} && \boldsymbol{\psi} \in \mathcal{D}'(\Omega, \mathbb{R}^{d\times d}).
\end{aligned}$$

In a two-dimensional setting we define the curl operator of a scalar($\mathbb{R}$)-valued function as

$$\operatorname{curl}(\psi) = \left(-\frac{\partial\psi}{\partial x_1}, \quad \frac{\partial\psi}{\partial x_0} \right)^{\mathrm{T}} \in \mathcal{D}'(\Omega, \mathbb{R}^2) \qquad \psi \in \mathcal{D}'(\Omega, \mathbb{R}).$$

Die approbierte gedruckte Originalversion dieser Diplomarbeit ist an der TU Wien Bibliothek verfügbar
The approved original version of this thesis is available in print at TU Wien Bibliothek.
TU Bibliothek Your knowledge hub WIEN

Let V be a *Sobolev* space, then we denote by $(\cdot,\cdot)_V$ the inner product and by $\|\cdot\|_V$ the norm of the space. When considering the space of real-valued square integrable functions on Ω

$$L^2(\Omega,\mathbb{R}) := \left\{ f : \int_\Omega f^2\,dx < \infty \right\},$$

we abbreviate the notion

$$\begin{aligned} (f,g) &:= \int_\Omega fg\,dx && \forall\, f,g \in L^2(\Omega,\mathbb{R}),\\ \|f\| &:= \sqrt{(f,f)} && \forall\, f,g \in L^2(\Omega,\mathbb{R}), \end{aligned}$$

otherwise for a subset $\Delta \subset \Omega$ we add the subscript

$$\begin{aligned} (f,g)_\Delta &:= \int_\Delta fg\,dx && \forall\, f,g \in L^2(\Delta,\mathbb{R}),\\ \|f\|_\Delta &:= \sqrt{(f,f)_\Delta} && \forall\, f,g \in L^2(\Delta,\mathbb{R}). \end{aligned}$$

We introduce the well known *Sobolev* spaces

$$\begin{aligned} H^1(\Omega,\mathbb{R}) &:= \left\{ \psi \in L^2(\Omega,\mathbb{R}) : \|\nabla\psi\| < \infty \right\},\\ H(\mathrm{div},\Omega) &:= \left\{ \boldsymbol{\psi} \in L^2(\Omega,\mathbb{R}^d) : \|\mathrm{div}(\boldsymbol{\psi})\| < \infty \right\}, \end{aligned}$$

and the subspaces with homogeneous traces

$$\begin{aligned} H_0^1(\Omega,\mathbb{R}) &:= \left\{ \psi \in H^1(\Omega,\mathbb{R}) : \psi = 0 \text{ on } \Gamma \right\},\\ H_0(\mathrm{div},\Omega) &:= \left\{ \boldsymbol{\psi} \in H(\mathrm{div},\Omega) : \boldsymbol{\psi}\cdot\boldsymbol{n} = 0 \text{ on } \Gamma \right\}, \end{aligned}$$

with the corresponding norms

$$\begin{aligned} \|\psi\|_{H^1}^2 &:= \|\psi\|^2 + \|\nabla\psi\|^2,\\ \|\boldsymbol{\psi}\|_{H(\mathrm{div})}^2 &:= \|\boldsymbol{\psi}\|^2 + \|\mathrm{div}(\boldsymbol{\psi})\|^2. \end{aligned}$$

A dual space V^* of all bounded linear forms on V is denoted by a superscript asterisk. The dual norm is given by

$$\|l\|_{V^*} := \sup_{v\in V} \frac{l(v)}{\|v\|_V} \qquad \forall\, l \in V^*$$

Every continuous and discrete variational formulations of *Stokes* equations we are going to derive have a saddle point structure. In order to guarantee uniqueness and solvability of such problems we need *Brezzis* [Bre74] Theorem 1.

Die approbierte gedruckte Originalversion dieser Diplomarbeit ist an der TU Wien Bibliothek verfügbar
The approved original version of this thesis is available in print at TU Wien Bibliothek.
TU Bibliothek Your knowledge hub WIEN

Theorem 1. *Consider the following problem:*

Find $(\boldsymbol{u}, p) \in V \times Q$ *such that*

$$\begin{aligned} a(\boldsymbol{u}, \overline{\boldsymbol{u}}) + b(\overline{\boldsymbol{u}}, p) &= f(\overline{\boldsymbol{u}}) && \forall \overline{\boldsymbol{u}} \in V, \\ b(\boldsymbol{u}, \overline{p}) &= 0 && \forall \overline{p} \in Q \end{aligned}$$

Assume:
The bilinear forms $a(\boldsymbol{u}, \overline{\boldsymbol{u}})$ *and* $b(\boldsymbol{u}, \overline{p})$ *are continuous*

$$\begin{aligned} a(\boldsymbol{u}, \overline{\boldsymbol{u}}) &\preceq \|\boldsymbol{u}\|_V \|\overline{\boldsymbol{u}}\|_V, \\ b(\boldsymbol{u}, \overline{p}) &\preceq \|\boldsymbol{u}\|_V \|\overline{p}\|_Q. \end{aligned}$$

The bilinear form $a(\boldsymbol{u}, \overline{\boldsymbol{u}})$ *is coercive(elliptic) on the kernel* V_0*, i.e.*

$$a(\boldsymbol{u}, \boldsymbol{u}) \succeq \|\boldsymbol{u}\|_V \qquad \forall \boldsymbol{u} \in V_0 := \{\boldsymbol{v} \in V : b(\boldsymbol{v}, \overline{p}) = 0 \ \forall \overline{p} \in Q\}.$$

The bilinear form $b(\boldsymbol{u}, \overline{p})$ *fulfils the LBB (Ladyshenskaya-Babuška-Brezzi) condition*

$$\sup_{\boldsymbol{u} \in V, \boldsymbol{u} \neq 0} \frac{b(\boldsymbol{u}, \overline{p})}{\|\boldsymbol{u}\|_V} \succeq \|\overline{p}\|_Q \qquad \forall \overline{p} \in Q.$$

Then the variational problem has an unique solution depending continuously on the input

$$\|\boldsymbol{u}\|_V + \|p\|_Q \preceq \|f\|_{V^*}.$$

The succeeding inequalities are useful to prove the conditions required to fulfil Theorem 1.

Proposition 2. ***Cauchy-Schwarz inequality***
For an inner product space V *it holds*

$$|\langle f, g \rangle_V| \leq \|f\|_V \|g\|_V \qquad \forall f, g \in V.$$

Proposition 3. ***Korn's inequality*** *[CDD+76]*
There exists a constant $c > 0$ *dependent on* Ω *such that it holds*

$$c\|\nabla \boldsymbol{u}\|_{H^1}^2 \leq \|\boldsymbol{\varepsilon}(\boldsymbol{u})\|^2 + \|\boldsymbol{u}\|^2 \qquad \forall \boldsymbol{u} \in H^1(\Omega, \mathbb{R}).$$

Governing equations

We recall *Stokes* equations for a Newtonian fluid and incompressible flow with homogeneous boundary conditions on $\Gamma_D = \partial\Omega$:

$$\begin{aligned} \boldsymbol{\tau} &= 2\mu\boldsymbol{\varepsilon}(\boldsymbol{u}) && \text{in } \Omega, && (3.1a) \\ -\operatorname{div}(\boldsymbol{\tau}) &= -\nabla p + \rho \boldsymbol{f} && \text{in } \Omega, && (3.1b) \\ \operatorname{div}(\boldsymbol{u}) &= 0 && \text{in } \Omega, && (3.1c) \\ \boldsymbol{u} &= 0 && \text{on } \Gamma_D. && (3.1d) \end{aligned}$$

Die approbierte gedruckte Originalversion dieser Diplomarbeit ist an der TU Wien Bibliothek verfügbar
The approved original version of this thesis is available in print at TU Wien Bibliothek.
TU Bibliothek Your knowledge hub WIEN

The solution to the system of equations (3.1) is unique up to a constant pressure. Choose $p = \tilde{p} + c$, then $\tilde{p}$ also solves the momentum equations. To guarantee uniqueness, one can either fix a pressure value in space, or perform a mathematical gauging

$$\int_\Omega p \, dx = 0.$$

We will use the latter technique and define the appropriate L^2-space with zero mean value

$$L_0^2(\Omega, \mathbb{R}) := \left\{ f \in L^2(\Omega, \mathbb{R}) : \int_\Omega f \, dx = 0 \right\}.$$

It is known that every tensor can be split in a symmetric and skew-symmetric part, in particular

$$\nabla \boldsymbol{u} = \operatorname{sym}(\nabla \boldsymbol{u}) + \operatorname{skw}(\nabla \boldsymbol{u}) = \boldsymbol{\varepsilon}(\boldsymbol{u}) + \boldsymbol{\omega}(\boldsymbol{u}). \tag{3.2}$$

Above relation, will be constantly used throughout this work. The rate-of-strain tensor $\boldsymbol{\varepsilon}(\boldsymbol{u})$ has already been introduced in Chapter 2

$$\boldsymbol{\varepsilon}(\boldsymbol{u}) = \frac{1}{2} \left(\nabla \boldsymbol{u} + (\nabla \boldsymbol{u})^{\mathrm{T}} \right) \tag{3.3}$$

whereas the rate-of-rotation tensor $\boldsymbol{\omega}(\boldsymbol{u})$ is defined as [Pop12, Section 2.8]

$$\boldsymbol{\omega}(\boldsymbol{u}) = \frac{1}{2} \left(\nabla \boldsymbol{u} - (\nabla \boldsymbol{u})^{\mathrm{T}} \right) \tag{3.4}$$

3.1 Velocity-pressure formulation

We aim to describe the system of equations (3.1) by two fields i.e. the velocity $\boldsymbol{u}$ and the pressure p. To form the rate-of-strain tensor $\boldsymbol{\varepsilon}(\boldsymbol{u})$ we require $\nabla \boldsymbol{u}$ to be in $L^2(\Omega, \mathbb{R}^{d \times d})$, therefore the appropriate space for the velocity is $\boldsymbol{u} \in V := H_0^1(\Omega, \mathbb{R}^d)$. The pressure suffices $p \in Q := L_0^2(\Omega, \mathbb{R})$.
To derive the weak formulation we multiply (3.1) with suitable test functions denoted by an overline $\overline{(\cdot)}$

$$\begin{aligned} -2\mu \int_\Omega \operatorname{div}(\boldsymbol{\varepsilon}(\boldsymbol{u})) \cdot \overline{\boldsymbol{u}} \, dx &= -\int_\Omega \nabla p \cdot \overline{\boldsymbol{u}} \, dx + \int_\Omega \rho \boldsymbol{f} \cdot \overline{\boldsymbol{u}} \, dx, \\ -\int_\Omega \operatorname{div}(\boldsymbol{u}) \overline{p} \, dx &= 0. \end{aligned}$$

Exploiting the identity of the *Frobenius* inner product for symmetric matrices

$$\boldsymbol{\varepsilon}(\boldsymbol{u}) : \nabla \overline{\boldsymbol{u}} = \boldsymbol{\varepsilon}(\boldsymbol{u}) : \boldsymbol{\varepsilon}(\overline{\boldsymbol{u}}) + \boldsymbol{\varepsilon}(\boldsymbol{u}) : \boldsymbol{\omega}(\overline{\boldsymbol{u}}) = \boldsymbol{\varepsilon}(\boldsymbol{u}) : \boldsymbol{\varepsilon}(\overline{\boldsymbol{u}}),$$

and applying integration by parts, we get a symmetric formulation

$$\begin{aligned} 2\mu \int_\Omega \boldsymbol{\varepsilon}(\boldsymbol{u}) : \boldsymbol{\varepsilon}(\overline{\boldsymbol{u}}) \, dx - \int_\Omega \operatorname{div}(\overline{\boldsymbol{u}}) p \, dx &= \int_\Omega \rho \boldsymbol{f} \cdot \overline{\boldsymbol{u}} \, dx, \\ -\int_\Omega \operatorname{div}(\boldsymbol{u}) \overline{p} \, dx &= 0. \end{aligned}$$

Die approbierte gedruckte Originalversion dieser Diplomarbeit ist an der TU Wien Bibliothek verfügbar
The approved original version of this thesis is available in print at TU Wien Bibliothek.
TU Bibliothek Your knowledge hub WIEN

The linear form and bilinear forms are redefined as

$$a(\boldsymbol{u}, \overline{\boldsymbol{u}}) := 2\mu \int_\Omega \boldsymbol{\varepsilon}(\boldsymbol{u}) : \boldsymbol{\varepsilon}(\overline{\boldsymbol{u}})\, dx, \tag{3.5}$$

$$b_1(\boldsymbol{u}, \overline{p}) := -\int_\Omega \operatorname{div}(\boldsymbol{u})\overline{p}\, dx, \tag{3.6}$$

$$f(\overline{\boldsymbol{u}}) := \int_\Omega \rho \boldsymbol{f} \cdot \overline{\boldsymbol{u}}\, dx. \tag{3.7}$$

such that variational formulation I is obtained.

Variational Formulation I
Find $(\boldsymbol{u}, p) \in V \times Q$ such that

$$\begin{aligned} a(\boldsymbol{u}, \overline{\boldsymbol{u}}) + b_1(\overline{\boldsymbol{u}}, p) &= f(\overline{\boldsymbol{u}}) && \forall \overline{\boldsymbol{u}} \in V, \\ b_1(\boldsymbol{u}, \overline{p}) &= 0 && \forall \overline{p} \in Q. \end{aligned}$$

Velocity-pressure stability aspects

Continuity of bilinear forms (3.5) and (3.6) is a direct consequence of applying *Cauchy-Schwarz* inequality to it

$$a(\boldsymbol{u}, \overline{\boldsymbol{u}}) \preceq \mu \|\boldsymbol{u}\|_V \|\overline{\boldsymbol{u}}\|_V \qquad \forall \boldsymbol{u}, \overline{\boldsymbol{u}} \in V, \tag{3.8}$$

$$b_1(\boldsymbol{u}, \overline{p}) \preceq \|\boldsymbol{u}\|_V \|\overline{p}\|_Q \qquad \forall \boldsymbol{u} \in V, \overline{p} \in Q. \tag{3.9}$$

Ellipticity on V (i.e. also on V_0) follows by making use of *Korn's* inequality

$$a(\boldsymbol{u}, \boldsymbol{u}) = 2\mu \|\boldsymbol{\varepsilon}(\boldsymbol{u})\|^2 \succeq \mu \|\boldsymbol{u}\|_V^2 \qquad \forall \boldsymbol{u} \in V.$$

The LBB condition is also fulfilled for the continuous setting

$$\sup_{\substack{\boldsymbol{u} \in V \\ \boldsymbol{u} \neq 0}} \frac{|b(\boldsymbol{u}, \overline{p})|}{\|\boldsymbol{u}\|_V} \succeq \|\overline{p}\|_Q \qquad \forall \overline{p} \in Q. \tag{3.10}$$

We refer to [BBF13, Section 8.2] for a detailed proof.

3.2 Mixed stress formulation

An alternative to the Velocity-pressure formulation is to introduce a third space for the deviatoric stress tensor $\boldsymbol{\tau}$. We will clarify later, why this choice is very well suited for Non-Newtonian flows. In the following we illustrate an option where $\boldsymbol{\tau}$ is sought in a $L^2(\Omega, \mathbb{R}^{d\times d})$-space. While in the two-field formulation the velocity $\boldsymbol{u}$ was the primal and the pressure p the dual variable, in the three-field formulation they undergo a role reversal. The primal variables become $(\boldsymbol{\tau}, p) \in X := \Sigma \times Q$ and the dual variable $\boldsymbol{u} \in V$. This will play an important part, when analysing the kernel ellipticity and the LBB condition.
Before deriving the variational formulation, we introduce the symmetric subset of the matrix-valued $L^2(\Omega, \mathbb{R}^{d\times d})$-space.

$$L^2_{\mathrm{sym}}(\Omega, \mathbb{R}^{d\times d}) := \left\{ \boldsymbol{\psi} \in L^2(\Omega, \mathbb{R}^{d\times d}) : \boldsymbol{\psi} = \boldsymbol{\psi}^{\mathrm{T}} \right\}.$$

Die approbierte gedruckte Originalversion dieser Diplomarbeit ist an der TU Wien Bibliothek verfügbar
The approved original version of this thesis is available in print at TU Wien Bibliothek.
TU Bibliothek Your knowledge hub WIEN

Recall from the angular momentum balance (2.4c) that the deviatoric stress tensor $\boldsymbol{\tau}$ must be symmetric. A suitable function space for this requirement is the above defined $\boldsymbol{\tau} \in \Sigma := L^2_{\mathrm{sym}}(\Omega, \mathbb{R}^{d\times d})$. Velocity and pressure spaces V, Q can be adopted from the velocity-pressure formulation 3.1.
With the help of the identity for symmetric matrices,

$$\boldsymbol{\tau} : \nabla \overline{\boldsymbol{u}} = \boldsymbol{\tau} : \boldsymbol{\varepsilon}(\overline{\boldsymbol{u}}) + \boldsymbol{\tau} : \boldsymbol{\omega}(\overline{\boldsymbol{u}}) = \boldsymbol{\tau} : \boldsymbol{\varepsilon}(\overline{\boldsymbol{u}}),$$

we derive the weak formulation by multiplication with appropriate test functions

$$\begin{aligned} -\frac{1}{2\mu}\int_\Omega \boldsymbol{\tau} : \overline{\boldsymbol{\tau}}\, dx + \int_\Omega \boldsymbol{\varepsilon}(\boldsymbol{u}) : \overline{\boldsymbol{\tau}}\, dx &= 0, \\ \int_\Omega \boldsymbol{\tau} : \boldsymbol{\varepsilon}(\overline{\boldsymbol{u}})\, dx - \int_\Omega \operatorname{div}(\overline{\boldsymbol{u}}) p\, dx &= \int_\Omega \rho \boldsymbol{f} \cdot \overline{\boldsymbol{u}}\, dx, \\ -\int_\Omega \operatorname{div}(\boldsymbol{u})\overline{p}\, dx &= 0. \end{aligned}$$

Subsequently, the linear form and bilinear forms

$$a(\boldsymbol{\tau}, \overline{\boldsymbol{\tau}}) := -\frac{1}{2\mu}\int_\Omega \boldsymbol{\tau} : \overline{\boldsymbol{\tau}}\, dx, \tag{3.11}$$

$$b_1(\boldsymbol{u}, \overline{p}) := -\int_\Omega \operatorname{div}(\boldsymbol{u})\overline{p}\, dx, \tag{3.12}$$

$$b_2(\boldsymbol{\tau}, \boldsymbol{\varepsilon}(\overline{\boldsymbol{u}})) := \int_\Omega \boldsymbol{\tau} : \boldsymbol{\varepsilon}(\overline{\boldsymbol{u}})\, dx, \tag{3.13}$$

$$f(\overline{\boldsymbol{u}}) := \int_\Omega \rho \boldsymbol{f} \cdot \overline{\boldsymbol{u}}\, dx. \tag{3.14}$$

form the variational formulation II.

Variational Formulation II
Find $((\boldsymbol{\tau}, p), \boldsymbol{u}) \in X \times V$ such that

$$\begin{aligned} a(\boldsymbol{\tau}, \overline{\boldsymbol{\tau}}) + b_2(\overline{\boldsymbol{\tau}}, \boldsymbol{\varepsilon}(\boldsymbol{u})) &= 0 && \forall \overline{\boldsymbol{\tau}} \in \Sigma, \\ b_2(\boldsymbol{\tau}, \boldsymbol{\varepsilon}(\overline{\boldsymbol{u}})) + b_1(\overline{\boldsymbol{u}}, p) &= f(\overline{\boldsymbol{u}}) && \forall \overline{\boldsymbol{u}} \in V, \\ b_1(\boldsymbol{u}, \overline{p}) &= 0 && \forall \overline{p} \in Q. \end{aligned}$$

Notice the solution of variational formulation I and II are identical in this linear setting, as it holds $\boldsymbol{\varepsilon}(\boldsymbol{u}) \subset \Sigma$ and from

$$a(\boldsymbol{\tau}, \overline{\boldsymbol{\tau}}) + b_2(\overline{\boldsymbol{\tau}}, \boldsymbol{\varepsilon}(\boldsymbol{u})) = 0 \qquad \forall \overline{\boldsymbol{\tau}} \in \Sigma,$$

it follows $\boldsymbol{\tau} = \boldsymbol{\varepsilon}(\boldsymbol{u})$.

Mixed stress stability aspects

Using *Cauchy-Schwarz* inequality the continuity of bilinear forms

$$\begin{aligned} a(\boldsymbol{\tau}, \overline{\boldsymbol{\tau}}) &\preceq \frac{1}{\mu}\|\boldsymbol{\tau}\|_\Sigma \|\overline{\boldsymbol{\tau}}\|_V && \forall \boldsymbol{\tau}, \overline{\boldsymbol{\tau}} \in \Sigma, \\ b_2(\boldsymbol{\tau}, \overline{\boldsymbol{u}}) &\preceq \|\boldsymbol{\tau}\|_\Sigma \|\overline{\boldsymbol{u}}\|_V && \forall \boldsymbol{\tau} \in \Sigma, \overline{\boldsymbol{u}} \in V, \end{aligned}$$

Die approbierte gedruckte Originalversion dieser Diplomarbeit ist an der TU Wien Bibliothek verfügbar
The approved original version of this thesis is available in print at TU Wien Bibliothek.
TU Bibliothek Your knowledge hub WIEN

can be shown. Note that the continuity of bilinear form (3.12) has already been proven in (3.9).

Lemma 4. *On the kernel X_0 bilinear form a is elliptic*

$$a(\boldsymbol{\tau},\boldsymbol{\tau}) \succeq \|\boldsymbol{\tau}\|_\Sigma^2 + \|p\|_Q^2 \qquad \forall (\boldsymbol{\tau},p) \in X_0. \tag{3.15}$$

Proof: The kernel is given by

$$X_0 := \{(\boldsymbol{\tau},p) \in X : b_2(\boldsymbol{\tau},\overline{\boldsymbol{u}}) + b_1(\overline{\boldsymbol{u}},p) = 0 \quad \forall \overline{\boldsymbol{u}} \in V\}.$$

To proof coercivity on the kernel we need a further estimate. For this recall the LBB condition from the two-field setting (3.10). With *Cauchy-Schwarz's* inequality

$$\begin{aligned}\|p\|_Q &\preceq \sup_{\substack{\boldsymbol{u}\in V\\ \boldsymbol{u}\neq 0}} \frac{|\int_\Omega \operatorname{div}(\overline{\boldsymbol{u}}) p\, dx|}{\|\overline{\boldsymbol{u}}\|_V} = \sup_{\substack{\boldsymbol{u}\in V\\ \boldsymbol{u}\neq 0}} \frac{|\int_\Omega \boldsymbol{\tau} : \boldsymbol{\varepsilon}(\boldsymbol{u})\, dx|}{\|\overline{\boldsymbol{u}}\|_V} \\ &\preceq \sup_{\substack{\boldsymbol{u}\in V\\ \boldsymbol{u}\neq 0}} \frac{\|\boldsymbol{\tau}\|_\Sigma \|\boldsymbol{\varepsilon}(\overline{\boldsymbol{u}})\|}{\|\overline{\boldsymbol{u}}\|_V} \preceq \|\boldsymbol{\tau}\|_\Sigma.\end{aligned}$$

With this result it follows

$$a(\boldsymbol{\tau},\boldsymbol{\tau}) = \frac{1}{2\mu}\|\boldsymbol{\tau}\|_\Sigma^2 \succeq \frac{1}{4\mu}\|\boldsymbol{\tau}\|_\Sigma^2 + \frac{1}{4\mu}\|p\|_Q^2 \succeq \frac{1}{\mu}\left(\|\boldsymbol{\tau}\|_\Sigma^2 + \|p\|_Q^2\right) = \frac{1}{\mu}\|(\boldsymbol{\tau},p)\|_X^2.$$

Lemma 5. *The LBB condition holds for any $\overline{\boldsymbol{u}} \in V$*

$$\sup_{(\boldsymbol{\tau},p)\in X} \frac{|b_2(\boldsymbol{\tau},\boldsymbol{\varepsilon}(\overline{\boldsymbol{u}})) + b_1(\overline{\boldsymbol{u}},p)|}{\|(\boldsymbol{\tau},p)\|_X} \succeq \|\overline{\boldsymbol{u}}\|_V \qquad \forall \overline{\boldsymbol{u}} \in V. \tag{3.16}$$

Proof: Since $(\boldsymbol{\tau},p)$ are arbitrary, we choose $\boldsymbol{\tau} := \boldsymbol{\varepsilon}(\overline{\boldsymbol{u}}), p := 0$

$$\sup_{(\boldsymbol{\tau},p)\in X} \frac{|b_2(\boldsymbol{\tau},\boldsymbol{\varepsilon}(\overline{\boldsymbol{u}})) + b_1(\overline{\boldsymbol{u}},p)|}{\|(\boldsymbol{\tau},p)\|_X} \succeq \sup_{\boldsymbol{\tau}\in\Sigma} \frac{|b_2(\boldsymbol{\tau},\boldsymbol{\varepsilon}(\overline{\boldsymbol{u}}))|}{\|\boldsymbol{\tau}\|_\Sigma} \geq \frac{|b_2(\boldsymbol{\varepsilon}(\overline{\boldsymbol{u}}),\boldsymbol{\varepsilon}(\overline{\boldsymbol{u}}))|}{\|\boldsymbol{\varepsilon}(\overline{\boldsymbol{u}})\|} = \|\boldsymbol{\varepsilon}(\overline{\boldsymbol{u}})\|.$$

We conclude by Korn's inequality (3). For a detailed proof of above stability analysis and additional error estimates consider the paper by *Fortin et al.* [FP89]

3.3 Mass conserving mixed stress formulation

Compared to the other formulations we aim to increase the regularity of the deviatoric stress tensor $\boldsymbol{\tau}$. Put into words, we seek a row-wise $H(\operatorname{div},\Omega)$-type space, such that $\operatorname{div}(\boldsymbol{\tau})$ is well defined. A recently developed formulation [GLS19] for *Stokes* equations (3.1) fulfills this prerequisite. Based on the authors findings, the regularity of the velocity space has been decreased to $\boldsymbol{u} \in V := H(\operatorname{div},\Omega)$, which is an appropriate space for the incompressibility constraint, especially in the discrete setting, while the pressure is still

Die approbierte gedruckte Originalversion dieser Diplomarbeit ist an der TU Wien Bibliothek verfügbar
The approved original version of this thesis is available in print at TU Wien Bibliothek.
TU Bibliothek Your knowledge hub WIEN

sought in $p \in Q := L_0^2(\Omega, \mathbb{R})$. The regularity of the deviatoric stress tensor has been increased to $\boldsymbol{\tau} \in \Sigma_{\text{sym}}$, where Σ_{sym} is given by

$$\begin{aligned} H(\operatorname{curl}\operatorname{div}, \Omega) &:= \left\{ \boldsymbol{\psi} \in L^2(\Omega, \mathbb{R}^{d\times d}) : \operatorname{div}(\boldsymbol{\psi}) \in H_0(\operatorname{div}, \Omega)^* \right\}, \\ \Sigma &:= \left\{ \boldsymbol{\psi} \in H(\operatorname{curl}\operatorname{div}, \Omega) : \operatorname{tr}(\boldsymbol{\psi}) = 0 \right\}, \\ \Sigma_{\text{sym}} &:= \left\{ \boldsymbol{\psi} \in H(\operatorname{curl}\operatorname{div}, \Omega) : \operatorname{tr}(\boldsymbol{\psi}) = 0, \boldsymbol{\psi} = \boldsymbol{\psi}^{\mathrm{T}} \right\}, \\ \|\boldsymbol{\psi}\|_{\Sigma}^2 &:= \|\boldsymbol{\psi}\|^2 + \|\operatorname{div}(\boldsymbol{\psi})\|_{H_0(\operatorname{div})^*}^2. \end{aligned}$$

We start deriving the weak formulation by multiplying (3.1) with suitable test functions

$$\begin{aligned} \frac{1}{2\mu} \int_\Omega \boldsymbol{\tau} : \overline{\boldsymbol{\tau}}\, dx - \int_\Omega \boldsymbol{\varepsilon}(\boldsymbol{u}) : \overline{\boldsymbol{\tau}}\, dx &= 0, \\ \langle \operatorname{div}(\boldsymbol{\tau}), \overline{\boldsymbol{u}} \rangle_V - \int_\Omega \nabla p \overline{\boldsymbol{u}}\, dx &= -\int_\Omega \rho \boldsymbol{f} \cdot \overline{\boldsymbol{u}}\, dx, \\ \int_\Omega \operatorname{div}(\boldsymbol{u}) \overline{p}\, dx &= 0. \end{aligned}$$

Using the identity for a *Frobenius* inner product with symmetric matrices, integration by parts and the homogeneous boundary condition we get

$$\begin{aligned} \int_\Omega \boldsymbol{\varepsilon}(\boldsymbol{u}) : \overline{\boldsymbol{\tau}}\, dx &= \int_\Omega \nabla \boldsymbol{u} : \overline{\boldsymbol{\tau}}\, dx = -\langle \operatorname{div}(\overline{\boldsymbol{\tau}}), \boldsymbol{u} \rangle_V, \\ -\int_\Omega \nabla p \overline{\boldsymbol{u}}\, dx &= \int_\Omega \operatorname{div}(\overline{\boldsymbol{u}}) p\, dx. \end{aligned}$$

Therefore in total it results in the symmetric weak formulation

$$\begin{aligned} \frac{1}{2\mu} \int_\Omega \boldsymbol{\tau} : \overline{\boldsymbol{\tau}}\, dx + \langle \operatorname{div}(\overline{\boldsymbol{\tau}}), \boldsymbol{u} \rangle_V &= 0, \\ \langle \operatorname{div}(\boldsymbol{\tau}), \overline{\boldsymbol{u}} \rangle_V + \int_\Omega \operatorname{div}(\overline{\boldsymbol{u}}) p\, dx &= -\int_\Omega \rho \boldsymbol{f} \cdot \overline{\boldsymbol{u}}\, dx, \\ \int_\Omega \operatorname{div}(\boldsymbol{u}) \overline{p}\, dx &= 0, \end{aligned}$$

where $\langle \cdot, \cdot \rangle_V$ denotes the duality pairing on V, see also [Led19].
In terms of bilinear forms and linear form

$$a(\boldsymbol{\tau}, \overline{\boldsymbol{\tau}}) := \frac{1}{2\mu} \int_\Omega \boldsymbol{\tau} : \overline{\boldsymbol{\tau}}\, dx, \tag{3.17}$$

$$b_1(\boldsymbol{u}, \overline{p}) := \int_\Omega \operatorname{div}(\boldsymbol{u}) \overline{p}\, dx, \tag{3.18}$$

$$b_2(\boldsymbol{\tau}, \overline{\boldsymbol{u}}) := \langle \operatorname{div}(\boldsymbol{\tau}), \overline{\boldsymbol{u}} \rangle_V, \tag{3.19}$$

$$f(\overline{\boldsymbol{u}}) := \int_\Omega \rho \boldsymbol{f} \cdot \overline{\boldsymbol{u}}\, dx. \tag{3.20}$$

we derived our third variational formulation III

Die approbierte gedruckte Originalversion dieser Diplomarbeit ist an der TU Wien Bibliothek verfügbar
The approved original version of this thesis is available in print at TU Wien Bibliothek.
TU Bibliothek Your knowledge hub WIEN

Variational Formulation III
Find $((\boldsymbol{\tau}, p), \boldsymbol{u}) \in X \times V$ such that

$$\begin{aligned} a(\boldsymbol{\tau}, \overline{\boldsymbol{\tau}}) + b_2(\overline{\boldsymbol{\tau}}, \boldsymbol{u}) &= 0 && \forall \overline{\boldsymbol{\tau}} \in \Sigma, \\ b_2(\boldsymbol{\tau}, \overline{\boldsymbol{u}}) + b_1(\overline{\boldsymbol{u}}, p) &= -f(\overline{\boldsymbol{u}}) && \forall \overline{\boldsymbol{u}} \in V, \\ b_1(\boldsymbol{u}, \overline{p}) &= 0 && \forall \overline{p} \in Q. \end{aligned}$$

Mass conserving mixed stress stability aspects

It follows immediately by *Cauchy-Schwarz's* inequality that bilinear form

$$a(\boldsymbol{\tau}, \overline{\boldsymbol{\tau}}) \preceq \frac{1}{\mu} \|\boldsymbol{\tau}\|_\Sigma \|\overline{\boldsymbol{\tau}}\|_\Sigma \qquad \forall \boldsymbol{\tau}, \overline{\boldsymbol{\tau}} \in \Sigma, \tag{3.21}$$

is continuous. Continuity of bilinear form $b_1(\boldsymbol{u}, \overline{p})$ is already known (3.9), whereas for $b_2(\boldsymbol{\tau}, \overline{\boldsymbol{u}})$ it follows from

$$b_2(\boldsymbol{\tau}, \overline{\boldsymbol{u}}) := \langle \operatorname{div}(\boldsymbol{\tau}), \overline{\boldsymbol{u}} \rangle \leq \|\operatorname{div}(\boldsymbol{\tau})\|_{V^*} \|\overline{\boldsymbol{u}}\|_V \leq \|\boldsymbol{\tau}\|_\Sigma \|\overline{\boldsymbol{u}}\|_V \qquad \forall \boldsymbol{\tau} \in \Sigma, \overline{\boldsymbol{u}} \in V.$$

Coercivity on the kernel follows similar arguments as in Lemma 4. For the detailed proof see [Led19, Lemma 9].

Lemma 6. *LBB condition is fulfilled*

$$\sup_{(\boldsymbol{\tau}, p) \in X} \frac{|b_2(\boldsymbol{\tau}, \overline{\boldsymbol{u}}) + b_1(\overline{\boldsymbol{u}}, p)|}{\|(\boldsymbol{\tau}, p)\|_X} \succeq \|\overline{\boldsymbol{u}}\|_V \qquad \forall \overline{\boldsymbol{u}} \in V. \tag{3.22}$$

Proof: Since $\operatorname{div}(V) \subset Q$, choose $p := \operatorname{div}(\overline{\boldsymbol{u}})$ then it follows

$$b_1(\overline{\boldsymbol{u}}, p) = \int_\Omega \operatorname{div}(\overline{\boldsymbol{u}}) p \, dx = \|\operatorname{div}(\overline{\boldsymbol{u}})\|^2 \qquad \forall \overline{\boldsymbol{u}} \in V,$$

and by definitions of the $L^2(\Omega)$ and $H(\operatorname{div})$ norms the estimate holds true

$$\|p\|_Q = \|\operatorname{div}(\overline{\boldsymbol{u}})\| \leq \|\overline{\boldsymbol{u}}\|_V.$$

From [Led19, Lemma 12] there further exists for all $\overline{\boldsymbol{u}} \in V$ a $\boldsymbol{\tau}$ such that

$$b_2(\boldsymbol{\tau}, \overline{\boldsymbol{u}}) \succeq \|\overline{\boldsymbol{u}}\|_V^2 \qquad \text{and} \qquad \|\boldsymbol{\tau}\|_\Sigma \preceq \|\overline{\boldsymbol{u}}\|_V.$$

Combining above estimates we get

$$\begin{aligned} \sup_{(\boldsymbol{\tau}, p) \in X} \frac{|b_2(\boldsymbol{\tau}, \overline{\boldsymbol{u}}) + b_1(\overline{\boldsymbol{u}}, p)|}{\|(\boldsymbol{\tau}, p)\|_X} &\succeq \frac{|b_2(\boldsymbol{\tau}, \overline{\boldsymbol{u}}) + b_1(\overline{\boldsymbol{u}}, p)|}{\|(\boldsymbol{\tau}, p)\|_X} \\ &\succeq \frac{\|\overline{\boldsymbol{u}}\|_V^2 + \|\operatorname{div}(\overline{\boldsymbol{u}})\|^2}{\|\boldsymbol{\tau}\|_\Sigma + \|p\|_Q} \succeq \|\overline{\boldsymbol{u}}\|_V \qquad \forall \overline{\boldsymbol{u}} \in V, \end{aligned}$$

which concludes the proof.

Die approbierte gedruckte Originalversion dieser Diplomarbeit ist an der TU Wien Bibliothek verfügbar
The approved original version of this thesis is available in print at TU Wien Bibliothek.
TU Bibliothek Your knowledge hub WIEN

Die approbierte gedruckte Originalversion dieser Diplomarbeit ist an der TU Wien Bibliothek verfügbar
The approved original version of this thesis is available in print at TU Wien Bibliothek.
TU Bibliothek Your knowledge hub WIEN

4

Mixed Finite Elements

In this chapter we introduce some Finite Elements approximating the three derived variational formulations I-III. As solvability of the discrete setting is by no means inherited from the continuous inf-sup variational formulation, we give a short comment on that. Ultimately, we present a new finite element method approximating a similar variational formulation to III in combination with an extensive discrete stability analysis.

Framework

Consider the domain $\Omega \subset \mathbb{R}^d$ introduced in Chapter 3. We define $\mathcal{T}_h$ as the partition of Ω into non overlapping triangles or tetrahedrons with following properties:

1. $\mathcal{T}_h$ is shape regular

$$\max_{T\in\mathcal{T}_h} \frac{\operatorname{diam}(T)^d}{|T|} \leq c_1 \qquad\qquad c_1 > 0, \forall T \in \mathcal{T}_h,$$

2. $\mathcal{T}_h$ is quasi-uniform

$$\operatorname{diam}(T) \leq c_2 h \qquad\qquad c_2 > 0, \forall T \in \mathcal{T}_h.$$

The mesh size h is defined as

$$h := \max_{T\in\mathcal{T}_h} \operatorname{diam}(T).$$

An example for a 2- and 3-simplex with the corresponding outer normal unit vector $\boldsymbol{n}$ and tangential unit vector $\boldsymbol{t}$ is given in Figure 4.1. The set $\mathcal{F}_h$ contains all triangulation facets, where we can further distinguish between interior and exterior facets $\mathcal{F}_h^{int} \cup \mathcal{F}_h^{ext} = \mathcal{F}_h$. The jump of a quantity on a common facet $F \in \mathcal{F}_h$ is denoted by $[\![\cdot]\!]$.
Further, the space of scalar-valued polynomials on a given element $T \in \mathcal{T}_h$ up to order k is denoted by $\mathbb{P}^k(T, \mathbb{R})$. Respectively, the space of vector- and matrix-valued polynomial spaces is given by $\mathbb{P}^k(T, \mathbb{R}^d)$ and $\mathbb{P}^k(T, \mathbb{R}^{d\times d})$. On a given triangulation $\mathcal{T}_h$ we define the space of polynomials as

$$\begin{aligned}
\mathbb{P}^k(\mathcal{T}_h, \mathbb{R}) &:= \prod_{T\in\mathcal{T}_h} \mathbb{P}^k(T, \mathbb{R}),\\
\mathbb{P}^k(\mathcal{T}_h, \mathbb{R}^d) &:= \prod_{T\in\mathcal{T}_h} \mathbb{P}^k(T, \mathbb{R}^d),\\
\mathbb{P}^k(\mathcal{T}_h, \mathbb{R}^{d\times d}) &:= \prod_{T\in\mathcal{T}_h} \mathbb{P}^k(T, \mathbb{R}^{d\times d}).
\end{aligned}$$

Die approbierte gedruckte Originalversion dieser Diplomarbeit ist an der TU Wien Bibliothek verfügbar
The approved original version of this thesis is available in print at TU Wien Bibliothek.
TU Bibliothek Your knowledge hub WIEN

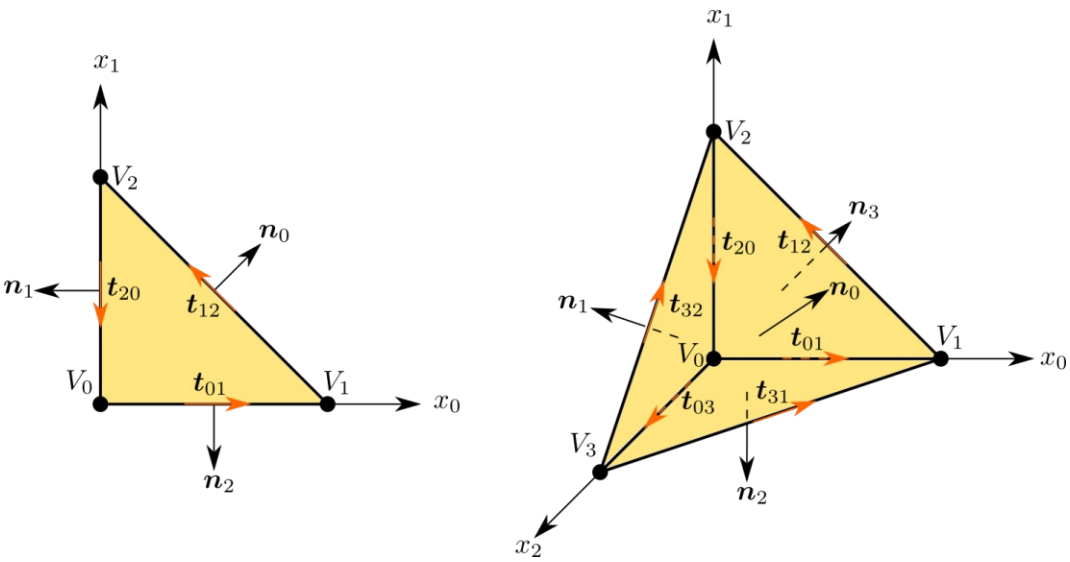

FIGURE 4.1 – Triangle and Tetrahedron with normal $\boldsymbol{n}$ and tangential vectors $\boldsymbol{t}$

Ultimately, we introduce the symmetric, skew-symmetric and trace-free matrix-valued polynomial spaces

$$\begin{aligned}
\mathbb{P}^k_{\mathrm{sym}}(\mathcal{T}_h, \mathbb{R}^{d\times d}) &:= \left\{\boldsymbol{\psi} \in \mathbb{P}^k(\mathcal{T}_h, \mathbb{R}^{d\times d}) : \boldsymbol{\psi}|_T = \boldsymbol{\psi}^{\mathrm{T}}|_T \ \forall T \in \mathcal{T}_h\right\},\\
\mathbb{P}^k_{\mathrm{skw}}(\mathcal{T}_h, \mathbb{R}^{d\times d}) &:= \left\{\boldsymbol{\psi} \in \mathbb{P}^k(\mathcal{T}_h, \mathbb{R}^{d\times d}) : \boldsymbol{\psi}|_T = -\boldsymbol{\psi}^{\mathrm{T}}|_T, (\boldsymbol{\psi}|_T)_{ii} = 0 \ \forall T \in \mathcal{T}_h\right\},\\
\mathbb{P}^k_{\mathrm{tr}}(\mathcal{T}_h, \mathbb{R}^{d\times d}) &:= \left\{\boldsymbol{\psi} \in \mathbb{P}^k(\mathcal{T}_h, \mathbb{R}^{d\times d}) : \mathrm{tr}(\boldsymbol{\psi}|_T) = 0 \ \forall T \in \mathcal{T}_h\right\},\\
\mathbb{P}^k_{\mathrm{sym,tr}}(\mathcal{T}_h, \mathbb{R}^{d\times d}) &:= \left\{\boldsymbol{\psi} \in \mathbb{P}^k(\mathcal{T}_h, \mathbb{R}^{d\times d}) : \boldsymbol{\psi}|_T = \boldsymbol{\psi}^{\mathrm{T}}|_T, \mathrm{tr}(\boldsymbol{\psi}|_T) = 0 \ \forall T \in \mathcal{T}_h\right\}.
\end{aligned}$$

4.1 Velocity-pressure approximation

We aim to approximate variational formulation I in means of a finite element method. By introducing a finite-dimensional subspaces $V_h \subset V := H^1_0(\Omega, \mathbb{R}^d)$ and $Q_h \subset Q := L^2_0(\Omega, \mathbb{R})$ we formulate the following discrete problem

Discrete Variational Formulation IV
Find $(\boldsymbol{u}_h, p_h) \in V_h \times Q_h$ such that

$$\begin{aligned}
a(\boldsymbol{u}_h, \overline{\boldsymbol{u}}_h) + b_1(\overline{\boldsymbol{u}}_h, p_h) &= f(\overline{\boldsymbol{u}}_h) && \forall \overline{\boldsymbol{u}}_h \in V_h,\\
b_1(\boldsymbol{u}_h, \overline{p}_h) &= 0 && \forall \overline{p}_h \in Q_h.
\end{aligned}$$

Recall that the bilinear forms and linear form are defined as in (3.5)-(3.7)

$$\begin{aligned}
a(\boldsymbol{u}_h, \overline{\boldsymbol{u}}_h) &:= 2\mu \int_\Omega \boldsymbol{\varepsilon}(\boldsymbol{u}_h) : \boldsymbol{\varepsilon}(\overline{\boldsymbol{u}}_h)\, dx,\\
b_1(\boldsymbol{u}_h, \overline{p}_h) &:= -\int_\Omega \mathrm{div}(\boldsymbol{u}_h)\overline{p}_h\, dx,\\
f(\overline{\boldsymbol{u}}_h) &:= \int_\Omega \rho \boldsymbol{f} \cdot \overline{\boldsymbol{u}}_h\, dx.
\end{aligned}$$

.

Die approbierte gedruckte Originalversion dieser Diplomarbeit ist an der TU Wien Bibliothek verfügbar
The approved original version of this thesis is available in print at TU Wien Bibliothek.

In literature [AMS+04, BBF13] many stable (i.e. the conditions of *Brezzi's* Theorem 1 are fulfilled) velocity-pressure finite elements solving the discrete problem IV can be found. For the sake of simplicity we will only introduce two of them.

4.1.1 Generalized Taylor-Hood element ($\mathcal{TH}$)

The well-known *Taylor-Hood* element[TH73] approximates both velocity $\boldsymbol{u}$ and pressure p in a continuous matter. Respectively, the discrete spaces are given by

$$V_h := \left\{ \boldsymbol{u}_h \in H_0^1(\Omega, \mathbb{R}^d) : \boldsymbol{u}_h|_T \in \mathbb{P}^k(T, \mathbb{R}^d) \ \forall T \in \mathcal{T}_h \right\},$$
$$Q_h := \left\{ p_h \in L_0^2(\Omega, \mathbb{R}) \cap \mathcal{C}^0(\Omega, \mathbb{R}) : p_h|_T \in \mathbb{P}^{k-1}(T, \mathbb{R}) \ \forall T \in \mathcal{T}_h \right\}.$$

An example of this mixed element is given for a polynomial order $k = 2$ in Figure 4.3.

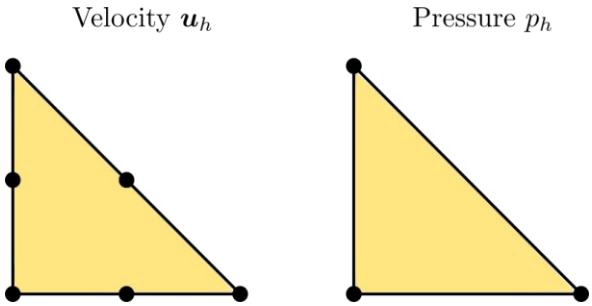

FIGURE 4.2 – 2-simplex *Taylor-Hood* element ($\mathcal{TH}$) of polynomial order $k = 2$

Discrete stability analysis

A proof of the discrete LBB condition can be found in many textbooks. In [AMS+04, Section 4.2.5] the authors present a proof for tetrahedrons of order $k = 2$, while in [BBF13, Section 8.8.2] the authors provide a proof for a 2D triangulation for any polynomial order $k > 2$.

4.1.2 Exactly divergence-free property

As discussed in Chapter 2 the incompressibility constraint reads as $\operatorname{div}(\boldsymbol{u}) = 0$. Unfortunately, in general at the discrete level the velocity $\boldsymbol{u}_h$ is approximated weakly divergence-free, since

$$\int_\Omega \operatorname{div}(\boldsymbol{u}_h)\overline{p}_h \, dx = 0 \qquad \forall \overline{p}_h \in Q_h,$$

does not imply $\operatorname{div}(\boldsymbol{u}_h) = 0$.
One way to obtain exactly divergence-free elements is to choose the discrete spaces such that $\operatorname{div}(V_h) \subset Q_h$, then by choosing $\overline{p}_h := \operatorname{div}(\boldsymbol{u}_h)$ [BBF13, Section 8.9.1] we get

$$\int_\Omega \operatorname{div}(\boldsymbol{u}_h)\overline{p}_h \, dx = \int_\Omega \operatorname{div}(\boldsymbol{u}_h)\operatorname{div}(\boldsymbol{u}_h) \, dx = 0 \qquad \Rightarrow \qquad \operatorname{div}(\boldsymbol{u}_h) = 0.$$

The above introduced *Taylor-Hood* element 4.1.1 is not exactly divergence-free and therefore not exactly mass conserving. An element that possesses this quality is introduced in the next subsection.

Die approbierte gedruckte Originalversion dieser Diplomarbeit ist an der TU Wien Bibliothek verfügbar
The approved original version of this thesis is available in print at TU Wien Bibliothek.
TU Bibliothek Your knowledge hub WIEN

4.1.3 Scott-Vogelius element ($\mathcal{SV}$)

As previously discussed a possibility to force conservation of mass on a discrete level is to choose the discrete spaces such that $\operatorname{div}(V_h) \subset Q_h$. Therefore the selection of spaces

$$V_h := \left\{ \boldsymbol{u}_h \in H_0^1(\Omega, \mathbb{R}^d) : \boldsymbol{u}_h|_T \in \mathbb{P}^k(T, \mathbb{R}^d) \; \forall T \in \mathcal{T}_h \right\},$$
$$Q_h := \left\{ p_h \in L_0^2(\Omega, \mathbb{R}) : p_h|_T \in \mathbb{P}^{k-1}(T, \mathbb{R}) \; \forall T \in \mathcal{T}_h \right\}.$$

leads to the so called *Scott-Vogelius* element [SV85]. Unfortunately, this choice is only stable on barycentric refined triangulations.

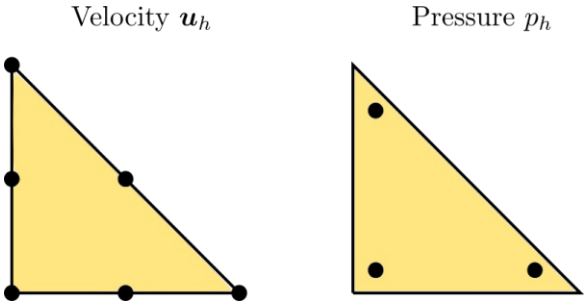

FIGURE 4.3 – 2-simplex *Scott-Vogelius* element ($\mathcal{SV}$) of polynomial order $k = 2$

The discrete inf-sup stability of this element is provided in [SV85, BBF13].

4.2 Mixed stress approximation

As in the previous section we aim to approximate variational formulation II by suitable finite elements. The discrete problem reads as

Discrete Variational Formulation V
Find $((\boldsymbol{\tau}_h, p_h), \boldsymbol{u}_h) \in X_h \times V_h$ such that

$$\begin{aligned} a(\boldsymbol{\tau}_h, \overline{\boldsymbol{\tau}}_h) + b_2(\overline{\boldsymbol{\tau}}_h, \boldsymbol{u}_h) &= 0 && \forall \overline{\boldsymbol{\tau}}_h \in \Sigma_h, \\ b_2(\boldsymbol{\tau}_h, \overline{\boldsymbol{u}}_h) + b_1(\overline{\boldsymbol{u}}_h, p_h) &= f(\overline{\boldsymbol{u}}_h) && \forall \overline{\boldsymbol{u}}_h \in V_h, \\ b_1(\boldsymbol{u}_h, \overline{p}_h) &= 0 && \forall \overline{p}_h \in Q_h. \end{aligned}$$

with bilinear forms and linear form (3.11)-(3.14).

$$\begin{aligned} a(\boldsymbol{\tau}_h, \overline{\boldsymbol{\tau}}_h) &:= -\frac{1}{2\mu} \int_\Omega \boldsymbol{\tau}_h : \overline{\boldsymbol{\tau}}_h \, dx, \\ b_1(\boldsymbol{u}_h, \overline{p}_h) &:= -\int_\Omega \operatorname{div}(\boldsymbol{u}_h) \overline{p}_h \, dx, \\ b_2(\boldsymbol{\tau}_h, \overline{\boldsymbol{u}}_h) &:= \int_\Omega \boldsymbol{\tau}_h : \boldsymbol{\varepsilon}(\overline{\boldsymbol{u}}_h) \, dx, \\ f(\overline{\boldsymbol{u}}_h) &:= \int_\Omega \rho \boldsymbol{f} \cdot \overline{\boldsymbol{u}}_h \, dx. \end{aligned}$$

Accordingly, we introduced the conforming finite-dimensional subspaces $\Sigma_h \subset \Sigma := L^2_{\mathrm{sym}}(\Omega, \mathbb{R}^{d\times d})$, $Q_h \subset Q := L_0^2(\Omega, \mathbb{R})$ and $V_h \subset V := H_0^1(\Omega, \mathbb{R}^d)$.

Die approbierte gedruckte Originalversion dieser Diplomarbeit ist an der TU Wien Bibliothek verfügbar
The approved original version of this thesis is available in print at TU Wien Bibliothek.
TU Bibliothek Your knowledge hub WIEN

4.2.1 Generalized Taylor-Hood + stress element ($\mathcal{TH}$-$\mathcal{S}$)

Let us recall the discrete spaces introduced in 4.1.1 and add the space of piecewise discontinuous symmetric matrix-valued polynomials

$$V_h := \left\{ \boldsymbol{u}_h \in H_0^1(\Omega, \mathbb{R}^d) : \boldsymbol{u}_h|_T \in \mathbb{P}^k(T, \mathbb{R}^d) \ \forall T \in \mathcal{T}_h \right\},$$
$$Q_h := \left\{ p_h \in L_0^2(\Omega, \mathbb{R}) \cap \mathcal{C}^0(\Omega, \mathbb{R}) : p_h|_T \in \mathbb{P}^{k-1}(T, \mathbb{R}) \ \forall T \in \mathcal{T}_h \right\},$$
$$\Sigma_h := \left\{ \boldsymbol{\tau}_h \in L_{\mathrm{sym}}^2(\Omega, \mathbb{R}^{d\times d}) : \boldsymbol{\tau}_h|_T \in \mathbb{P}_{\mathrm{sym}}^{k-1}(T, \mathbb{R}^{d\times d}) \ \forall T \in \mathcal{T}_h \right\}.$$

An illustration of the degrees of freedom of mixed finite element is shown for a polynomial order $k = 2$ in Figure 4.4.

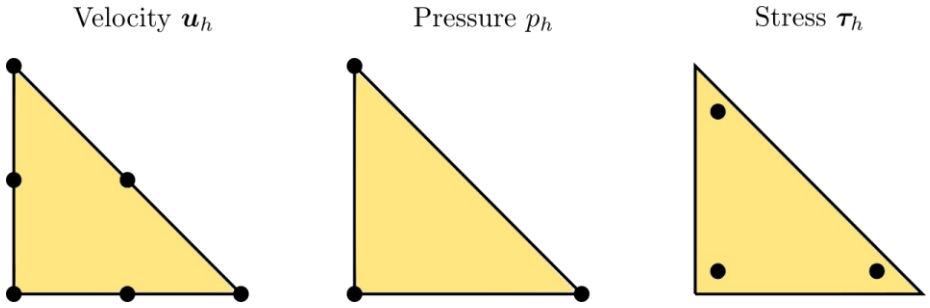

FIGURE 4.4 – 2-simplex *Taylor-Hood* element augmented with a piecewise discontinuous approximation for the stresses ($\mathcal{TH}$-$\mathcal{S}$) of polynomial order $k = 2$

Discrete stability analysis

The stability of above mixed finite element follows similar to the continuous setting and from the inf-sup condition of the *Taylor-Hood* element. Continuity of the bilinear forms is inherited from the continuous setting.

Lemma 7. *On the kernel $X_{h,0}$ bilinear form $a(\boldsymbol{\tau}, \overline{\boldsymbol{\tau}})$ is elliptic*

$$a(\boldsymbol{\tau}_h, \boldsymbol{\tau}_h) \succeq \|\boldsymbol{\tau}_h\|_\Sigma^2 + \|p_h\|_Q^2 \qquad \forall (\boldsymbol{\tau}_h, p_h) \in X_{h,0}.$$

Proof: The discrete kernel is defined as

$$X_{h,0} := \{(\boldsymbol{\tau}_h, p_h) \in X_h : b_2(\boldsymbol{\tau}_h, \overline{\boldsymbol{u}}_h) + b_1(\overline{\boldsymbol{u}}_h, p_h) = 0 \quad \forall \overline{\boldsymbol{u}}_h \in V_h\}.$$

From the discrete LBB condition of the *Taylor-Hood* element 4.1.1 it follows

$$\|p_h\|_Q \preceq \sup_{\overline{\boldsymbol{u}}_h \in V_h} \frac{|\int_\Omega \operatorname{div}(\overline{\boldsymbol{u}}_h) p_h \, dx|}{\|\overline{\boldsymbol{u}}_h\|_V} = \sup_{\overline{\boldsymbol{u}}_h \in V_h} \frac{|\int_\Omega \boldsymbol{\tau}_h : \boldsymbol{\varepsilon}(\overline{\boldsymbol{u}}_h) \, dx|}{\|\overline{\boldsymbol{u}}_h\|_V}.$$

By applying *Cauchy-Schwarz* and *Korn's* inequality the next estimate is derived

$$\|p_h\|_Q \preceq \sup_{\overline{\boldsymbol{u}}_h \in V_h} \frac{\|\boldsymbol{\tau}_h\|_\Sigma \|\boldsymbol{\varepsilon}(\overline{\boldsymbol{u}}_h)\|}{\|\overline{\boldsymbol{u}}_h\|_V} \preceq \|\boldsymbol{\tau}_h\|_\Sigma.$$

The discrete kernel ellipticity is then straightforward

$$a(\boldsymbol{\tau}_h, \boldsymbol{\tau}_h) = \frac{1}{2\mu}\|\boldsymbol{\tau}_h\|_\Sigma^2 \succeq \frac{1}{4\mu}\|\boldsymbol{\tau}_h\|_\Sigma^2 + \frac{1}{4\mu}\|p_h\|_Q^2 \succeq \frac{1}{\mu}\|(\boldsymbol{\tau}_h, p_h)\|_X^2 \qquad \forall (\boldsymbol{\tau}_h, p_h) \in X_{h,0}.$$

Die approbierte gedruckte Originalversion dieser Diplomarbeit ist an der TU Wien Bibliothek verfügbar
The approved original version of this thesis is available in print at TU Wien Bibliothek.
TU Bibliothek Your knowledge hub WIEN

Lemma 8. *The discrete LBB condition is fulfilled*

$$\sup_{(\boldsymbol{\tau}_h,p_h)\in X_h} \frac{|b_2(\boldsymbol{\tau}_h,\overline{\boldsymbol{u}}_h)+b_1(\overline{\boldsymbol{u}}_h,p_h)|}{\|(\boldsymbol{\tau}_h,p_h)\|_X} \succeq \|\overline{\boldsymbol{u}}_h\|_V \qquad \forall \overline{\boldsymbol{u}}_h \in V_h.$$

Proof: The proof follows similar arguments as in the continuous setting. Choose $\boldsymbol{\tau}_h := \boldsymbol{\varepsilon}(\overline{\boldsymbol{u}}_h)$ and $p_h := 0$ with the upper bound $\|\boldsymbol{\tau}_h\|_\Sigma \leq \|\boldsymbol{\varepsilon}(\overline{\boldsymbol{u}}_h)\|$. Then there holds

$$\begin{aligned}\sup_{(\boldsymbol{\tau}_h,p_h)\in X_h} \frac{|b_2(\boldsymbol{\tau}_h,\overline{\boldsymbol{u}}_h)+b_1(\overline{\boldsymbol{u}}_h,p_h)|}{\|(\boldsymbol{\tau}_h,p_h)\|_X} &\geq \frac{|b_2(\boldsymbol{\tau}_h,\overline{\boldsymbol{u}}_h)+b_1(\overline{\boldsymbol{u}}_h,p_h)|}{\|(\boldsymbol{\tau}_h,p_h)\|_X} \\ &\geq \frac{\|\boldsymbol{\varepsilon}(\overline{\boldsymbol{u}}_h)\|^2}{\|\boldsymbol{\varepsilon}(\overline{\boldsymbol{u}}_h)\|} \\ &\overset{(3)}{\succeq} \|\overline{\boldsymbol{u}}_h\|_V \qquad \forall \overline{\boldsymbol{u}}_h \in V_h.\end{aligned}$$

4.2.2 Scott-Vogelius + stress element ($\mathcal{SV}$-$\mathcal{S}$)

In a similar matter as in the previous Subsection 4.2.1 we can add the space of piecewise discontinuous symmetric matrix-valued polynomials to the *Scott-Vogelius* element. In this particular case, we can further impose on the discrete stress tensor $\boldsymbol{\tau}_h$ to be trace-free, as the discrete velocity u_h is pointwise divergence-free and therefore it holds $\mathrm{tr}(\boldsymbol{\varepsilon}(\boldsymbol{u}_h)) = 0$. The discrete spaces are then

$$\begin{aligned}V_h &:= \left\{\boldsymbol{u}_h \in H^1_0(\Omega,\mathbb{R}^d) : \boldsymbol{u}_h|_T \in \mathbb{P}^k(T,\mathbb{R}^d)\ \forall T \in \mathcal{T}_h\right\}, \\ Q_h &:= \left\{p_h \in L^2_0(\Omega,\mathbb{R}) : p_h|_T \in \mathbb{P}^{k-1}(T,\mathbb{R})\ \forall T \in \mathcal{T}_h\right\}, \\ \Sigma_h &:= \left\{\boldsymbol{\tau}_h \in L^2_{\mathrm{sym,tr}}(\Omega,\mathbb{R}^{d\times d}) : \boldsymbol{\tau}_h|_T \in \mathbb{P}^{k-1}_{\mathrm{sym,tr}}(T,\mathbb{R}^{d\times d})\ \forall T \in \mathcal{T}_h\right\}\end{aligned}$$

Again, we point out that this mixed element is only stable on barycentric refined triangulations.

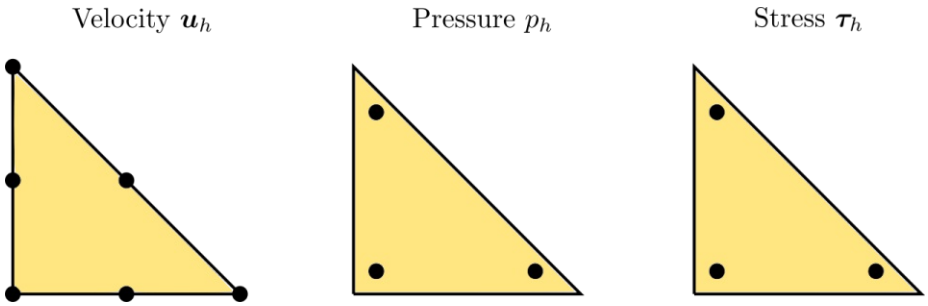

FIGURE 4.5 – 2-simplex *Scott-Vogelius* element augmented with a piecewise discontinuous approximation for the stresses ($\mathcal{SV}$-$\mathcal{S}$) of polynomial order $k = 2$

Discrete stability analysis

The discrete stability of the $\mathcal{SV}$-$\mathcal{S}$element follows in the same way as the $\mathcal{TH}$-$\mathcal{S}$element.

Die approbierte gedruckte Originalversion dieser Diplomarbeit ist an der TU Wien Bibliothek verfügbar
The approved original version of this thesis is available in print at TU Wien Bibliothek.
TU Bibliothek Your knowledge hub WIEN

4.3 Mass conserving mixed stress approximation

Recall variational formulation III and the corresponding spaces $\boldsymbol{u} \in V := H(\operatorname{div}, \Omega)$, $p \in Q := L^2_0(\Omega, \mathbb{R})$ and $\boldsymbol{\tau} \in \Sigma_{\text{sym}} := \left\{\boldsymbol{\psi} \in H(\operatorname{curl}\operatorname{div}, \Omega) : \operatorname{tr}(\boldsymbol{\psi}) = 0, \boldsymbol{\psi} = \boldsymbol{\psi}^{\mathrm{T}}\right\}$. With the conforming finite-dimensional subspaces $V_h \subset V$, $Q_h \subset Q$ and $\Sigma_h \subset \Sigma$ the discrete problem reads as

Discrete Variational Formulation VI
Find $((\boldsymbol{\tau}_h, p_h), \boldsymbol{u}_h) \in X_h \times V_h$ such that

$$\begin{aligned} a(\boldsymbol{\tau}_h, \overline{\boldsymbol{\tau}}_h) + b_2(\overline{\boldsymbol{\tau}}_h, \boldsymbol{u}_h) &= 0 && \forall \overline{\boldsymbol{\tau}}_h \in \Sigma_h, \\ b_2(\boldsymbol{\tau}_h, \overline{\boldsymbol{u}}_h) + b_1(\overline{\boldsymbol{u}}_h, p_h) &= -f(\overline{\boldsymbol{u}}_h) && \forall \overline{\boldsymbol{u}}_h \in V_h, \\ b_1(\boldsymbol{u}_h, \overline{p}_h) &= 0 && \forall \overline{p}_h \in Q_h. \end{aligned}$$

Respectively, the bilinear forms and linear form (3.17)-(3.20)

$$\begin{aligned} a(\boldsymbol{\tau}_h, \overline{\boldsymbol{\tau}}_h) &:= \frac{1}{2\mu} \int_\Omega \boldsymbol{\tau}_h : \overline{\boldsymbol{\tau}}_h \, dx, \\ b_1(\boldsymbol{u}_h, \overline{p}_h) &:= \int_\Omega \operatorname{div}(\boldsymbol{u}_h) \overline{p}_h \, dx, \\ b_2(\boldsymbol{\tau}_h, \overline{\boldsymbol{u}}_h) &:= \langle \operatorname{div}(\boldsymbol{\tau}_h), \overline{\boldsymbol{u}}_h \rangle, \\ f(\overline{\boldsymbol{u}}_h) &:= -\int_\Omega \rho \boldsymbol{f} \cdot \overline{\boldsymbol{u}}_h \, dx. \end{aligned}$$

Conformity in $\boldsymbol{\psi} \in H(\operatorname{curl}\operatorname{div}, \Omega)$-space is given by the continuity of the normal-tangential component $\boldsymbol{\psi}_{nt}$ and the requirement for the normal-normal component $\psi_{nn} \in H^{1/2}(\partial T)$, the former being a sufficient condition [GLS19].

4.3.1 Mass conserving mixed stress element ($\mathcal{MCS}$)

In [GLS19] the authors introduced a new finite element $\mathcal{MCS}$, which approximates the space $H(\operatorname{curl}\operatorname{div}, \Omega)$, but it is slightly non-conforming $\Sigma_h \not\subset \Sigma_{\text{sym}}$ as the normal-normal component ψ_{nn} continuity at vertices in two and edges in three dimensions is too restrictive. Nevertheless, the continuity of the discrete normal-tangential ψ_{nt} component is granted.

$$\Sigma_h^{k-1} := \left\{\boldsymbol{\tau}_h \in \mathbb{P}^{k-1}(\mathcal{T}_h, \mathbb{R}^{d\times d}) : \operatorname{tr}(\boldsymbol{\tau}_h|_T) = 0 \; \forall T \in \mathcal{T}_h, [\![(\boldsymbol{\tau}_h)_{nt}]\!] = 0 \; \forall F \in \mathcal{F}_h^{\text{int}}\right\}.$$

On the other hand, Σ_h is in general not symmetric. To circumvent this, in [GLS20] the authors applied *Stenberg*'s concept [Ste15] of weak-symmetry by introducing an additional space of skew-symmetric matrices $W_h \subset W := L^2_{\text{skw}}(\Omega, \mathbb{R}^{d\times d})$ and by enriching the discrete stress space Σ_h with interior $\mathbb{P}^k$-bubbles given by

$$\mathcal{B}_h^k := \left\{\boldsymbol{\tau}_h \in \Sigma_h^k : (\boldsymbol{\tau}_h)_{nt} = 0\right\}. \tag{4.1}$$

This technique enforces the L^2-orthogonality of the skew-symmetric $\mathbb{P}^{k-1}$ part of $\boldsymbol{\tau}_h \in \Sigma_h$. Ultimately, we define the discrete space augmented with this interior bubbles as

$$\Sigma_h^{\oplus} := \left\{\boldsymbol{\tau}_h \in \Sigma_h^k : (\boldsymbol{\tau}_h)_{nt} \in \mathbb{P}^{k-1}(F, \mathbb{R}^{d-1}) \; \forall F \in \mathcal{F}_h^{\text{int}}\right\}.$$

Die approbierte gedruckte Originalversion dieser Diplomarbeit ist an der TU Wien Bibliothek verfügbar
The approved original version of this thesis is available in print at TU Wien Bibliothek.
TU Bibliothek Your knowledge hub WIEN

With the decomposition of the rate-of-strain tensor $\boldsymbol{\varepsilon}(\boldsymbol{u})$ in its asymmetric part $\nabla \boldsymbol{u}$ and the skew-symmetric rate-of-rotation tensor $\boldsymbol{\omega}$

$$\boldsymbol{\varepsilon}(\boldsymbol{u}_h) = \nabla \boldsymbol{u}_h - \frac{1}{2}\left(\nabla \boldsymbol{u}_h - (\nabla \boldsymbol{u}_h)^T\right) = \nabla \boldsymbol{u}_h - \boldsymbol{\omega}_h,$$

we define the new discrete variational formulation

Discrete Variational Formulation VII
Find $((\boldsymbol{\tau}_h, p_h), (\boldsymbol{u}_h, \boldsymbol{\omega}_h)) \in X_h \times U_h$ such that

$$\begin{aligned} a(\boldsymbol{\tau}_h, \overline{\boldsymbol{\tau}}_h) + b_{2h}(\overline{\boldsymbol{\tau}}_h, (\boldsymbol{u}_h, \boldsymbol{\omega}_h)) &= 0 && \forall \overline{\boldsymbol{\tau}}_h \in \Sigma_h^{\oplus}, \\ b_{2h}(\boldsymbol{\tau}_h, (\overline{\boldsymbol{u}}_h, \overline{\boldsymbol{\omega}}_h)) + b_1(\overline{\boldsymbol{u}}_h, p_h) &= f(\overline{\boldsymbol{u}}_h) && \forall (\overline{\boldsymbol{u}}_h, \overline{\boldsymbol{\omega}}_h) \in U_h, \\ b_1(\boldsymbol{u}_h, \overline{p}_h) &= 0 && \forall \overline{p}_h \in Q_h, \end{aligned}$$

where $X_h := \Sigma_h^{\oplus} \times Q_h$ and $U_h := V_h \times W_h$.
The bilinear forms and linear form in VII correspond to the ones of the discrete problem VI, except for the discrete bilinearform $b_{2h}(\boldsymbol{\tau}_h, (\overline{\boldsymbol{u}}_h, \overline{\boldsymbol{\omega}}))$

$$b_{2h}(\boldsymbol{\tau}_h, (\overline{\boldsymbol{u}}_h, \overline{\boldsymbol{\omega}}_h)) := \sum_{T \in \mathcal{T}_h} \int_T \operatorname{div}(\boldsymbol{\tau}_h) \cdot \overline{\boldsymbol{u}}_h \, dx + \sum_{T \in \mathcal{T}_h} \int_T \boldsymbol{\tau}_h : \overline{\boldsymbol{\omega}}_h \, dx - \sum_{F \in \mathcal{F}_h} \int_F [\![(\boldsymbol{\tau}_h)_{nn}]\!](\overline{\boldsymbol{u}}_h)_n \, ds.$$

With integration by parts respectively

$$b_{2h}(\boldsymbol{\tau}_h, (\overline{\boldsymbol{u}}_h, \overline{\boldsymbol{\omega}}_h)) := -\sum_{T \in \mathcal{T}_h} \int_T \boldsymbol{\tau}_h : (\nabla \overline{\boldsymbol{u}}_h - \overline{\boldsymbol{\omega}}_h) \, dx + \sum_{F \in \mathcal{F}_h} \int_F (\boldsymbol{\tau}_h)_{nt} [\![(\overline{\boldsymbol{u}}_h)_t]\!] \, ds.$$

This choice is inspired by the definition of the distributional divergence [GLS20, Eq. 11].
Eventually, we can define the remaining discrete spaces

$$\begin{aligned} V_h &:= \left\{ \boldsymbol{u}_h \in H(\operatorname{div}, \Omega) : \boldsymbol{u}_h|_T \in \mathbb{P}^k(T, \mathbb{R}^d) \ \forall T \in \mathcal{T}_h, [\![(\boldsymbol{u}_h)_n]\!] = 0 \ \forall F \in \mathcal{F}_h^{\text{int}} \right\}, \\ Q_h &:= \left\{ p_h \in L_0^2(\Omega, \mathbb{R}) : p_h|_T \in \mathbb{P}^{k-1}(T, \mathbb{R}) \ \forall T \in \mathcal{T}_h \right\}, \\ W_h &:= \left\{ \boldsymbol{\omega}_h \in L_{\text{skw}}^2(\Omega, \mathbb{R}^{d \times d}) : \boldsymbol{\omega}_h|_T \in \mathbb{P}_{\text{skw}}^{k-1}(T, \mathbb{R}^{d \times d}) \ \forall T \in \mathcal{T}_h \right\}. \end{aligned}$$

An example of the mass conserving mixed stress finite element of polynomial order $k = 2$ can be seen in Figure 4.6.

The introduced discrete space V_h for the velocity is also known as the *Brezzi-Douglas-Marini* ($\mathcal{BDM}$) space and it contains all polynomials of degree k in contrast to the alternative *Raviart-Thomas* space [BBF13, Section 2.3]. Additionally, we see that by construction $\operatorname{div}(V_h) \subset Q_h$ holds, therefore this mixed finite element is exactly mass preserving as was pointed out in Subsection 4.1.2.

Die approbierte gedruckte Originalversion dieser Diplomarbeit ist an der TU Wien Bibliothek verfügbar
The approved original version of this thesis is available in print at TU Wien Bibliothek.
TU Bibliothek Your knowledge hub WIEN

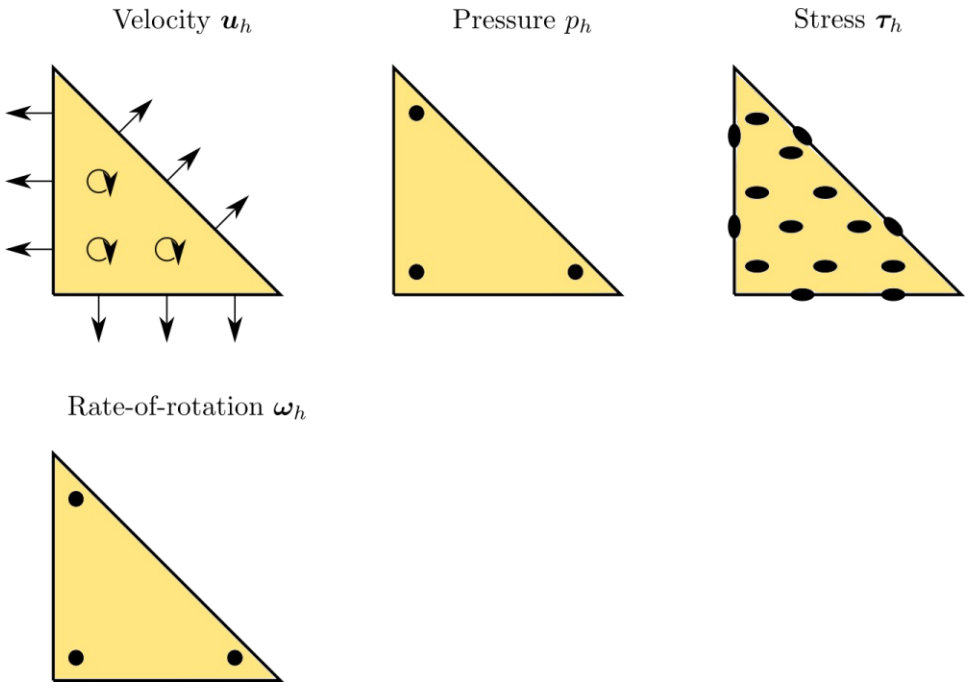

FIGURE 4.6 – 2-simplex mass conserving mixed stress element ($\mathcal{MCS}$) of polynomial order $k = 2$

Discrete stability analysis

To proof solvability of the discrete problem VII we follow the proof presented in [GLS19, GLS20]. Following norms are needed

$$\|(\boldsymbol{u}_h, \boldsymbol{\omega}_h)\|^2_{U_h} := \sum_{T\in\mathcal{T}_h} \|\boldsymbol{\varepsilon}(\boldsymbol{u}_h)\|^2_T + \sum_{T\in\mathcal{T}_h} \|\boldsymbol{\omega}(\boldsymbol{u}_h) - \boldsymbol{\omega}_h\|^2_T + \sum_{F\in\mathcal{F}_h} \frac{1}{h}\|[\![(\boldsymbol{u}_h)_t]\!]\|^2_F,$$

$$\|(\boldsymbol{u}_h, \boldsymbol{\omega}_h)\|^2_{U_h,\Pi} := \sum_{T\in\mathcal{T}_h} \|\boldsymbol{\varepsilon}(\boldsymbol{u}_h)\|^2_T + \sum_{T\in\mathcal{T}_h} \|\boldsymbol{\omega}(\boldsymbol{u}_h) - \boldsymbol{\omega}_h\|^2_T + \sum_{F\in\mathcal{F}_h} \frac{1}{h}\|\Pi^1_F[\![(\boldsymbol{u}_h)_t]\!]\|^2_F,$$

$$\|(\boldsymbol{u}_h, \boldsymbol{\omega}_h)\|^2_{U_h,*} := \sum_{T\in\mathcal{T}_h} \|\mathrm{dev}(\nabla\boldsymbol{u}_h) - \boldsymbol{\omega}_h\|^2_T + \sum_{F\in\mathcal{F}_h} \frac{1}{h}\|\Pi^1_F[\![(\boldsymbol{u}_h)_t]\!]\|^2_F,$$

$$\|(\boldsymbol{\tau}_h, p_h)\|^2_{X_h} = \left(\|\boldsymbol{\tau}_h\| + \|p_h\|\right)^2,$$

where $\boldsymbol{\varepsilon}(\boldsymbol{u}_h)$ and $\boldsymbol{\omega}(\boldsymbol{u}_h)$ have been defined in (3.3) and (3.4) and $\Pi^1_F\overline{\boldsymbol{u}}_h \in \mathbb{P}^1(F, \boldsymbol{t}_f)$ denotes a tangential projection $\boldsymbol{t}_f \perp \boldsymbol{n}_F$ on a facet $F \in \mathcal{F}_h$, such that $(\Pi^1_F\overline{\boldsymbol{u}}_h, r) = (\overline{\boldsymbol{u}}_h, r)\ \forall r \in \mathbb{P}^1(F, \boldsymbol{t}_F)$. Further, we need the norm equivalences derived in [GLS20]

$$\|\boldsymbol{\tau}_h\|^2_{L^2} \overset{[Eq.\ 26]}{\sim} \sum_{T\in\mathcal{T}_h} \|\boldsymbol{\tau}_h\|^2_T + \sum_{F\in\mathcal{F}_h} h\|[\![(\boldsymbol{\tau}_h)_{nn}]\!]\|^2_F \qquad \forall\boldsymbol{\tau}_h \in \Sigma^{\oplus}_h, \tag{4.2}$$

$$\|(\boldsymbol{u}_h, \boldsymbol{\omega}_h)\|^2_{U_h} \overset{[Lemma\ 9]}{\sim} \|(\boldsymbol{u}_h, \boldsymbol{\omega}_h)\|^2_{U_h,\Pi} \qquad \forall(\boldsymbol{u}_h, \boldsymbol{\omega}_h) \in U_h. \tag{4.3}$$

Die approbierte gedruckte Originalversion dieser Diplomarbeit ist an der TU Wien Bibliothek verfügbar
The approved original version of this thesis is available in print at TU Wien Bibliothek.
TU Bibliothek Your knowledge hub WIEN

Lemma 9. *Bilinear forms $a(\boldsymbol{\tau}_h, \overline{\boldsymbol{\tau}}_h)$, $b_1(\boldsymbol{u}_h, \overline{p}_h)$ and $b_{2h}(\boldsymbol{\tau}_h, (\overline{\boldsymbol{u}}_h, \overline{\boldsymbol{\omega}}_h))$ are continuous [GLS20, Lemma 22].*

$$\begin{aligned} a(\boldsymbol{\tau}_h, \overline{\boldsymbol{\tau}}_h) &\preceq \|\boldsymbol{\tau}_h\|\|\overline{\boldsymbol{\tau}}_h\| && \forall \boldsymbol{\tau}_h, \overline{\boldsymbol{\tau}}_h \in \Sigma_h^{\oplus}, \\ b_1(\boldsymbol{u}_h, \overline{p}_h) &\preceq \|(\boldsymbol{u}_h, 0)\|_{U_h}\|p_h\| && \forall \boldsymbol{u}_h \in V_h, \overline{p}_h \in Q_h, \\ b_{2h}(\boldsymbol{\tau}_h, (\overline{\boldsymbol{u}}_h, \overline{\boldsymbol{\omega}}_h)) &\preceq \|\boldsymbol{\tau}_h\|\|(\overline{\boldsymbol{u}}_h, \overline{\boldsymbol{\omega}}_h)\|_{U_h} && \forall \boldsymbol{\tau}_h \in \Sigma_h^{\oplus}, (\overline{\boldsymbol{u}}_h, \overline{\boldsymbol{\omega}}_h) \in U_h. \end{aligned}$$

Proof: Continuity of bilinear form $a(\boldsymbol{\tau}_h, \overline{\boldsymbol{\tau}}_h)$ and $b_1(\boldsymbol{u}_h, \overline{p}_h)$ is inherited from the continuous setting (3.21), whereas for the discrete bilinear form $b_{2h}(\boldsymbol{\tau}_h, (\overline{\boldsymbol{u}}_h, \overline{\boldsymbol{\omega}}_h))$ it follows from

$$\begin{aligned} b_{2h}(\boldsymbol{\tau}_h, (\overline{\boldsymbol{u}}_h, \overline{\boldsymbol{\omega}}_h)) &:= -\sum_{T\in\mathcal{T}_h} \int_T \boldsymbol{\tau}_h : (\nabla \overline{\boldsymbol{u}}_h - \overline{\boldsymbol{\omega}}_h)\, dx + \sum_{F\in\mathcal{F}_h} \int_F (\boldsymbol{\tau}_h)_{nt} [\![(\overline{\boldsymbol{u}}_h)_t]\!]\, ds, \\ &:= -\sum_{T\in\mathcal{T}_h} \int_T \boldsymbol{\tau}_h : [\boldsymbol{\varepsilon}(\overline{\boldsymbol{u}}_h) + (\boldsymbol{\omega}(\overline{\boldsymbol{u}}_h) - \overline{\boldsymbol{\omega}}_h)]\, dx + \sum_{F\in\mathcal{F}_h} \int_F (\boldsymbol{\tau}_h)_{nt} [\![(\overline{\boldsymbol{u}}_h)_t]\!]\, ds. \end{aligned}$$

By Cauchy-Schwarz 2 and the norm equivalence (4.11) we conclude the proof.

Lemma 10. *Bilinear form $a(\boldsymbol{\tau}_h, \overline{\boldsymbol{\tau}}_h)$ is elliptic on the kernel $X_{h,0}$*

$$a(\boldsymbol{\tau}_h, \boldsymbol{\tau}_h) \succeq \|(\boldsymbol{\tau}_h, \overline{p}_h)\|_{X_h}^2 \qquad \forall (\boldsymbol{\tau}_h, p_h) \in X_{h,0}.$$

Proof: The kernel is given as

$$X_{h,0} := \{(\boldsymbol{\tau}_h, p_h) \in X_h : b_{2h}(\boldsymbol{\tau}_h, (\overline{\boldsymbol{u}}_h, \overline{\boldsymbol{\omega}}_h)) + b_1(\overline{\boldsymbol{u}}_h, p_h) = 0 \quad \forall (\overline{\boldsymbol{u}}_h, \overline{\boldsymbol{\omega}}_h) \in U_h\}$$

In [LS16, GLS20] the authors state there exists a $(\overline{\boldsymbol{u}}_h, \overline{\boldsymbol{\omega}}_h) \in U_h$ such that

$$\begin{aligned} \overline{\boldsymbol{\omega}}_h &= \boldsymbol{\omega}(\overline{\boldsymbol{u}}_h), \\ \|(\overline{\boldsymbol{u}}_h, \overline{\boldsymbol{\omega}}_h)\|_{U_h} &\preceq \|p_h\| && \forall p_h \in Q_h, \\ \|p_h\|^2 &\preceq b_1(\overline{\boldsymbol{u}}_h, p_h) && \forall p_h \in Q_h. \end{aligned}$$

These findings are a direct consequence of considering a two-field discontinuous Stokes problem. The following estimate then holds true on the kernel $X_{h,0}$

$$\|p_h\|^2 \preceq |b_1(\overline{\boldsymbol{u}}_h, p_h)| = |b_{2h}(\boldsymbol{\tau}_h, (\overline{\boldsymbol{u}}_h, \overline{\boldsymbol{\omega}}_h))| \preceq \|\boldsymbol{\tau}_h\|\|(\overline{\boldsymbol{u}}_h, \overline{\boldsymbol{\omega}}_h)\|_{U_h} \preceq \|\boldsymbol{\tau}_h\|\|p_h\|,$$

thus

$$\|p_h\| \preceq \|\boldsymbol{\tau}_h\| \qquad \forall (\boldsymbol{\tau}_h, p_h) \in X_{h,0}.$$

The discrete kernel ellipticity follows then similar to the ($\mathcal{TH}$-$\mathcal{S}$) element 4.2.1

$$a(\boldsymbol{\tau}_h, \boldsymbol{\tau}_h) = \frac{1}{2\mu}\|\boldsymbol{\tau}_h\|^2 \succeq \frac{1}{8\mu}\left(\|\boldsymbol{\tau}_h\| + \|p_h\|\right)^2 \succeq \frac{1}{\mu}\|(\boldsymbol{\tau}_h, p_h)\|_{X_h}^2 \qquad \forall (\boldsymbol{\tau}_h, p_h) \in X_{h,0}.$$

Lemma 11. *For all $(\overline{\boldsymbol{u}}_h, \overline{\boldsymbol{\omega}}_h)$ the discrete LBB condition*

$$\sup_{(\boldsymbol{\tau}_h, p_h)\in X_h} \frac{|b_1(\overline{\boldsymbol{u}}_h, p_h) + b_{2h}(\boldsymbol{\tau}_h, (\overline{\boldsymbol{u}}_h, \overline{\boldsymbol{\omega}}_h))|}{\|(\boldsymbol{\tau}_h, p_h)\|_{X_h}} \succeq \|(\overline{\boldsymbol{u}}_h, \overline{\boldsymbol{\omega}}_h)\|_{U_h} \qquad \forall (\overline{\boldsymbol{u}}_h, \overline{\boldsymbol{\omega}}_h) \in U_h,$$

holds true.

Die approbierte gedruckte Originalversion dieser Diplomarbeit ist an der TU Wien Bibliothek verfügbar
The approved original version of this thesis is available in print at TU Wien Bibliothek.
TU Bibliothek Your knowledge hub WIEN

Proof: By the L^2-orthogonality of trace-free and diagonal matrices in the *Frobenius* inner product it holds

$$\begin{aligned}
\|\boldsymbol{\varepsilon}(\boldsymbol{u}_h)\|_T^2 &= \|\operatorname{dev}(\boldsymbol{\varepsilon}(\boldsymbol{u}_h))\|_T^2 + \frac{1}{d^2}\|\operatorname{tr}(\boldsymbol{\varepsilon}(\boldsymbol{u}_h))\|_T^2, \\
&= \|\operatorname{dev}(\boldsymbol{\varepsilon}(\boldsymbol{u}_h))\|_T^2 + \frac{1}{d^2}\|\operatorname{div}(\boldsymbol{u}_h)\|_T^2, \\
\|\nabla \boldsymbol{u}_h - \boldsymbol{\omega}_h\|_T^2 &= \|\boldsymbol{\varepsilon}(\boldsymbol{u}_h)\|_T^2 + \|\boldsymbol{\omega}(\boldsymbol{u}_h) - \boldsymbol{\omega}_h\|_T^2, \\
\|\operatorname{dev}(\nabla \boldsymbol{u}_h) - \boldsymbol{\omega}_h\|_T^2 &= \|\operatorname{dev}(\boldsymbol{\varepsilon}(\boldsymbol{u}_h))\|_T^2 + \|\boldsymbol{\omega}(\boldsymbol{u}_h) - \boldsymbol{\omega}_h\|_T^2.
\end{aligned}$$

Combining the upper results yields the norm equivalences

$$\begin{aligned}
\|\boldsymbol{\varepsilon}(\boldsymbol{u}_h)\|_T^2 &\sim \|\operatorname{dev}(\boldsymbol{\varepsilon}(\boldsymbol{u}_h))\|_T^2 + \|\operatorname{div}(\boldsymbol{u}_h)\|_T^2, \\
\|\boldsymbol{\varepsilon}(\boldsymbol{u}_h)\|_T^2 + \|\boldsymbol{\omega}(\boldsymbol{u}_h) - \boldsymbol{\omega}_h\|_T^2 &\sim \|\operatorname{dev}(\nabla \boldsymbol{u}_h) - \boldsymbol{\omega}_h\|_T^2 + \|\operatorname{div}(\boldsymbol{u}_h)\|_T^2, \\
\|(\boldsymbol{u}_h, \boldsymbol{\omega}_h)\|_{U_h,\Pi}^2 &\sim \|(\boldsymbol{u}_h, \boldsymbol{\omega}_h)\|_{U_h,*}^2 + \|\operatorname{div}(\boldsymbol{u}_h)\|^2.
\end{aligned}$$

In a similar way to [GLS20, Lemma 19] we continue by showing in two dimensions that there exists a $\boldsymbol{\tau}_h \in \Sigma_h^{\oplus}$ such that

$$b_{2h}(\boldsymbol{\tau}_h, (\overline{\boldsymbol{u}}_h, \overline{\boldsymbol{\omega}}_h)) \succeq \|(\overline{\boldsymbol{u}}_h, \overline{\boldsymbol{\omega}}_h)\|_{U_{h,*}} \|\boldsymbol{\tau}_h\| \qquad \forall (\overline{\boldsymbol{u}}_h, \overline{\boldsymbol{\omega}}_h) \in U_h.$$

The three dimensional proof is similar. Consider the local element basis matrix functions $\boldsymbol{\xi}^i := \operatorname{dev}(\nabla \lambda_{i+1} \otimes \operatorname{curl}(\lambda_{i+2}))$, where λ_i are the barycentric coordinates and the index i is taken by modulo 3. By the requirement of the discrete space $\Sigma_h^{\oplus}$ for normal-tangential continuity and trace-free basis functions it is obvious that for every facet $F \in \mathcal{F}_h$ there exists a constant basis $\boldsymbol{\xi}^F$ with the attribute $\boldsymbol{\xi}^F \in \mathbb{P}^0(F, \boldsymbol{t}), \|\boldsymbol{\xi}_{nt}^F\|_F = 1$ and vanishing normal-tangential component on the remaining facets. Define

$$\boldsymbol{\tau}_h^0 := \sum_{T \in \mathcal{T}_h} \sum_{F \in \mathcal{F}_h} - \left[\boldsymbol{\xi}^F : \operatorname{dev}(\nabla \overline{\boldsymbol{u}}_h - \overline{\boldsymbol{\omega}}_h)\right] \lambda_T^F \boldsymbol{\xi}^F \qquad \forall (\overline{\boldsymbol{u}}_h, \overline{\boldsymbol{\omega}}_h) \in U_h, \tag{4.4a}$$

$$\boldsymbol{\tau}_h^1 := \sum_{F \in \mathcal{F}_h} \frac{1}{\sqrt{h}} \Pi_F^1 \left([\![(\overline{\boldsymbol{u}}_h)_t]\!]\right) \boldsymbol{\xi}^F \qquad \forall (\overline{\boldsymbol{u}}_h, \overline{\boldsymbol{\omega}}_h) \in U_h, \tag{4.4b}$$

where λ_T^F is the barycentric coordinate opposite to the facet F. Note, that $\boldsymbol{\tau}_h^0 \in \mathcal{B}_h^k$ as $(\lambda_T^F \boldsymbol{\xi}^F)_{nt} = 0 \; \forall F \in \mathcal{F}_h$ and $\boldsymbol{\tau}_h^1 \in \Sigma_h^{k-1}$. Obviously, by $\operatorname{tr}(\boldsymbol{\xi}^F) = 0$ it holds $\operatorname{tr}(\boldsymbol{\tau}_h^0) = \operatorname{tr}(\boldsymbol{\tau}_h^1) = 0$. Now by scaling arguments from the reference element to the physical element in [GLS19, Eqs. 6.1 and 6.2] and [GLS20, Eq. 10] we get the estimates

$$\begin{aligned}
\|\boldsymbol{\tau}_h^0\|^2 &\preceq \sum_{T \in \mathcal{T}_h} \|\operatorname{dev}(\nabla \overline{\boldsymbol{u}}_h - \overline{\boldsymbol{\omega}}_h)\|_T^2, \\
\|\boldsymbol{\tau}_h^1\|^2 &\preceq \sum_{F \in \mathcal{F}_h} \frac{1}{h} \|\Pi_F^1 \left([\![(\overline{\boldsymbol{u}}_h)_t]\!]\right)\|_F^2.
\end{aligned}$$

By a linear combination $\boldsymbol{\tau}_h = c_1 \boldsymbol{\tau}_h^0 + c_2 \boldsymbol{\tau}_h^1$ we immediately see $\boldsymbol{\tau}_h \in \Sigma_h^{\oplus}$. Combining above estimates

$$\|\boldsymbol{\tau}_h\|^2 \preceq \sum_{T \in \mathcal{T}_h} \|\operatorname{dev}(\nabla \overline{\boldsymbol{u}}_h - \overline{\boldsymbol{\omega}}_h)\|_T^2 + \sum_{F \in \mathcal{F}_h} \frac{1}{h} \|\Pi_F^1 \left([\![(\overline{\boldsymbol{u}}_h)_t]\!]\right)\|_F^2,$$

TU Bibliothek Your knowledge hub WIEN
Die approbierte gedruckte Originalversion dieser Diplomarbeit ist an der TU Wien Bibliothek verfügbar
The approved original version of this thesis is available in print at TU Wien Bibliothek.

there holds

$$\|\boldsymbol{\tau}_h\| \preceq \|(\overline{\boldsymbol{u}}_h, \overline{\boldsymbol{\omega}}_h)\|_{U_{h,*}} \qquad \forall (\overline{\boldsymbol{u}}_h, \overline{\boldsymbol{\omega}}_h) \in U_h,$$

and following the same steps as in [GLS19, Lemma 6.5], there also exist constants $c_1, c_2 \neq 0$ such that

$$\begin{aligned} b_{2h}(\boldsymbol{\tau}_h, (\overline{\boldsymbol{u}}_h, \overline{\boldsymbol{\omega}}_h)) &\succeq \sum_{T\in\mathcal{T}_h} \|\mathrm{dev}(\nabla \boldsymbol{u}_h) - \boldsymbol{\omega}_h\|_T^2 + \sum_{F\in\mathcal{F}_h} \frac{1}{h}\|\Pi_F^1[\![(\boldsymbol{u}_h)_t]\!]\|_F^2 \\ &= \|(\overline{\boldsymbol{u}}_h, \overline{\boldsymbol{\omega}}_h)\|_{U_{h,*}}^2 \succeq \|(\overline{\boldsymbol{u}}_h, \overline{\boldsymbol{\omega}}_h)\|_{U_{h,*}} \|\boldsymbol{\tau}_h\| \qquad \forall (\overline{\boldsymbol{u}}_h, \overline{\boldsymbol{\omega}}_h) \in U_h. \end{aligned}$$

Equipped with this estimates we can now turn to the discrete LBB condition. Choose $\boldsymbol{\tau}_h$ as in (4.4) and $p_h := \mathrm{div}(\overline{\boldsymbol{u}}_h)$ as $\mathrm{div}(V_h) \in Q_h$ then it clearly holds

$$\|\boldsymbol{\tau}_h\| + \|p_h\| \preceq \|\mathrm{div}(\overline{\boldsymbol{u}}_h)\| + \|(\overline{\boldsymbol{u}}_h, \overline{\boldsymbol{\omega}}_h)\|_{U_{h,*}} \qquad \forall (\overline{\boldsymbol{u}}_h, \overline{\boldsymbol{\omega}}_h) \in U_h.$$

Inserting above estimates and norm equivalences, we get for all $(\overline{\boldsymbol{u}}_h, \overline{\boldsymbol{\omega}}_h) \in U_h$

$$\begin{aligned} \sup_{(\boldsymbol{\tau}_h, p_h)\in X_h} \frac{|b_1(\overline{\boldsymbol{u}}_h, p_h) + b_{2h}(\boldsymbol{\tau}_h, (\overline{\boldsymbol{u}}_h, \overline{\boldsymbol{\omega}}_h))|}{\|(\boldsymbol{\tau}_h, p_h)\|_{X_h}} &\succeq \frac{|b_1(\overline{\boldsymbol{u}}_h, p_h) + b_{2h}(\boldsymbol{\tau}_h, (\overline{\boldsymbol{u}}_h, \overline{\boldsymbol{\omega}}_h))|}{\|(\boldsymbol{\tau}_h, p_h)\|_{X_h}} \\ &\succeq \frac{\|\mathrm{div}(\overline{\boldsymbol{u}}_h)\|^2 + \|(\overline{\boldsymbol{u}}_h, \overline{\boldsymbol{\omega}}_h)\|_{U_{h,*}}^2}{\|\boldsymbol{\tau}_h\| + \|p_h\|} \\ &\gtrsim \|(\overline{\boldsymbol{u}}_h, \overline{\boldsymbol{\omega}}_h)\|_{U_{h,*}} + \|\mathrm{div}(\overline{\boldsymbol{u}}_h)\| \\ &\sim \|(\overline{\boldsymbol{u}}_h, \overline{\boldsymbol{\omega}}_h)\|_{U_{h,\Pi}} \overset{(4.3)}{\sim} \|(\overline{\boldsymbol{u}}_h, \overline{\boldsymbol{\omega}}_h)\|_{U_h}. \end{aligned}$$

4.3.2 Mass conserving mixed stress-strain rate element ($\mathcal{MCS}$-$\mathcal{S}$)

After an insight in different stable finite elements for the simulation of Newtonian flows, we finally turn to the finite element developed during these thesis. It is strongly based on the previous introduced finite element ($\mathcal{MCS}$) in Subsection 4.3.1 and the *Hu-Washizu* principle [Was75] from continuum mechanics, which uses an additional piecewise discontinuous unknown $\boldsymbol{\varepsilon}$ for the mechanical strains - in our case the $\boldsymbol{\varepsilon}$ denotes the rate-of-strain tensor. The reason for this special choice is that in the mass conserving mixed stress method ($\mathcal{MCS}$), the velocity gradient $\nabla \boldsymbol{u}$, which is needed for the construction of the rate-of-strain tensor $\boldsymbol{\varepsilon}(\boldsymbol{u})$, is not globally defined as for $\boldsymbol{u} \in H(\mathrm{div}, \Omega), \nabla \boldsymbol{u} \notin L^2(\Omega)$. It is precisely the definiteness of the rate-of-strain tensor $\boldsymbol{\varepsilon}(\boldsymbol{u})$ that is desirable, since many non-Newtonian models rely on them, as we saw in Chapter 2. According to the frequent used argument (3.2) it holds

$$\nabla \boldsymbol{u} = \boldsymbol{\varepsilon}(\boldsymbol{u}) + \boldsymbol{\omega} = \boldsymbol{\varepsilon} + \boldsymbol{\omega},$$

by which we extend the discrete ($\mathcal{MCS}$) variational formulation VII to our new discrete problem VIII

Discrete Variational Formulation VIII

Find $((\boldsymbol{\varepsilon}_h, (\boldsymbol{u}_h, \boldsymbol{\omega}_h)), (\boldsymbol{\tau}_h, p_h)) \in Y_h \times X_h$ such that

$$\begin{aligned} a(\boldsymbol{\varepsilon}_h, \overline{\boldsymbol{\varepsilon}}_h) + b_3(\overline{\boldsymbol{\varepsilon}}_h, \boldsymbol{\tau}_h) &= 0 && \forall \overline{\boldsymbol{\varepsilon}}_h \in \Xi_h, \\ b_3(\boldsymbol{\varepsilon}_h, \overline{\boldsymbol{\tau}}_h) + b_{2h}(\overline{\boldsymbol{\tau}}_h, (\boldsymbol{u}_h, \boldsymbol{\omega}_h)) &= 0 && \forall \overline{\boldsymbol{\tau}}_h \in \Sigma_h^{\oplus}, \\ b_{2h}(\boldsymbol{\tau}_h, (\overline{\boldsymbol{u}}_h, \overline{\boldsymbol{\omega}}_h)) + b_1(\overline{\boldsymbol{u}}_h, p_h) &= f(\overline{\boldsymbol{u}}_h) && \forall (\overline{\boldsymbol{u}}_h, \overline{\boldsymbol{\omega}}_h) \in U_h, \\ b_1(\boldsymbol{u}_h, \overline{p}_h) &= 0 && \forall \overline{p}_h \in Q_h. \end{aligned}$$

Die approbierte gedruckte Originalversion dieser Diplomarbeit ist an der TU Wien Bibliothek verfügbar
The approved original version of this thesis is available in print at TU Wien Bibliothek.
TU Bibliothek Your knowledge hub WIEN

The approximated system can easily be derived by the standard procedure. Bilinear forms and linear form are then given as

$$
\begin{aligned}
a(\boldsymbol{\varepsilon}_h, \overline{\boldsymbol{\varepsilon}}_h) &:= -2\mu \int_\Omega \boldsymbol{\varepsilon}_h : \overline{\boldsymbol{\varepsilon}}_h \, dx, \\
b_1(\boldsymbol{u}_h, \overline{p}_h) &:= \int_\Omega \operatorname{div}(\boldsymbol{u}_h)\overline{p}_h \, dx, \\
b_{2h}(\boldsymbol{\tau}_h, (\overline{\boldsymbol{u}}_h, \overline{\boldsymbol{\omega}}_h)) &:= \sum_{T\in\mathcal{T}_h} \int_T \operatorname{div}(\boldsymbol{\tau}_h)\cdot\overline{\boldsymbol{u}}_h \, dx + \sum_{T\in\mathcal{T}_h} \int_T \boldsymbol{\tau}_h : \overline{\boldsymbol{\omega}}_h \, dx - \sum_{F\in\mathcal{F}_h} \int_F [\![(\boldsymbol{\tau}_h)_{nn}]\!](\overline{\boldsymbol{u}}_h)_n \, ds, \\
b_3(\boldsymbol{\varepsilon}_h, \overline{\boldsymbol{\tau}}_h) &:= \int_\Omega \boldsymbol{\varepsilon}_h : \overline{\boldsymbol{\tau}}_h \, dx, \\
f(\overline{\boldsymbol{u}}_h) &:= -\int_\Omega \rho \boldsymbol{f}\cdot\overline{\boldsymbol{u}}_h \, dx.
\end{aligned}
$$

Note, that in contrast to the ($\mathcal{MCS}$) method our primal variables have become $(\boldsymbol{\varepsilon}_h, (\boldsymbol{u}_h, \boldsymbol{\omega}_h)) \in Y_h := \Xi_h \times U_h$ and $(\boldsymbol{\tau}_h, p_h) \in X_h := \Sigma_h^{\oplus} \times Q_h$ have become dual variables. The discrete spaces have been chosen equivalently to the previous ($\mathcal{MCS}$) method, namely

$$
\begin{aligned}
V_h &:= \left\{\boldsymbol{u}_h \in H(\operatorname{div},\Omega) : \boldsymbol{u}_h|_T \in \mathbb{P}^k(T,\mathbb{R}^d)\ \forall T\in\mathcal{T}_h, [\![(\boldsymbol{u}_h)_n]\!] = 0\ \forall F\in\mathcal{F}_h^{\text{int}}\right\}, \\
\Sigma_h^{\oplus} &:= \left\{\boldsymbol{\tau}_h \in \Sigma_h^k : (\boldsymbol{\tau}_h)_{nt} \in \mathbb{P}^{k-1}(F,\mathbb{R}^{d-1})\ \forall F\in\mathcal{F}_h^{\text{int}}\right\}, \\
Q_h &:= \left\{p_h \in L_0^2(\Omega,\mathbb{R}) : p_h|_T \in \mathbb{P}^{k-1}(T,\mathbb{R})\ \forall T\in\mathcal{T}_h\right\}, \\
W_h &:= \left\{\boldsymbol{\omega}_h \in L^2_{\text{skw}}(\Omega,\mathbb{R}^{d\times d}) : \boldsymbol{\omega}_h|_T \in \mathbb{P}^{k-1}_{\text{skw}}(T,\mathbb{R}^{d\times d})\ \forall T\in\mathcal{T}_h\right\}.
\end{aligned}
$$

Recall: For this special choice $\operatorname{div}(V_h) \subset Q_h$ we acquire a mass preserving property as explained in Subsection 4.1.2. Since in general $\boldsymbol{\varepsilon}$ is symmetric, as shown in (3.3), and on the discrete setting it holds $\operatorname{tr}(\nabla\boldsymbol{u}_h) = \operatorname{tr}(\boldsymbol{\tau}_h) = 0$, it is appropriate to choose piecewise discontinuous trace-free symmetric matrix-valued polynomials as our approximating space

$$
\Xi_h = \left\{\boldsymbol{\varepsilon}_h \in L^2_{\text{sym,tr}}(\Omega,\mathbb{R}^{d\times d}) : \boldsymbol{\varepsilon}_h|_T \in \mathbb{P}^k_{\text{sym,tr}}(\Omega,\mathbb{R}^{d\times d})\ \forall T\in\mathcal{T}_h\right\}.
$$

The stability analysis, which is carried out later, suggests a polynomial order of k for the rate-of-strain tensor $\boldsymbol{\varepsilon}_h$ in order to control the interior stress $\mathbb{P}^k$ bubbles $\mathcal{B}_h^k$ introduced in equation (4.1).
As for the previous finite elements we provide an illustration of this newly introduced mixed finite element ($\mathcal{MCS}$-$\mathcal{S}$) in Figure 4.7 for a polynomial order $k = 2$.

Discrete stability analysis

We continue by showing the stability of the above introduced finite element. As in the discrete stability analysis of the mass conserving mixed stress finite element ($\mathcal{MCS}$) we use a discontinuous *Galerkin* norm for the velocity $\boldsymbol{u}_h$, while for the remaining quantities a L^2-norm suffices

$$
\begin{aligned}
\|(\boldsymbol{u}_h,\boldsymbol{\omega}_h)\|_{U_h}^2 &:= \sum_{T\in\mathcal{T}_h} \|\boldsymbol{\varepsilon}(\boldsymbol{u}_h)\|_T^2 + \sum_{T\in\mathcal{T}_h} \|\boldsymbol{\omega}(\boldsymbol{u}_h) - \boldsymbol{\omega}_h\|_T^2 + \sum_{F\in\mathcal{F}_h} \frac{1}{h}\|[\![(\boldsymbol{u}_h)_t]\!]\|_F^2, \\
\|(\boldsymbol{\varepsilon}_h,(\boldsymbol{u}_h,\boldsymbol{\omega}_h))\|_{Y_h}^2 &= \|\boldsymbol{\varepsilon}_h\|^2 + \|(\boldsymbol{u}_h,\boldsymbol{\omega}_h)\|_{U_h}^2, \\
\|(\boldsymbol{\tau}_h,p_h)\|_{X_h}^2 &= \left(\|\boldsymbol{\tau}_h\| + \|p_h\|\right)^2.
\end{aligned}
$$

Die approbierte gedruckte Originalversion dieser Diplomarbeit ist an der TU Wien Bibliothek verfügbar
The approved original version of this thesis is available in print at TU Wien Bibliothek.
TU Bibliothek Your knowledge hub WIEN

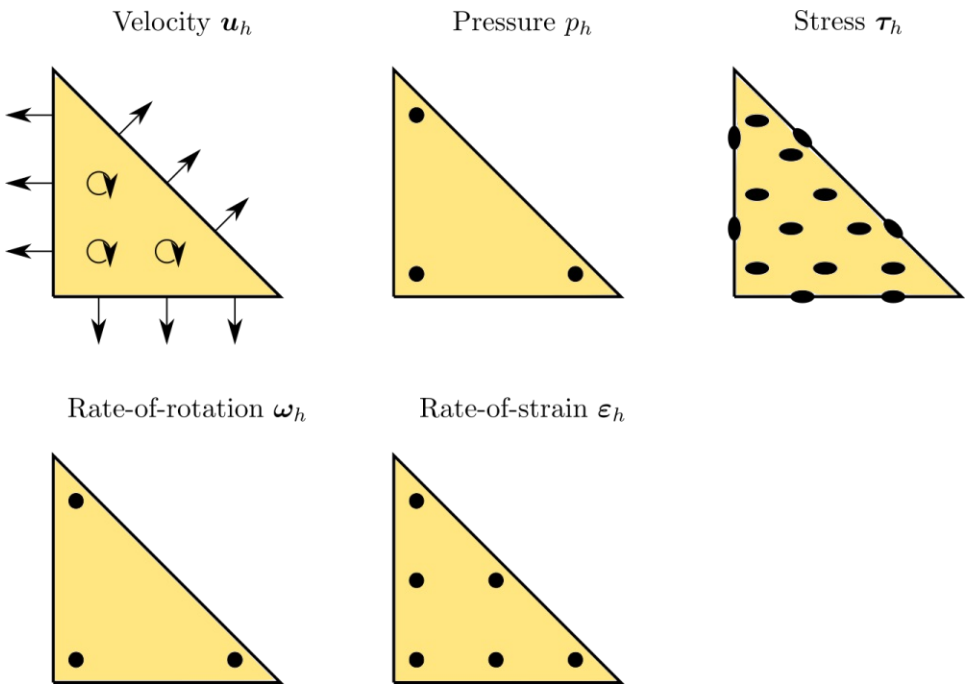

FIGURE 4.7 – 2-simplex mass conserving mixed stress-strain rate element ($\mathcal{MCS}$-$\mathcal{S}$) of polynomial order $k = 2$

Lemma 12. *Bilinear forms* $a(\boldsymbol{\varepsilon}_h, \overline{\boldsymbol{\varepsilon}}_h)$, $b_1(\boldsymbol{u}_h, \overline{p}_h)$, $b_{2h}(\boldsymbol{\tau}_h, (\overline{\boldsymbol{u}}_h, \overline{\boldsymbol{\omega}}_h))$ *and* $b_3(\boldsymbol{\varepsilon}_h, \overline{\boldsymbol{\tau}}_h)$ *are continuous*

$$\begin{aligned}
a(\boldsymbol{\varepsilon}_h, \overline{\boldsymbol{\varepsilon}}_h) &\preceq \|\boldsymbol{\varepsilon}_h\|\|\overline{\boldsymbol{\varepsilon}}_h\| && \forall \boldsymbol{\varepsilon}_h, \overline{\boldsymbol{\varepsilon}}_h \in \Xi_h,\\
b_1(\boldsymbol{u}_h, \overline{p}_h) &\preceq \|(\boldsymbol{u}_h, 0)\|_{U_h}\|p_h\| && \forall \boldsymbol{u}_h \in V_h, \overline{p}_h \in Q_h,\\
b_{2h}(\boldsymbol{\tau}_h, (\overline{\boldsymbol{u}}_h, \overline{\boldsymbol{\omega}}_h)) &\preceq \|\boldsymbol{\tau}_h\|\|(\overline{\boldsymbol{u}}_h, \overline{\boldsymbol{\omega}}_h)\|_{U_h} && \forall \boldsymbol{\tau}_h \in \Sigma_h^{\oplus}, (\overline{\boldsymbol{u}}_h, \overline{\boldsymbol{\omega}}_h) \in U_h,\\
b_3(\boldsymbol{\varepsilon}_h, \overline{\boldsymbol{\tau}}_h) &\preceq \|\boldsymbol{\varepsilon}_h\|\|\overline{\boldsymbol{\tau}}_h\| && \forall \boldsymbol{\varepsilon}_h \in \Xi_h, \overline{\boldsymbol{\tau}}_h \in \Sigma_h^{\oplus}.
\end{aligned}$$

Proof: Continuity of $b_1(\boldsymbol{u}_h, \overline{p}_h), b_{2h}(\boldsymbol{\tau}_h, (\overline{\boldsymbol{u}}_h, \overline{\boldsymbol{\omega}}_h))$ has been shown in Lemma 9, while continuity of $a(\boldsymbol{\varepsilon}_h, \overline{\boldsymbol{\varepsilon}}_h)$ and $b_3(\boldsymbol{\varepsilon}_h, \overline{\boldsymbol{\tau}}_h)$ is straightforward by a *Cauchy-Schwarz*.

Lemma 13. *Bilinear form* $a(\boldsymbol{\varepsilon}_h, \boldsymbol{\varepsilon}_h)$ *is elliptic on the kernel* $Y_{h,0}$

$$a(\boldsymbol{\varepsilon}_h, \boldsymbol{\varepsilon}_h) \succeq \|(\boldsymbol{\varepsilon}_h, (\boldsymbol{u}_h, \boldsymbol{\omega}_h))\|_{Y_h}^2 \qquad \forall (\boldsymbol{\varepsilon}_h, (\boldsymbol{u}_h, \boldsymbol{\omega}_h)) \in Y_{h,0}.$$

Proof: First of all, the kernel is given as $Y_{h,0}$

$$Y_{h,0} := \{(\boldsymbol{\varepsilon}_h, (\boldsymbol{u}_h, \boldsymbol{\omega}_h)) \in Y_h : b_3(\boldsymbol{\varepsilon}_h, \overline{\boldsymbol{\tau}}_h) + b_{2h}(\overline{\boldsymbol{\tau}}_h, (\boldsymbol{u}_h, \boldsymbol{\omega}_h)) + b_1(\boldsymbol{u}_h, \overline{p}_h) = 0 \quad \forall (\overline{\boldsymbol{\tau}}_h, \overline{p}_h) \in X_h\}.$$

By the LBB condition Lemma 11 of the standard mass conserving mixed stress approximation ($\mathcal{MCS}$) there exists a $(\boldsymbol{\tau}_h, p_h) \in X_h$ such that

$$\frac{|b_1(\overline{\boldsymbol{u}}_h, p_h) + b_{2h}(\boldsymbol{\tau}_h, (\overline{\boldsymbol{u}}_h, \overline{\boldsymbol{\omega}}_h))|}{\|(\boldsymbol{\tau}_h, p_h)\|_{X_h}} \succeq \|(\overline{\boldsymbol{u}}_h, \overline{\boldsymbol{\omega}}_h)\|_{U_h} \qquad \forall (\overline{\boldsymbol{u}}_h, \overline{\boldsymbol{\omega}}_h) \in U_h,$$

with

$$\|\boldsymbol{\tau}_h\| + \|p_h\| \preceq \|(\overline{\boldsymbol{u}}_h, \overline{\boldsymbol{\omega}}_h)\|_{U_h} \qquad \forall (\overline{\boldsymbol{u}}_h, \overline{\boldsymbol{\omega}}_h) \in U_h.$$

Die approbierte gedruckte Originalversion dieser Diplomarbeit ist an der TU Wien Bibliothek verfügbar
The approved original version of this thesis is available in print at TU Wien Bibliothek.
TU Bibliothek Your knowledge hub WIEN

By the continuity of bilinear form $b_3(\boldsymbol{\varepsilon}_h, \overline{\boldsymbol{\tau}}_h)$ it clearly holds on the kernel

$$\begin{aligned}\|(\overline{\boldsymbol{u}}_h, \overline{\boldsymbol{\omega}}_h)\|_{U_h} &\preceq \frac{|b_1(\overline{\boldsymbol{u}}_h, p_h) + b_{2h}(\boldsymbol{\tau}_h, (\overline{\boldsymbol{u}}_h, \overline{\boldsymbol{\omega}}_h))|}{\|(\boldsymbol{\tau}_h, p_h)\|_{X_h}} = \frac{|b_3(\overline{\boldsymbol{\varepsilon}}_h, \boldsymbol{\tau}_h)|}{\|(\boldsymbol{\tau}_h, p_h)\|_{X_h}} \\ &\preceq \frac{\|\overline{\boldsymbol{\varepsilon}}_h\|\|\boldsymbol{\tau}_h\|}{\|(\overline{\boldsymbol{u}}_h, \overline{\boldsymbol{\omega}}_h)\|_{U_h}} \preceq \|\overline{\boldsymbol{\varepsilon}}_h\| \qquad \forall (\overline{\boldsymbol{\varepsilon}}_h, (\overline{\boldsymbol{u}}_h, \overline{\boldsymbol{\omega}}_h)) \in Y_{h,0}.\end{aligned}$$

The proof of kernel ellipticity is then straightforward

$$a(\boldsymbol{\varepsilon}_h, \boldsymbol{\varepsilon}_h) \succeq 2\mu\|\boldsymbol{\varepsilon}_h\|^2 \succeq \mu\|\boldsymbol{\varepsilon}_h\|^2 + \mu\|(\boldsymbol{u}_h, \boldsymbol{\omega}_h)\|_{U_h}^2 \succeq \|(\boldsymbol{\varepsilon}_h, (\boldsymbol{u}_h, \boldsymbol{\omega}_h))\|_{Y_h}^2 \quad \forall (\boldsymbol{\varepsilon}_h, (\boldsymbol{u}_h, \boldsymbol{\omega}_h)) \in Y_{h,0}.$$

Lemma 14. *The discrete LBB condition holds for all* $(\overline{\boldsymbol{\tau}}_h, p_h) \in X_h$

$$\sup_{(\boldsymbol{\varepsilon}_h, (\boldsymbol{u}_h, \boldsymbol{\omega}_h)) \in Y_h} \frac{|b_3(\boldsymbol{\varepsilon}_h, \overline{\boldsymbol{\tau}}_h) + b_{2h}(\overline{\boldsymbol{\tau}}_h, (\boldsymbol{u}_h, \boldsymbol{\omega}_h)) + b_1(\boldsymbol{u}_h, \overline{p}_h)|}{\|(\boldsymbol{\varepsilon}_h, (\boldsymbol{u}_h, \boldsymbol{\omega}_h))\|_{Y_h}} \succeq \|(\overline{\boldsymbol{\tau}}_h, \overline{p}_h)\|_{X_h}.$$

Proof: For sake of simplicity we present the proof of the LBB condition in a two-dimensional setting. Although we did not prove solvability in three dimensions, it should follow similar steps as presented here. A crucial point of the proof is to bound the skew-symmetric part of the high order $\mathcal{B}_h^k$-bubbles, defined in (4.1). For this consider the partition of the deviatoric stress tensor $\overline{\boldsymbol{\tau}}_h$

$$\overline{\boldsymbol{\tau}}_h = \operatorname{sym}(\overline{\boldsymbol{\tau}}_h) + \operatorname{skw}(\overline{\boldsymbol{\tau}}_h) = \operatorname{sym}(\overline{\boldsymbol{\tau}}_h) + \operatorname{skw}(\Pi^{\mathcal{B}_h^k}\overline{\boldsymbol{\tau}}_h) + \operatorname{skw}((\mathrm{id} - \Pi^{\mathcal{B}_h^k})\overline{\boldsymbol{\tau}}_h),$$

where $\Pi^{\mathcal{B}_h^k}$ denotes the projection on the bubbles $\mathcal{B}_h^k$, given by

$$\int_T \overline{\boldsymbol{\tau}}_h|_T : \boldsymbol{\psi}_h = \int_T \Pi^{\mathcal{B}_h^k}\overline{\boldsymbol{\tau}}_h|_T : \boldsymbol{\psi}_h \qquad \forall \boldsymbol{\psi}_h \in \mathcal{B}_h^k(T). \tag{4.5}$$

By the definition of $\Sigma_h^{\oplus}$ the highest order polynomials consist only of bubbles $\mathcal{B}_h^k$, therefore it is clear that

$$\operatorname{skw}((\mathrm{id} - \Pi^{\mathcal{B}_h^k})\overline{\boldsymbol{\tau}}_h|_T) \in \mathbb{P}_{\mathrm{skw}}^{k-1}(T, \mathbb{R}^{d\times d}) \qquad \forall T \in \mathcal{T}_h.$$

Again we exploit the L^2-orthogonality in the *Frobenius* inner product to get the norm

$$\|\overline{\boldsymbol{\tau}}_h\|^2 = \|\operatorname{sym}(\overline{\boldsymbol{\tau}}_h)\|^2 + \|\operatorname{skw}(\Pi^{\mathcal{B}_h^k}\overline{\boldsymbol{\tau}}_h)\|^2 + \|\operatorname{skw}((\mathrm{id} - \Pi^{\mathcal{B}_h^k})\overline{\boldsymbol{\tau}}_h)\|^2.$$

Of course it holds

$$\|\operatorname{sym}(\overline{\boldsymbol{\tau}}_h)\|^2 + \|\operatorname{skw}((\mathrm{id} - \Pi^{\mathcal{B}_h^k})\overline{\boldsymbol{\tau}}_h)\|^2 \leq \|\overline{\boldsymbol{\tau}}_h\|^2.$$

As we will control $\operatorname{sym}(\overline{\boldsymbol{\tau}}_h) \in \Xi_h \subset \Sigma_h^{\oplus}$ and $\operatorname{skw}((\mathrm{id} - \Pi^{\mathcal{B}_h^k})\overline{\boldsymbol{\tau}}_h) \in W_h \subset \Sigma_h^{\oplus}$, we need to bound the remaining quantity $\operatorname{skw}(\Pi^{\mathcal{B}_h^k}\overline{\boldsymbol{\tau}}_h)$. To do this a closer look at $\Pi^{\mathcal{B}_h^k}\overline{\boldsymbol{\tau}}_h$ is needed.

Norm equivalences

Recall the three local normal-tangential basis matrix functions given by the expression [GLS19, Eq. 5.2]

$$\boldsymbol{\xi}^i := \operatorname{dev}(\nabla\lambda_{i+1} \otimes \operatorname{curl}(\lambda_{i+2})). \tag{4.6}$$

TU Bibliothek Your knowledge hub WIEN
Die approbierte gedruckte Originalversion dieser Diplomarbeit ist an der TU Wien Bibliothek verfügbar
The approved original version of this thesis is available in print at TU Wien Bibliothek.

Obviously, the indices are taken by modulo 3 and λ_i stands for the barycentric coordinates such that

$$\lambda_i(\mathcal{V}_j) = \delta_{ij} \qquad \forall i,j \in \mathcal{I}_{\mathcal{V}_h(T)} \qquad \lambda_i \in \mathbb{P}^1(T,\mathbb{R}),$$

where the index set of the local vertices $\mathcal{V}_h(T)$ is denoted as $\mathcal{I}_{\mathcal{V}_h(T)}$ [Led19, Section 5.1]. Any element local normal-tangential bubble $\boldsymbol{\beta} \in \mathcal{B}_h^k(T)$ of a 2-simplex can be constructed by [GLS19, Lemma 5.2]

$$\boldsymbol{\beta} = \sum_{i \in \mathcal{I}_{\mathcal{V}_h(T)}} \mu_i \lambda_i \boldsymbol{\xi}^i \qquad \forall \mu_i \in \mathbb{P}^{k-1}(T).$$

A very important property is that by construction it holds

$$\operatorname{tr}(\boldsymbol{\xi}^i) = \sum_{j=0}^{1} \boldsymbol{\xi}^i_{jj} = 0, \qquad \boldsymbol{\xi}^i_{jj} \neq 0, \tag{4.7}$$

hence $\boldsymbol{\xi}^i$ is never fully skew-symmetric. This follows from the fact that

$$\operatorname{tr}(\nabla\lambda_{i+1} \otimes \operatorname{curl}(\lambda_{i+2})) = \nabla\lambda_{i+1} \cdot \operatorname{curl}(\lambda_{i+2}) \neq 0,$$

as $\lambda_{i+1} \neq \lambda_{i+2}$, which arises from our assumption of a non overlapping triangulation, otherwise we would deal with a degenerated 2-simplex.

Proposition 15. *Consider the skew-symmetric subset $\mathcal{P}_h^b(T) \subset \mathcal{B}_h^k(T)$ of high order polynomials $k \geq 3$ with vanishing component on the boundary ∂T*

$$\mathcal{P}_h^b(T) := \left\{ \boldsymbol{\beta} \in \mathcal{B}_h^k(T) : \boldsymbol{\xi} \lambda_i^{l+1} \lambda_{i+1}^{m+1} \lambda_{i+2}^{n+1} \big|_{l,n,m \geq 0}^{l+n+m=k-3} \qquad \boldsymbol{\xi} \in \mathbb{P}^0_{\mathrm{skw}}(T, \mathbb{R}^{2\times 2}) \right\}.$$

For any $\boldsymbol{\beta} \in \mathcal{B}_h^k(T)$ such that

$$\|\operatorname{sym}(\boldsymbol{\beta})\|_T = 0 \text{ and } \|\operatorname{skw}(\boldsymbol{\beta})\|_T \neq 0 \Rightarrow \boldsymbol{\beta} \in \mathcal{P}_h^b(T).$$

By norm equivalence on finite dimensional spaces it holds

$$\|\operatorname{skw}(\boldsymbol{\beta})\|_T \preceq \|\operatorname{sym}(\boldsymbol{\beta})\|_T \qquad \forall \boldsymbol{\beta} \in \mathcal{B}_h^k(T), k < 3,$$
$$\|\operatorname{skw}(\boldsymbol{\beta})\|_T \preceq \|\operatorname{sym}(\boldsymbol{\beta})\|_T \qquad \forall \boldsymbol{\beta} \in (\mathcal{B}_h^k(T) \setminus P_h^b(T)), k \geq 3.$$

Proposition 15 follows by exploiting the structure of an arbitrary bubble $\boldsymbol{\beta} \in \mathcal{B}_h^k(T)$. For this consider an arbitrary non overlapping 2-simplex with the index set $\mathcal{I}_{\mathcal{V}_h(T)} := \{l,m,n\}$ as shown in Figure 4.8. The bubble $\boldsymbol{\beta}$ and its corresponding symmetric and skew-symmetric part are defined as

$$\boldsymbol{\beta} = \sum_{i \in \mathcal{I}_{\mathcal{V}_h(T)}} \alpha_i \mu_i \lambda_i \begin{pmatrix} a_i & b_i \\ c_i & -a_i \end{pmatrix} \qquad \forall \mu_i \in \mathbb{P}^{k-1}(T),$$

$$\operatorname{sym}(\boldsymbol{\beta}) = \sum_{i \in \mathcal{I}_{\mathcal{V}_h(T)}} \alpha_i \mu_i \lambda_i \begin{pmatrix} a_i & 0.5(b_i+c_i) \\ 0.5(b_i+c_i) & -a_i \end{pmatrix} \qquad \forall \mu_i \in \mathbb{P}^{k-1}(T),$$

$$\operatorname{skw}(\boldsymbol{\beta}) = \sum_{i \in \mathcal{I}_{\mathcal{V}_h(T)}} \alpha_i \mu_i \lambda_i \begin{pmatrix} 0 & 0.5(b_i-c_i) \\ 0.5(-b_i+c_i) & 0 \end{pmatrix} \qquad \forall \mu_i \in \mathbb{P}^{k-1}(T).$$

Die approbierte gedruckte Originalversion dieser Diplomarbeit ist an der TU Wien Bibliothek verfügbar
The approved original version of this thesis is available in print at TU Wien Bibliothek.
TU Bibliothek Your knowledge hub WIEN

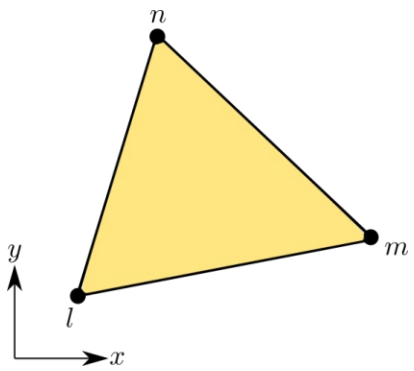

FIGURE 4.8 – Arbitrary 2-simplex with index set $\mathcal{I}_{\mathcal{V}_h(T)} := \{l, m, n\}$

The question now is whether there exists a linear combination such that $\mathrm{sym}(\boldsymbol{\beta})$ vanishes. In order to meet this specific requirements, it must hold

$$\sum_{i \in \mathcal{I}_{\mathcal{V}_h(T)}} \alpha_i \mu_i \lambda_i a_i = 0 \qquad \forall \mu_i \in \mathbb{P}^{k-1}(T), \tag{4.8a}$$

$$\sum_{i \in \mathcal{I}_{\mathcal{V}_h(T)}} \alpha_i \mu_i \lambda_i (b_i + c_i) = 0 \qquad \forall \mu_i \in \mathbb{P}^{k-1}(T), \tag{4.8b}$$

$$\sum_{i \in \mathcal{I}_{\mathcal{V}_h(T)}} \alpha_i \mu_i \lambda_i (b_i - c_i) \neq 0 \qquad \forall \mu_i \in \mathbb{P}^{k-1}(T), \tag{4.8c}$$

where α_i, a_i, b_i, c_i are arbitrary scalars. From (4.7) we know that $a_i \neq 0$, which is automatically a crucial property of our proof. A further necessity is

$$\mu_l \lambda_l = \mu_m \lambda_m = \mu_n \lambda_n, \tag{4.9}$$

otherwise it is clear that $\mu_l\lambda_l, \mu_m\lambda_m, \mu_n\lambda_n$ are linearly independent.
Hence for a polynomial order $k = 1$ it is straightforward from (4.8a) as $a_l, a_m, a_n \neq 0$ and $\mu_l\lambda_l \neq \mu_m\lambda_m \neq \mu_n\lambda_n$ that the only admissible choice is $\alpha_l = \alpha_m = \alpha_n = 0$.
For a polynomial order $k = 2$ it becomes more intriguing as we have to distinguish between multiple cases. All arguments presented in the following apply to an arbitrary index $\mathcal{I}_{\mathcal{V}_h(T)}$ permutation.

1. $\alpha_l = \alpha_m = 0$ and $\alpha_n \neq 0$.
   Likewise to a polynomial order $k = 1$ by (4.8a) and $a_n \neq 0$ it follows $\alpha_n = 0$.

2. $\alpha_l \neq 0, \alpha_m \neq 0$ and $\alpha_n \neq 0$.
   For an arbitrary $\mu \in \mathbb{P}^1(T)$ we can not fulfil condition (4.9). Thus the only admissible choice is $\alpha_l = \alpha_m = \alpha_n = 0$.

3. $\alpha_l = 0, \alpha_m \neq 0$ and $\alpha_n \neq 0$.
   In the 2nd subitem we stated that for an arbitrary $\mu \in \mathbb{P}^1(T)$ we can not fulfil condition (4.9). There exists one special case, in which we choose $\alpha_l = 0$ and $\mu_m\lambda_m = \mu_n\lambda_n = \mu\lambda$. Thus $\mu_l\lambda_l$ can be arbitrary as it vanishes anyway. To proof that $\alpha_m = \alpha_n = 0$ we need to explicitly define the coefficients $a_m, a_n, b_m, b_n, c_m, c_n$ in terms of the barycentric coordinates $\lambda_l, \lambda_m, \lambda_n$. By (4.6) the symmetric constant

Die approbierte gedruckte Originalversion dieser Diplomarbeit ist an der TU Wien Bibliothek verfügbar
The approved original version of this thesis is available in print at TU Wien Bibliothek.
TU Bibliothek Your knowledge hub WIEN

normal-tangential basis functions are given as

$$\operatorname{sym}(\boldsymbol{\xi}^m) = \frac{1}{2}\begin{pmatrix} -\lambda_{n,x}\lambda_{l,y} - \lambda_{n,y}\lambda_{l,x} & \lambda_{n,x}\lambda_{l,x} - \lambda_{n,y}\lambda_{l,y} \\ \lambda_{n,x}\lambda_{l,x} - \lambda_{n,y}\lambda_{l,y} & \lambda_{n,x}\lambda_{l,y} + \lambda_{n,y}\lambda_{l,x} \end{pmatrix},$$
$$\operatorname{sym}(\boldsymbol{\xi}^n) = \frac{1}{2}\begin{pmatrix} -\lambda_{l,x}\lambda_{m,y} - \lambda_{l,y}\lambda_{m,x} & \lambda_{l,x}\lambda_{m,x} - \lambda_{l,y}\lambda_{m,y} \\ \lambda_{l,x}\lambda_{m,x} - \lambda_{l,y}\lambda_{m,y} & \lambda_{l,x}\lambda_{m,y} + \lambda_{l,y}\lambda_{m,x} \end{pmatrix}.$$

where for sake of readability the derivative along a spatial coordinate is denoted by a second subscript. Inserting upper definition of a_m, a_n in (4.8a) yields

$$\underbrace{\cancel{\mu\lambda}}_{\neq 0} \sum_{i\in\{m,n\}} \alpha_i a_i = \alpha_m\left(\lambda_{n,x}\lambda_{l,y} + \lambda_{n,y}\lambda_{l,x}\right) + \alpha_n\left(\lambda_{l,x}\lambda_{m,y} + \lambda_{l,y}\lambda_{m,x}\right) = 0,$$
$$\alpha_m = -\alpha_n \frac{\left(\lambda_{l,x}\lambda_{m,y} + \lambda_{l,y}\lambda_{m,x}\right)}{\left(\lambda_{n,x}\lambda_{l,y} + \lambda_{n,y}\lambda_{l,x}\right)}.$$

Note, that the property $a_m \neq 0, a_n \neq 0$ is important, otherwise we could not divide by a_m so easily. Now we substitute upper intermediate result for α_m into (4.8b), which results into

$$\underbrace{\cancel{\mu\lambda}}_{\neq 0} \sum_{i\in\{m,n\}} \alpha_i(b_i + c_i) = \alpha_m\left(\lambda_{n,x}\lambda_{l,x} - \lambda_{n,y}\lambda_{l,y}\right) + \alpha_n\left(\lambda_{l,x}\lambda_{m,x} - \lambda_{l,y}\lambda_{m,y}\right) = 0,$$
$$-\left(\lambda_{l,x}\lambda_{m,y} + \lambda_{l,y}\lambda_{m,x}\right)\left(\lambda_{n,x}\lambda_{l,x} - \lambda_{n,y}\lambda_{l,y}\right) +$$
$$\left(\lambda_{n,x}\lambda_{l,y} + \lambda_{n,y}\lambda_{l,x}\right)\left(\lambda_{l,x}\lambda_{m,x} - \lambda_{l,y}\lambda_{m,y}\right) = 0.$$

Ultimately, we expand the brackets

$$-\lambda_{l,x}\lambda_{m,y}\lambda_{n,x}\lambda_{l,x} + \cancel{\lambda_{l,x}\lambda_{m,y}\lambda_{n,y}\lambda_{l,y}} - \cancel{\lambda_{l,y}\lambda_{m,x}\lambda_{n,x}\lambda_{l,x}} + \lambda_{l,y}\lambda_{m,x}\lambda_{n,y}\lambda_{l,y} +$$
$$\cancel{\lambda_{n,x}\lambda_{l,y}\lambda_{l,x}\lambda_{m,x}} - \lambda_{n,x}\lambda_{l,y}\lambda_{l,y}\lambda_{m,y} + \lambda_{n,y}\lambda_{l,x}\lambda_{l,x}\lambda_{m,x} - \cancel{\lambda_{n,y}\lambda_{l,x}\lambda_{l,y}\lambda_{m,y}} = 0,$$

and simplify the expression

$$-\lambda_{l,x}\lambda_{m,y}\lambda_{n,x}\lambda_{l,x} + \lambda_{l,y}\lambda_{m,x}\lambda_{n,y}\lambda_{l,y} - \lambda_{n,x}\lambda_{l,y}\lambda_{l,y}\lambda_{m,y} + \lambda_{n,y}\lambda_{l,x}\lambda_{l,x}\lambda_{m,x} = 0,$$
$$(\lambda_{m,x}\lambda_{n,y} - \lambda_{m,y}\lambda_{n,x})(\lambda_{l,x}^2 + \lambda_{l,y}^2) = 0,$$
$$(\nabla\lambda_n \cdot \operatorname{curl}(\lambda_m))(\lambda_{l,x}^2 + \lambda_{l,y}^2) = 0.$$

Which is a contradiction because $\nabla\lambda_n \cdot \operatorname{curl}(\lambda_m) \neq 0$, as stated in (4.7), and $\lambda_{l,x}^2 + \lambda_{l,y}^2 \neq 0$, otherwise $\lambda_l \notin \mathbb{P}^1(T)$. Hence the only possible solution is $\alpha_m = \alpha_n = 0$.

To summarise we have just proven that it is not possible to construct a skew-symmetric bubble $\boldsymbol{\beta} \in \mathcal{B}_h^k(T)$, solely by the linear combination of two constant normal-tangential basis matrix functions $\boldsymbol{\xi}^i$.

If we now turn our attention to high order polynomials $k \geq 3$ the same arguments as for the $k = 2$ cases apply, except for the case $\alpha_l \neq 0, \alpha_m \neq 0$ and $\alpha_n \neq 0$. For this particular setting we always find a combination $\mu\lambda$ such that (4.9)

$$\mu\lambda = \mu_l\lambda_l = \mu_m\lambda_m = \mu_n\lambda_n,$$

is fulfilled. The system of equations (4.8) can then be expressed in the following form

$$\underbrace{\begin{pmatrix} a_l & a_m & a_n \\ (b_l + c_l) & (b_m + c_m) & (b_n + c_n) \\ (b_l - c_l) & (b_m - c_m) & (b_n - c_n) \end{pmatrix}}_{A} \begin{pmatrix} \alpha_l \\ \alpha_m \\ \alpha_n \end{pmatrix} = \begin{pmatrix} 0 \\ 0 \\ \neq 0 \end{pmatrix},$$

Die approbierte gedruckte Originalversion dieser Diplomarbeit ist an der TU Wien Bibliothek verfügbar
The approved original version of this thesis is available in print at TU Wien Bibliothek.
TU Bibliothek Your knowledge hub WIEN

where for a unique solution $\alpha_l, \alpha_m, \alpha_n$ the system matrix A has to be invertible, thus $\det(A) \neq 0$. For sake of readability we omit the step by step calculation of the determinant, on the contrary we just present the result

$$\begin{aligned}\det(A) =&\lambda_{l,x}\lambda_{l,y}(\lambda_{m,x}^2\lambda_{n,y}^2 - \lambda_{m,y}^2\lambda_{n,x}^2)+\\ &\lambda_{m,x}\lambda_{m,y}(\lambda_{n,x}^2\lambda_{l,y}^2 - \lambda_{n,y}^2\lambda_{l,x}^2)+\\ &\lambda_{n,x}\lambda_{n,y}(\lambda_{l,x}^2\lambda_{m,y}^2 - \lambda_{l,y}^2\lambda_{m,x}^2).\end{aligned}$$

Eventually, we exploit the property $\lambda_l + \lambda_m + \lambda_n = 1 \Rightarrow \nabla\lambda_l + \nabla\lambda_m + \nabla\lambda_n = \mathbf{0}$ to get

$$\det(A) = (\lambda_{m,y}\lambda_{n,x} - \lambda_{m,x}\lambda_{n,y})^3 = (\nabla\lambda_m \cdot \operatorname{curl}(\lambda_n))^3 \neq 0,$$

for the same reason discussed in (4.7). Hence, for a polynomial order $k \geq 3$ such that (4.9) is fulfilled e.g.

$$\begin{aligned} k &= 3 && \mu\lambda \in \{\lambda_l\lambda_m\lambda_n\}, \\ k &= 4 && \mu\lambda \in \{\lambda_l^2\lambda_m\lambda_n, \lambda_l\lambda_m^2\lambda_n, \lambda_l\lambda_m\lambda_n^2\}, \end{aligned}$$

we always find a linear combination $\alpha_l \neq 0, \alpha_m \neq 0, \alpha_n \neq 0$ such that $\operatorname{sym}(\boldsymbol{\beta})$ vanishes. To recapitulate the insights gained, which are also listed in Proposition 15: For any interior degree of freedom $\beta \in \mathcal{B}_h^k(T)$ and a polynomial order $k < 3$, the bubble $\boldsymbol{\beta}$ becomes never fully skew-symmetric, thus by norm equivalence on finite dimensional spaces it holds

$$\|\operatorname{skw}(\boldsymbol{\beta})\|_T \preceq \|\operatorname{sym}(\boldsymbol{\beta})\|_T \qquad \forall \boldsymbol{\beta} \in \mathcal{B}_h^k(T), k < 3.$$

On the other hand for a polynomial order $k \geq 3$ we found a subset $\mathcal{P}_h^b(T) \subset \mathcal{B}_h^k(T)$,

$$\mathcal{P}_h^b(T) := \left\{\boldsymbol{\beta} \in \mathcal{B}_h^k(T) : \boldsymbol{\xi}\lambda_i^{l+1}\lambda_{i+1}^{m+1}\lambda_{i+2}^{n+1}\Big|_{l,n,m\geq 0}^{l+n+m=k-3} \quad \boldsymbol{\xi} \in \mathbb{P}^0_{\operatorname{skw}}(T, \mathbb{R}^{2\times 2})\right\},$$

of all skew-symmetric bubbles $\boldsymbol{\beta}$. Therefore, by taking the set difference we can state

$$\|\operatorname{skw}(\boldsymbol{\beta})\|_T \preceq \|\operatorname{sym}(\boldsymbol{\beta})\|_T \qquad \forall \boldsymbol{\beta} \in (\mathcal{B}_h^k(T) \setminus P^b(T)), k \geq 3.$$

Equipped with the found norm equivalences, we can turn back to the proof of the LBB condition. We present two proofs for a low order case $k < 3$ and a high order case $k \geq 3$.

Low order LBB condition $k < 3$

Recall the norm partition

$$\|\overline{\boldsymbol{\tau}}_h\|^2 = \|\operatorname{sym}(\overline{\boldsymbol{\tau}}_h)\|^2 + \|\operatorname{skw}(\Pi^{\mathcal{B}_h^k}\overline{\boldsymbol{\tau}}_h)\|^2 + \|\operatorname{skw}((\mathrm{id} - \Pi^{\mathcal{B}_h^k})\overline{\boldsymbol{\tau}}_h)\|^2. \tag{4.10}$$

By Propositon 15 and the continuity of (4.5), there holds

$$\|\operatorname{skw}(\Pi^{\mathcal{B}_h^k}\overline{\boldsymbol{\tau}}_h)\|^2 \preceq \|\operatorname{sym}(\Pi^{\mathcal{B}_h^k}\overline{\boldsymbol{\tau}}_h)\|^2 \leq \|\operatorname{sym}(\overline{\boldsymbol{\tau}}_h)\|^2,$$

and therefore the norm equivalence

$$\|\overline{\boldsymbol{\tau}}_h\|^2 \sim \|\operatorname{sym}(\overline{\boldsymbol{\tau}}_h)\|^2 + \|\operatorname{skw}((\mathrm{id} - \Pi^{\mathcal{B}_h^k})\overline{\boldsymbol{\tau}}_h)\|^2. \tag{4.11}$$

Die approbierte gedruckte Originalversion dieser Diplomarbeit ist an der TU Wien Bibliothek verfügbar
The approved original version of this thesis is available in print at TU Wien Bibliothek.
TU Bibliothek Your knowledge hub WIEN

Now select

$$\begin{aligned} &\Xi_h \subset \Sigma_h^{\oplus}, && W_h \subset \Sigma_h^{\oplus}, && \operatorname{div}(V_h) \subset Q_h, \\ &\boldsymbol{\varepsilon}_h := \alpha \operatorname{sym}(\overline{\boldsymbol{\tau}}_h), && \boldsymbol{\omega}_h := \beta \operatorname{skw}((\mathrm{id} - \Pi^{\mathcal{B}_h^k})\overline{\boldsymbol{\tau}}_h), && \operatorname{div}(\boldsymbol{u}_h) := \gamma\, \overline{p}_h, \\ &\|\boldsymbol{\varepsilon}_h\| \leq \|\overline{\boldsymbol{\tau}}_h\|, && \|\boldsymbol{\omega}_h\| \leq \|\overline{\boldsymbol{\tau}}_h\|, && \|(\boldsymbol{u}_h, 0)\|_{U_h} \leq \|\overline{p}_h\|, \end{aligned}$$

where the scalars α, β, γ are currently arbitrary. By this special choice it readily follows for the norms

$$\|(\boldsymbol{\varepsilon}_h, (\boldsymbol{u}_h, \boldsymbol{\omega}_h))\|_{Y_h} \preceq \|(\overline{\boldsymbol{\tau}}_h, \overline{p}_h)\|_{X_h}, \tag{4.12}$$

and for the b_i bilinear forms

$$\begin{aligned} b_3(\boldsymbol{\varepsilon}_h, \overline{\boldsymbol{\tau}}_h) &= \alpha \|\operatorname{sym}(\overline{\boldsymbol{\tau}}_h)\|^2, \\ b_{2h}(\overline{\boldsymbol{\tau}}_h, (\boldsymbol{u}_h, \boldsymbol{\omega}_h)) &= \beta \|\operatorname{skw}((\mathrm{id} - \Pi^{\mathcal{B}_h^k})\overline{\boldsymbol{\tau}}_h)\|^2 - \sum_{T \in \mathcal{T}_h} \int_T \overline{\boldsymbol{\tau}}_h : \nabla \boldsymbol{u}_h \, dx + \sum_{F \in \mathcal{F}_h} \int_F (\overline{\boldsymbol{\tau}}_h)_{nt} [\![(\boldsymbol{u}_h)_t]\!] \, ds, \\ b_1(\boldsymbol{u}_h, \overline{p}_h) &= \gamma \|\overline{p}_h\|^2. \end{aligned}$$

By *Cauchy-Schwarz* and *Young's* inequality we bound $b_{2h}(\overline{\boldsymbol{\tau}}_h, (\boldsymbol{u}_h, \boldsymbol{\omega}_h))$ from below

$$\begin{aligned} b_{2h}(\overline{\boldsymbol{\tau}}_h, (\boldsymbol{u}_h, \boldsymbol{\omega}_h)) &\geq \beta \|\operatorname{skw}((\mathrm{id} - \Pi^{\mathcal{B}_h^k})\overline{\boldsymbol{\tau}}_h)\|^2 - \frac{\|\overline{\boldsymbol{\tau}}_h\|^2}{2} - \frac{\|(\boldsymbol{u}_h, 0)\|_{U_h}^2}{2} \\ &\succeq \beta \|\operatorname{skw}((\mathrm{id} - \Pi^{\mathcal{B}_h^k})\overline{\boldsymbol{\tau}}_h)\|^2 - \frac{\|\overline{\boldsymbol{\tau}}_h\|^2}{2} - \frac{\|\overline{p}_h\|^2}{2}. \end{aligned}$$

Now choose α, β, γ big enough and exploit the norm equivalence (4.11), then it follows

$$b_3(\boldsymbol{\varepsilon}_h, \overline{\boldsymbol{\tau}}_h) + b_{2h}(\overline{\boldsymbol{\tau}}_h, (\boldsymbol{u}_h, \boldsymbol{\omega}_h)) + b_1(\boldsymbol{u}_h, \overline{p}_h) \succeq \|\overline{\boldsymbol{\tau}}_h\|^2 + \|\overline{p}_h\|^2 \simeq \|(\overline{\boldsymbol{\tau}}_h, \overline{p}_h)\|_{X_h}^2. \tag{4.13}$$

Ultimately, by combining results (4.12) and (4.13) it yields

$$\begin{aligned} \sup_{(\boldsymbol{\varepsilon}_h, (\boldsymbol{u}_h, \boldsymbol{\omega}_h)) \in Y_h} \frac{|b_3(\boldsymbol{\varepsilon}_h, \overline{\boldsymbol{\tau}}_h) + b_{2h}(\overline{\boldsymbol{\tau}}_h, (\boldsymbol{u}_h, \boldsymbol{\omega}_h)) + b_1(\boldsymbol{u}_h, \overline{p}_h)|}{\|(\boldsymbol{\varepsilon}_h, (\boldsymbol{u}_h, \boldsymbol{\omega}_h))\|_{Y_h}} &\succeq \frac{\|(\overline{\boldsymbol{\tau}}_h, \overline{p}_h)\|_{X_h}^2}{\|(\overline{\boldsymbol{\tau}}_h, \overline{p}_h)\|_{X_h}} \\ &= \|(\overline{\boldsymbol{\tau}}_h, \overline{p}_h)\|_{X_h} \quad \forall (\overline{\boldsymbol{\tau}}_h, \overline{p}_h) \in X_h. \end{aligned}$$

Therefore we have proven the LBB condition (see Lemma 14) for the low order case $k < 3$.

High order LBB condition $k \geq 3$

For high order methods the norm equivalence (4.11) does not hold anymore, since we have seen in Proposition 15 that

$$\|\operatorname{skw}(\Pi^{\mathcal{B}_h^k} \overline{\boldsymbol{\tau}}_h)\|^2 \not\preceq \|\operatorname{sym}(\Pi^{\mathcal{B}_h^k} \overline{\boldsymbol{\tau}}_h)\|^2,$$

as there exists some fully skew symmetric bubbles $\boldsymbol{\beta} \in \mathcal{P}_h^b(T)$. To circumvent this problem we introduce a further projection onto the subset $\mathcal{P}_h^b(T)$

$$\int_T (\Pi^{\mathcal{B}_h^k} \overline{\boldsymbol{\tau}}_h|_T) : \boldsymbol{\psi}_h = \int_T \Pi^{\mathcal{P}_h^b} (\Pi^{\mathcal{B}_h^k} \overline{\boldsymbol{\tau}}_h|_T) : \boldsymbol{\psi}_h \qquad \forall \boldsymbol{\psi}_h \in \mathcal{P}_h^b(T), \tag{4.14}$$

TU Bibliothek Your knowledge hub WIEN
Die approbierte gedruckte Originalversion dieser Diplomarbeit ist an der TU Wien Bibliothek verfügbar
The approved original version of this thesis is available in print at TU Wien Bibliothek.

and we decompose

$$\|\mathrm{skw}(\Pi^{\mathcal{B}_h^k}\overline{\boldsymbol{\tau}}_h)\|^2 = \|\mathrm{skw}(\Pi^{\mathcal{P}_h^b}(\Pi^{\mathcal{B}_h^k}\overline{\boldsymbol{\tau}}_h))\|^2 + \|\underbrace{\mathrm{skw}((\mathrm{id}-\Pi^{\mathcal{P}_h^b})(\Pi^{\mathcal{B}_h^k}\overline{\boldsymbol{\tau}}_h))}_{\in(\mathcal{B}_h^k(T)\setminus P_h^b(T))}\|^2.$$

By Proposition 15 and continuity of the projections (4.5) and (4.14) it holds now, similarly to the low order case,

$$\|\mathrm{skw}((\mathrm{id}-\Pi^{\mathcal{P}_h^b})(\Pi^{\mathcal{B}_h^k}\overline{\boldsymbol{\tau}}_h))\|^2 \preceq \|\mathrm{sym}((\mathrm{id}-\Pi^{\mathcal{P}_h^b})(\Pi^{\mathcal{B}_h^k}\overline{\boldsymbol{\tau}}_h))\|^2 \leq \|\mathrm{sym}(\overline{\boldsymbol{\tau}}_h)\|^2.$$

Due to the definition of $\mathcal{P}_h^b$ we can omit $\mathrm{skw}(\cdot)$ in

$$\|\mathrm{skw}(\Pi^{\mathcal{P}_h^b}(\Pi^{\mathcal{B}_h^k}\overline{\boldsymbol{\tau}}_h))\|^2 = \|\Pi^{\mathcal{P}_h^b}(\Pi^{\mathcal{B}_h^k}\overline{\boldsymbol{\tau}}_h)\|^2.$$

In two dimensions, a skew-symmetric matrix $\Pi^{\mathcal{P}_h^b}(\Pi^{\mathcal{B}_h^k}\overline{\boldsymbol{\tau}}_h|_T) \in \mathcal{P}_h^b(T)$ consists of only one component with different signs. Let w_s denote this scalar component on an arbitrary element T

$$w_s = c\lambda_i^{l+1}\lambda_{i+1}^{m+1}\lambda_{i+2}^{n+1}\big|_{l,n,m\geq 0}^{l+n+m=k-3},$$

where $c \in \mathbb{R}$. It is clear, that $w_s(T)$ vanishes on the boundary ∂T. For this reason we can use *Poincaré*'s inequality [BBF13, Eq.1.2.14]

$$\|\Pi^{\mathcal{P}_h^b}(\Pi^{\mathcal{B}_h^k}\overline{\boldsymbol{\tau}}_h|_T)\|_T^2 = 2\|w_s\|_T^2 \leq 2h_T^2\|\nabla w_s\|_T^2.$$

Since in a two dimensional setting there holds $\|\nabla w_s\|_T = \|\mathrm{curl}(w_s)\|_T$, we get that

$$\|\Pi^{\mathcal{P}_h^b}(\Pi^{\mathcal{B}_h^k}\overline{\boldsymbol{\tau}}_h|_T)\|_T^2 = 2\|w_s\|_T^2 \leq 2h_T^2\|\nabla w_s\|_T^2 = 2h_T^2\|\mathrm{curl}(w_s)\|_T^2 = 2h_T^2\|\mathrm{div}(\Pi^{\mathcal{P}_h^b}(\Pi^{\mathcal{B}_h^k}\overline{\boldsymbol{\tau}}_h|_T))\|_T^2,$$

and therefore the upper bound on the domain Ω

$$\|\mathrm{skw}(\Pi^{\mathcal{B}_h^k}\overline{\boldsymbol{\tau}}_h)\|^2 \preceq \|\mathrm{sym}(\overline{\boldsymbol{\tau}}_h)\|^2 + \|\mathrm{div}(\Pi^{\mathcal{P}_h^b}(\Pi^{\mathcal{B}_h^k}\overline{\boldsymbol{\tau}}_h))\|^2 = \|\mathrm{sym}(\overline{\boldsymbol{\tau}}_h)\|^2 + \|\mathrm{curl}(w_s)\|^2, \tag{4.15a}$$

$$\|\overline{\boldsymbol{\tau}}_h\|^2 \preceq \|\mathrm{sym}(\overline{\boldsymbol{\tau}}_h)\|^2 + \|\mathrm{curl}(w_s)\|^2 + \|\mathrm{skw}((\mathrm{id}-\Pi^{\mathcal{B}_h^k})\overline{\boldsymbol{\tau}}_h)\|^2. \tag{4.15b}$$

In comparison to the lower order case (4.11), a new term appeared in the upper bound, namely $\|\mathrm{curl}(w_s)\|^2$, which has to be controlled. A closer look shows that $\mathrm{curl}(w_s)$ is divergence-free by definition on every element T, therefore on the whole domain Ω

$$\int_T \mathrm{div}(\mathrm{curl}(w_s)) = 0$$

Additionally, $\mathrm{curl}(w_s)$ has also continuous normal component, namely zero

$$\int_{\partial T} \mathrm{curl}(w_s)\cdot\boldsymbol{n} = \int_{\partial T} \nabla w_s \cdot \boldsymbol{t} = 0.$$

Upper property is crucial, as it implies that $\mathrm{curl}(w_s) \in V_h$. For this reason we construct $\boldsymbol{u}_h = \boldsymbol{u}_{h,1} + \boldsymbol{u}_{h,2}$ such that

$$\begin{aligned} \mathrm{div}(V_h) &\subset Q_h, & \mathrm{div}(\mathcal{P}_h^b) &\subset V_h,\\ \mathrm{div}(\boldsymbol{u}_{h,1}) &:= \gamma\overline{p}_h, & \boldsymbol{u}_{h,2} &:= \delta\,\mathrm{curl}(w_s),\\ \|(\boldsymbol{u}_{h,1},0)\|_{U_h} &\leq \|\overline{p}_h\|, & \|(\boldsymbol{u}_{h,2},0)\|_{U_h} &\leq \|\overline{\boldsymbol{\tau}}_h\|, \end{aligned}$$

TU Bibliothek Your knowledge hub WIEN
Die approbierte gedruckte Originalversion dieser Diplomarbeit ist an der TU Wien Bibliothek verfügbar
The approved original version of this thesis is available in print at TU Wien Bibliothek.

and chose the remaining quantities $\boldsymbol{\varepsilon}_h$ and $\boldsymbol{\omega}_h$ as in the lower order case, namely

$$\begin{aligned} \Xi_h &\subset \Sigma_h^{\oplus}, & W_h &\subset \Sigma_h^{\oplus}, \\ \boldsymbol{\varepsilon}_h &:= \alpha\,\mathrm{sym}(\overline{\boldsymbol{\tau}}_h), & \boldsymbol{\omega}_h &:= \beta\,\mathrm{skw}((\mathrm{id} - \Pi^{\mathcal{B}_h^k})\overline{\boldsymbol{\tau}}_h), \\ \|\boldsymbol{\varepsilon}_h\| &\leq \|\overline{\boldsymbol{\tau}}_h\|, & \|\boldsymbol{\omega}_h\| &\leq \|\overline{\boldsymbol{\tau}}_h\|. \end{aligned}$$

For the time being the scalars $\alpha, \beta, \gamma, \delta \in \mathbb{R}$ are arbitrary. Once again, by this choice it holds

$$\|(\boldsymbol{\varepsilon}_h, (\boldsymbol{u}_h, \boldsymbol{\omega}_h))\|_{Y_h} \preceq \|(\overline{\boldsymbol{\tau}}_h, \overline{p}_h)\|_{X_h}. \tag{4.16}$$

The b_i bilinear forms differ compared to the low order case, because of the linear combination $\boldsymbol{u}_h = \boldsymbol{u}_{h,1} + \boldsymbol{u}_{h,2}$

$$\begin{aligned} b_3(\boldsymbol{\varepsilon}_h, \overline{\boldsymbol{\tau}}_h) &= \alpha \|\mathrm{sym}(\overline{\boldsymbol{\tau}}_h)\|^2, \\ b_{2h}(\overline{\boldsymbol{\tau}}_h, (0, \boldsymbol{\omega}_h)) &= \beta \|\mathrm{skw}((\mathrm{id} - \Pi^{\mathcal{B}_h^k}))\|^2, \\ b_{2h}(\overline{\boldsymbol{\tau}}_h, (\boldsymbol{u}_{h,1}, 0)) &= -\sum_{T \in \mathcal{T}_h} \int_T \overline{\boldsymbol{\tau}}_h : \nabla \boldsymbol{u}_{h,1}\, dx + \sum_{F \in \mathcal{F}_h} \int_F (\overline{\boldsymbol{\tau}}_h)_{nt} [\![(\boldsymbol{u}_{h,1})_t]\!]\, ds, \\ b_{2h}(\overline{\boldsymbol{\tau}}_h, (\boldsymbol{u}_{h,2}, 0)) &= \sum_{T \in \mathcal{T}_h} \int_T \mathrm{div}(\overline{\boldsymbol{\tau}}_h) : \boldsymbol{u}_{h,2}\, dx - \sum_{F \in \mathcal{F}_h} \int_F (\overline{\boldsymbol{\tau}}_h)_{nn} \underbrace{[\![(\boldsymbol{u}_{h,2})_n]\!]}_{=0}\, ds, \\ b_1(\boldsymbol{u}_h, \overline{p}_h) &= \int_\Omega \mathrm{div}(\boldsymbol{u}_{h,1}) \overline{p}_h\, dx + \int_\Omega \underbrace{\mathrm{div}(\boldsymbol{u}_{h,2})}_{=0} \overline{p}_h\, dx = \gamma \|\overline{p}_h\|^2. \end{aligned}$$

Reusing *Cauchy-Schwarz* and *Young's* inequality we bound $b_{2h}(\overline{\boldsymbol{\tau}}_h, (\boldsymbol{u}_{h,1}, 0))$ from below

$$b_{2h}(\overline{\boldsymbol{\tau}}_h, (\boldsymbol{u}_{h,1}, 0)) \geq -\frac{\|\overline{\boldsymbol{\tau}}_h\|^2}{2} - \frac{\|(\boldsymbol{u}_{h,1}, 0)\|_{U_h}^2}{2} \geq -\frac{\|\overline{\boldsymbol{\tau}}_h\|^2}{2} - \frac{\|\overline{p}_h\|^2}{2},$$

while $b_{2h}(\overline{\boldsymbol{\tau}}_h, (\boldsymbol{u}_{h,2}, 0))$ can also bound from below by

$$\begin{aligned} b_{2h}(\overline{\boldsymbol{\tau}}_h, (\boldsymbol{u}_{h,2}, 0)) &= \delta \sum_{T \in \mathcal{T}_h} \int_T \mathrm{div}(\overline{\boldsymbol{\tau}}_h) : \mathrm{div}(\Pi^{\mathcal{P}_h^b}(\Pi^{\mathcal{B}_h^k} \overline{\boldsymbol{\tau}}_h))\, dx \\ &\geq \delta \|\mathrm{div}(\Pi^{\mathcal{P}_h^b}(\Pi^{\mathcal{B}_h^k} \overline{\boldsymbol{\tau}}_h))\|^2 = \delta \|\mathrm{curl}(w_s)\|^2. \end{aligned}$$

By choosing $\alpha, \beta, \gamma, \delta$ big enough, using the norm equivalence (4.15b) and the expression

$$b_{2h}(\overline{\boldsymbol{\tau}}_h, (\boldsymbol{u}_h, \boldsymbol{\omega}_h)) = b_{2h}(\overline{\boldsymbol{\tau}}_h, (\boldsymbol{u}_{h,1}, 0)) + b_{2h}(\overline{\boldsymbol{\tau}}_h, (\boldsymbol{u}_{h,2}, 0)) + b_{2h}(\overline{\boldsymbol{\tau}}_h, (0, \boldsymbol{\omega}_h)),$$

it does hold

$$b_3(\boldsymbol{\varepsilon}_h, \overline{\boldsymbol{\tau}}_h) + b_{2h}(\overline{\boldsymbol{\tau}}_h, (\boldsymbol{u}_h, \boldsymbol{\omega}_h)) + b_1(\boldsymbol{u}_h, \overline{p}_h) \succeq \|\overline{\boldsymbol{\tau}}_h\|^2 + \|\overline{p}_h\|^2 \simeq \|(\overline{\boldsymbol{\tau}}_h, \overline{p}_h)\|_{X_h}^2. \tag{4.17}$$

In a similar fashion as for the low order case, does the high order LBB condition follow from the combination of (4.16) and (4.17)

$$\begin{aligned} \sup_{(\boldsymbol{\varepsilon}_h, (\boldsymbol{u}_h, \boldsymbol{\omega}_h)) \in Y_h} \frac{|b_3(\boldsymbol{\varepsilon}_h, \overline{\boldsymbol{\tau}}_h) + b_{2h}(\overline{\boldsymbol{\tau}}_h, (\boldsymbol{u}_h, \boldsymbol{\omega}_h)) + b_1(\boldsymbol{u}_h, \overline{p}_h)|}{\|(\boldsymbol{\varepsilon}_h, (\boldsymbol{u}_h, \boldsymbol{\omega}_h))\|_{Y_h}} &\succeq \frac{\|(\overline{\boldsymbol{\tau}}_h, \overline{p}_h)\|_{X_h}^2}{\|(\overline{\boldsymbol{\tau}}_h, \overline{p}_h)\|_{X_h}} \\ &= \|(\overline{\boldsymbol{\tau}}_h, \overline{p}_h)\|_{X_h} \quad \forall (\overline{\boldsymbol{\tau}}_h, \overline{p}_h) \in X_h. \end{aligned}$$

In summary, we have presented a low and high order proof of the LBB condition (see Lemma 14) and shown the remaining conditions of *Brezzi's* theorem (see Theorem 1). For this reason the newly introduced mass conserving mixed stress-strain rate finite element ($\mathcal{MCS}$-$\mathcal{S}$) solves the discrete variational formulation VIII.

Die approbierte gedruckte Originalversion dieser Diplomarbeit ist an der TU Wien Bibliothek verfügbar
The approved original version of this thesis is available in print at TU Wien Bibliothek.
TU Bibliothek Your knowledge hub WIEN

4.4 Non-Newtonian extension

So far, we presented inf-sup stable finite elements suitable for the simulation of Newtonian flows. We will now discuss the inclusion of a non-linear constitutive relation between the deviatoric stress tensor $\boldsymbol{\tau}$ and the rate-of-strain tensor $\boldsymbol{\varepsilon}(\boldsymbol{u})$. Solvability of the arising non-linear discrete variational formulation will not be discussed in this work, but only referenced.
Consider an implicit constitutive relation of the form $\mathcal{G}(\boldsymbol{\tau}, \boldsymbol{\varepsilon}(\boldsymbol{u})) = 0$. The governing equations for a Stokes flow with homogeneous boundary conditions become

$$\begin{aligned} \mathcal{G}(\boldsymbol{\tau}, \boldsymbol{\varepsilon}(\boldsymbol{u})) &= 0 && \text{in } \Omega, \\ -\operatorname{div}(\boldsymbol{\tau}) &= -\nabla p + \rho \boldsymbol{f} && \text{in } \Omega, \\ \operatorname{div}(\boldsymbol{u}) &= 0, && \text{in } \Omega, \\ \boldsymbol{u} &= 0 && \text{on } \Gamma_D. \end{aligned}$$

In some cases the implicit form $\mathcal{G}(\boldsymbol{\tau}, \boldsymbol{\varepsilon}(\boldsymbol{u})) = 0$ can be reformulated in an explicit matter e.g. for

$$\mathcal{G}(\boldsymbol{\tau}, \boldsymbol{\varepsilon}(\boldsymbol{u})) = \boldsymbol{\tau} - 2\mu\boldsymbol{\varepsilon}(\boldsymbol{u}) = 0$$

we recover the Newtonian Stokes problem (3.1). In every non-Newtonian model presented in Chapter 2 the deviatoric stress tensor $\boldsymbol{\tau}$ is given explicitly. Consider e.g. the power-law model (2.7)

$$\boldsymbol{\tau} = 2K\left(2|\boldsymbol{\varepsilon}(\boldsymbol{u})|\right)^{r-2}\boldsymbol{\varepsilon}(\boldsymbol{u}) \qquad K > 0, 2 > r > 1$$

For this particular case the finite elements ($\mathcal{TH}$, $\mathcal{SV}$, $\mathcal{TH}$-$\mathcal{S}$, $\mathcal{SV}$-$\mathcal{S}$, $\mathcal{MCS}$, $\mathcal{MCS}$-$\mathcal{S}$) are all suited to approximate the arising non-linear problem. It starts to become problematic for the two-field *Taylor-Hood* ($\mathcal{TH}$) and *Scott-Vogelius* ($\mathcal{SV}$) element if the deviatoric stress tensor $\boldsymbol{\tau}$ is given implicitly as e.g. for the *Ellis* model [GO20, Eq. 1.15]

$$\boldsymbol{\tau} = \frac{\mu_0}{1 + \alpha|\boldsymbol{\tau}|^{q-2}}\boldsymbol{\varepsilon}(\boldsymbol{u}) \qquad \alpha > 0, q > 1$$

Since these velocity-pressure finite elements ($\mathcal{TH}$, $\mathcal{SV}$) do not model stresses, it is impossible for them to resolve such a constitutive relation. Although the ($\mathcal{MCS}$) mixed finite element is capable to solve the non-linear Stokes problem with an implicit relation for the stresses, it has a major drawback, namely the requirement for the deviatoric stress tensor $\boldsymbol{\tau}$ to be proportional to the rate-of-strain tensor $\boldsymbol{\varepsilon}(\boldsymbol{u})$. This follows from the splitting of $\boldsymbol{\varepsilon}(\boldsymbol{u})$ in the derivation of the discrete (non-)linear variational formulation in a asymmetric and a skew-symmetric part

$$\boldsymbol{\varepsilon}(\boldsymbol{u}) = \nabla\boldsymbol{u} - \boldsymbol{\omega}$$

For this reason the integration of more sophisticated models is in general not possible for the ($\mathcal{MCS}$) method. On the other hand, the inclusion of an arbitrary implicit constitutive relation of the form $\mathcal{G}(\boldsymbol{\tau}, \boldsymbol{\varepsilon}(\boldsymbol{u})) = 0$ is very natural for the ($\mathcal{TH}$-$\mathcal{S}$, $\mathcal{SV}$-$\mathcal{S}$, $\mathcal{MCS}$-$\mathcal{S}$) mixed finite elements. For these discrete methods, the entire implicit relationship is tested with piecewise discontinuous symmetric matrix-valued polynomials

$$\begin{aligned} (\mathcal{TH}\text{-}\mathcal{S},\ \mathcal{SV}\text{-}\mathcal{S}) \qquad & \int_\Omega \mathcal{G}(\boldsymbol{\tau}_h, \boldsymbol{\varepsilon}(\boldsymbol{u}_h)) : \overline{\boldsymbol{\tau}}_h \, dx = 0 && \forall \overline{\boldsymbol{\tau}}_h \in \Sigma_h, \\ (\mathcal{MCS}\text{-}\mathcal{S}) \qquad & \int_\Omega \mathcal{G}(\boldsymbol{\tau}_h, \boldsymbol{\varepsilon}_h) : \overline{\boldsymbol{\varepsilon}}_h \, dx = 0 && \forall \overline{\boldsymbol{\varepsilon}}_h \in \Xi_h \end{aligned}$$

Die approbierte gedruckte Originalversion dieser Diplomarbeit ist an der TU Wien Bibliothek verfügbar
The approved original version of this thesis is available in print at TU Wien Bibliothek.
TU Bibliothek Your knowledge hub WIEN

without the necessity to reshape the implicit constitutive law in an explicit matter. This is a big plus.
The cornerstone of implicit constitutive relations was laid by *Rajagopal* in [Raj03, Raj06]. His concept introduced in these papers provides a new framework for the formulation of sophisticated constitutive relations in harmony with the second law of thermodynamics. Such implicit constitutive relation e.g. allow for a pressure i.e. mean normal stress dependent viscosity [GO20, Eq. 1.17]

$$\mathcal{G}(\boldsymbol{\sigma}, \boldsymbol{\varepsilon}(\boldsymbol{u})) = \boldsymbol{\sigma} - \left(2\mu(|\boldsymbol{\varepsilon}(\boldsymbol{u})|, \tfrac{1}{d}\mathrm{tr}(\boldsymbol{\sigma})) + \frac{\tau_y(\frac{1}{d}\mathrm{tr}(\boldsymbol{\sigma}))}{|\boldsymbol{\varepsilon}(\boldsymbol{u})|} \right) \boldsymbol{\varepsilon}(\boldsymbol{u}) = 0$$

The *Bingham* model (2.9) presented in Chapter 2 can be described very naturally by a continuous implicit relation [GO20, Eq. 1.13]

$$\mathcal{G}(\boldsymbol{\tau}, \boldsymbol{\varepsilon}(\boldsymbol{u})) = 2\mu \left(\tau_y + (|\boldsymbol{\tau}| - \tau_y)^+ \right) \boldsymbol{\varepsilon}(\boldsymbol{u}) - (|\boldsymbol{\tau}| - \tau_y)^+ \boldsymbol{\tau} = 0$$

where $\psi^+ := \max(\psi, 0)$.

Die approbierte gedruckte Originalversion dieser Diplomarbeit ist an der TU Wien Bibliothek verfügbar
The approved original version of this thesis is available in print at TU Wien Bibliothek.
TU Bibliothek Your knowledge hub WIEN

5

Non-Newtonian Numerical Experiments

In this chapter we perform non-Newtonian numerical experiments of the steady *Stokes* equations (3.1) using the mixed finite elements ($\mathcal{TH}$-$\mathcal{S}$, $\mathcal{SV}$-$\mathcal{S}$, $\mathcal{MCS}$) and the new finite element ($\mathcal{MCS}$-$\mathcal{S}$) introduced in Chapter 4. In particular we focus on the two-dimensional simulation of power-law (2.7) and *Bingham* (2.9) like fluids.

5.1 Experimental setting

All experiments have been carried out using the open-source finite element software *NGSolve/Netgen* (Version 6.2.2102) [Sch97, Sch14] on the local cluster *Matrix* at the Institute of Analysis and Scientific Computing, Vienna University of Technology. The cluster consists of two *Intel Xeon E5-2670 v3* processors with 30 Mb Cache and in total 48 threads when Hyper-Threading enabled.
For every numerical experiment we used a unstructured two-dimensional triangulation $\mathcal{T}_h$, even if the geometry would allow for a structured mesh. This decision is motivated by the intention to consider a more general setting, where a structured triangulation is not applicable.
To solve the arising non-linear system either *Newton's* or a fixed point method has been implemented following the scheme in operator form

***Newton's* method:**

$$\begin{aligned} \boldsymbol{x}^{k+1} &= \boldsymbol{x}^k + d\,\boldsymbol{\delta x} \\ \mathcal{R}(\boldsymbol{x}) &:= \boldsymbol{f} - \boldsymbol{g}(\boldsymbol{x}) \\ \delta\boldsymbol{x} &= -\underline{A}^{-1}(\boldsymbol{x}^k)\mathcal{R}(\boldsymbol{x}^k) \end{aligned}$$

Fixed point method:

$$\begin{aligned} \boldsymbol{x}^{k+1} &= \boldsymbol{x}^k + d\,\boldsymbol{\delta x} \\ \mathcal{R}(\boldsymbol{x}) &:= \boldsymbol{f} - A(\boldsymbol{x}^k)\boldsymbol{x} \\ \delta\boldsymbol{x} &= -A^{-1}(\boldsymbol{x}^k)\mathcal{R}(\boldsymbol{x}^k) \end{aligned}$$

where $\boldsymbol{x}^k$ is the solution vector at iteration k, $\boldsymbol{\delta x}$ the search direction, d a damping parameter, $\mathcal{R}(\boldsymbol{x})$ the residual vector, $\underline{A}(\boldsymbol{x})$ the linearised system matrix, $A(\boldsymbol{x})$ a suitable fixed point system matrix, $\boldsymbol{g}(\boldsymbol{x})$ a non-linear operator and $\boldsymbol{f}$ the right-hand side. In *NGSolve/Netgen* the assembly of the linearised system matrix $\underline{A}$ is done by automatic differentiation [GSMS20]. Although two Line Search algorithms (L^2 Line Search, Backtracking Line Search) [BKST15, Alg. 2, Alg. 3] for the damping parameter d have been implemented, it did not appear to converge any better. For this reason the damping parameter d has been determined empirically. The solution is deemed to have converged when the search direction $\boldsymbol{\delta x}$ is almost orthogonal to the residual $\mathcal{R}(\boldsymbol{x}^k)$

$$\sqrt{|\boldsymbol{\delta x} \cdot \mathcal{R}(\boldsymbol{x}^k)|} \leq 10^{-8}$$

Die approbierte gedruckte Originalversion dieser Diplomarbeit ist an der TU Wien Bibliothek verfügbar
The approved original version of this thesis is available in print at TU Wien Bibliothek.
TU Bibliothek Your knowledge hub WIEN

where in each iteration step the linear system gets solved by the Intel MKL PARDISO parallel direct sparse solver [SG04]. As an inital guess $\boldsymbol{x}^0$ for the non-linear solution process, we found it appropriate to use the discrete result from a Newtonian simulation. To speed up the solution process static condensation was applied such that internal degrees of freedom are eliminated from the global linear system.

5.2 Newtonian convergence order

Before we focused on the simulation of non-Newtonian flows, all implemented finite elements ($\mathcal{TH}$-$\mathcal{S}$, $\mathcal{SV}$-$\mathcal{S}$, $\mathcal{MCS}$, $\mathcal{MCS}$-$\mathcal{S}$) underwent a Newtonian convergence order test [GLS19, Section 7]. For this recall *Stokes equations* in Newtonian setting with homogeneous boundary conditions (3.1)

$$\begin{aligned} \boldsymbol{\tau} &= 2\mu\boldsymbol{\varepsilon}(\boldsymbol{u}) && \text{in } \Omega, && \text{(5.1a)}\\ -\operatorname{div}(\boldsymbol{\tau}) &= -\nabla p + \rho\boldsymbol{f} && \text{in } \Omega, && \text{(5.1b)}\\ \operatorname{div}(\boldsymbol{u}) &= 0, && \text{in } \Omega, && \text{(5.1c)}\\ \boldsymbol{u} &= 0 && \text{on } \Gamma_D && \text{(5.1d)} \end{aligned}$$

Consider a two-dimensional domain $\Omega = [0,1]^2$ with coordinates x and y. We prescribe on the unit square a potential ϕ and a pressure p

$$\begin{aligned} \phi &= x^2(1-x)^2y^2(1-y)^2\\ p &= x^5 + y^5 - \frac{1}{3} \end{aligned}$$

Note, that the pressure has zero mean value on Ω. The velocity $\boldsymbol{u}$ is determined by $\operatorname{curl}(\phi)$

$$\boldsymbol{u} = \operatorname{curl}(\phi) = \begin{pmatrix} 2x^2(1-x)^2y(1-y)(1-2y)\\ -2y^2(1-y)^2x(1-x)(1-2x) \end{pmatrix}$$

On the boundary Γ_D we see that the homogeneous boundary conditions are fulfilled. Further, also the incompressibility constraint is trivial, as by construction $\operatorname{div}(\boldsymbol{u}) = \operatorname{div}(\operatorname{curl}(\phi)) = 0$. The rate-of-strain tensor $\boldsymbol{\varepsilon}(\boldsymbol{u})$ is given as

$$\begin{aligned} \varepsilon_{xx} &= 4xy\,(x-1)\,(y-1)\,(xy + x\,(y-1) + y\,(x-1) + (x-1)\,(y-1))\\ \varepsilon_{xy} &= 5x^2y^2((x-1)^2 - (y-1)^2) - 4xy(x\,(x-1)^2 - y\,(y-1)^2) + (x^2-y^2)\,(x-1)^2\,(y-1)^2\\ \varepsilon_{yx} &= \varepsilon_{xy}\\ \varepsilon_{yy} &= -4xy\,(x-1)\,(y-1)\,(xy + x\,(y-1) + y\,(x-1) + (x-1)\,(y-1)) \end{aligned}$$

A contour plot of the magnitude of the velocity $\boldsymbol{u}$ and rate-of-strain $\boldsymbol{\varepsilon}(\boldsymbol{u})$ is shown in Figure 5.1 Consequently, by the constitutive relation (5.1a) the deviatoric stress tensor $\boldsymbol{\tau}$ is then just a multiple of the rate-of-strain tensor $\boldsymbol{\varepsilon}(\boldsymbol{u})$. By substituting τ and the gradient of the prescribed pressure p into the momentum equation (5.1b) we obtain an expression for the forcing $\boldsymbol{f}$, which is our input for the numerical simulation and is omitted for sake of simplicity.
In [GLS19, FP89, AMS+04] it is proven, that for smooth enough $\boldsymbol{u} \in H^1(\Omega,\mathbb{R}^d) \cap H^m(\mathcal{T}_h,\mathbb{R}^d)$, $\boldsymbol{\tau} \in H^1(\Omega,\mathbb{R}^d) \cap H^{m-1}(\mathcal{T}_h,\mathbb{R}^d)$ and $p \in L^2_0(\Omega,\mathbb{R}) \cap H^{m-1}(\mathcal{T}_h,\mathbb{R})$ the following

Die approbierte gedruckte Originalversion dieser Diplomarbeit ist an der TU Wien Bibliothek verfügbar
The approved original version of this thesis is available in print at TU Wien Bibliothek.
TU Bibliothek Your knowledge hub WIEN

(a) Velocity magnitude $\|\boldsymbol{u}\|$ (b) Rate-of-strain magnitude $\|\boldsymbol{\varepsilon}\|$

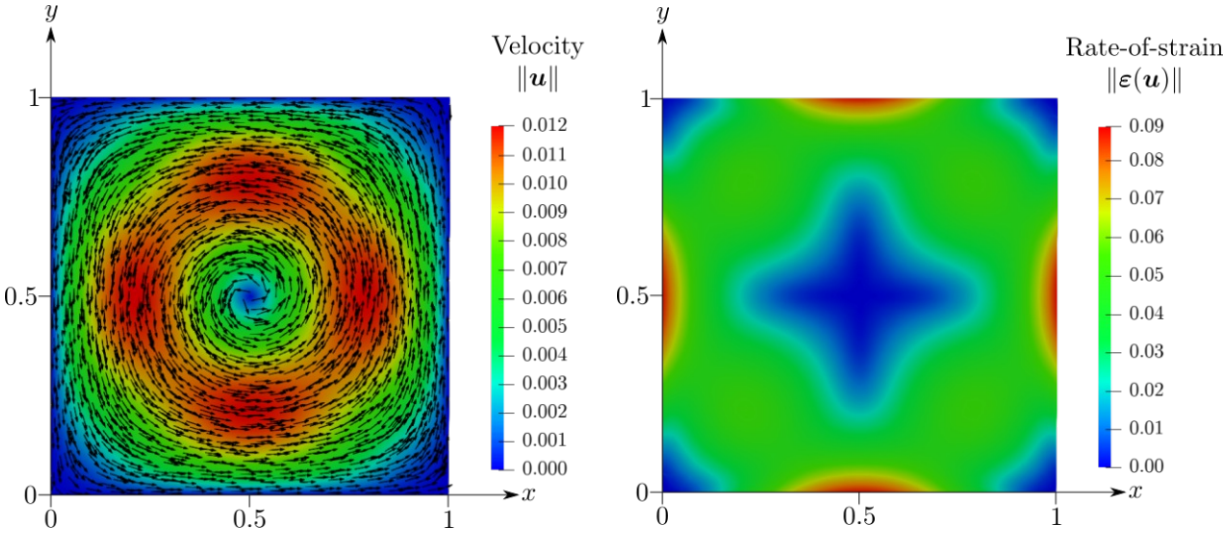

FIGURE 5.1 – Exact solution contour plots of Newtonian benchmark

error estimate holds

$$\|\boldsymbol{u}-\boldsymbol{u}_h\|_V + \frac{\rho}{\mu}\|\boldsymbol{\tau}-\boldsymbol{\tau}_h\|_\Sigma + \frac{\rho}{\mu}\|p-p_h\|_Q \preceq h^s\left(\|u\|_{H^{s+1}} + \frac{\rho}{\mu}\|\boldsymbol{\tau}\|_{H^s} + \frac{\rho}{\mu}\|p\|_{H^s}\right) \tag{5.2}$$

$$\|\boldsymbol{u}-\boldsymbol{u}_h\|_{L_2} \preceq h^{s+1}\|u\|_{H^{s+1}} \tag{5.3}$$

where the quantities $\{\boldsymbol{u}, \boldsymbol{\tau}, \boldsymbol{\varepsilon}(\boldsymbol{u}), p\}$ represent the exact solution of the mixed Stokes problem, while $\{\boldsymbol{u}_h, \boldsymbol{\tau}_h, \boldsymbol{\varepsilon}(\boldsymbol{u}_h), p_h\}$ is the finite element solution and $s = \min(m-1, k)$. In order to avoid a blow up of the errors $\|\boldsymbol{\psi} - \boldsymbol{\psi}_h\|$ of non mass-conserving finite elements due to the viscosity, the dynamic viscosity and density is chosen as $\mu = 1$ and $\rho = 1$, equivalently the kinematic viscosity $\nu = 1$. As the prescribed quantities in the test case are all polynomials of some degree, we can safely assume enough regularity of the exact solutions $\{\boldsymbol{u}, \boldsymbol{\tau}, \boldsymbol{\varepsilon}(\boldsymbol{u}), p\}$, therefore $s = k$.
In Figure 5.2 we see the obtained errors over different mesh sizes h for a polynomial order $k = 2$, which are in good agreement with the error estimate (5.2). Although we have not provided an error estimate for the finite element ($\mathcal{MCS}$-$\mathcal{S}$), the method recovers the same order of convergence as ($\mathcal{TH}$-$\mathcal{S}$, $\mathcal{SV}$-$\mathcal{S}$, $\mathcal{MCS}$).

5.3 Non-Newtonian channel flow

Finally, we shall tackle Non-Newtonian flows. To do this we consider a geometry, which is often used [HMST17, GW11, GO20] for its beneficial properties, namely a two-dimensional channel. For a steady laminar flow between two plates, it is known that the velocity field is purely unidirectional. This facilitates the determination of an analytical solution for non-Newtonian fluids (see Appendix A). Another advantage is the application of boundary conditions, because all quantities can be regarded as periodic. This means that we do not have to specify an inlet velocity profile $\boldsymbol{u}_{inlet}$, but only a forcing term $\boldsymbol{f}$, which in our numerical examples is constant e.g. gravity or a pressure drop. Of course, on the walls we apply the standard homogeneous no-slip boundary condition for the velocity $\boldsymbol{u}$. Furthermore, because of the periodic boundary conditions, the computational domain in

Die approbierte gedruckte Originalversion dieser Diplomarbeit ist an der TU Wien Bibliothek verfügbar
The approved original version of this thesis is available in print at TU Wien Bibliothek.
TU Bibliothek Your knowledge hub WIEN

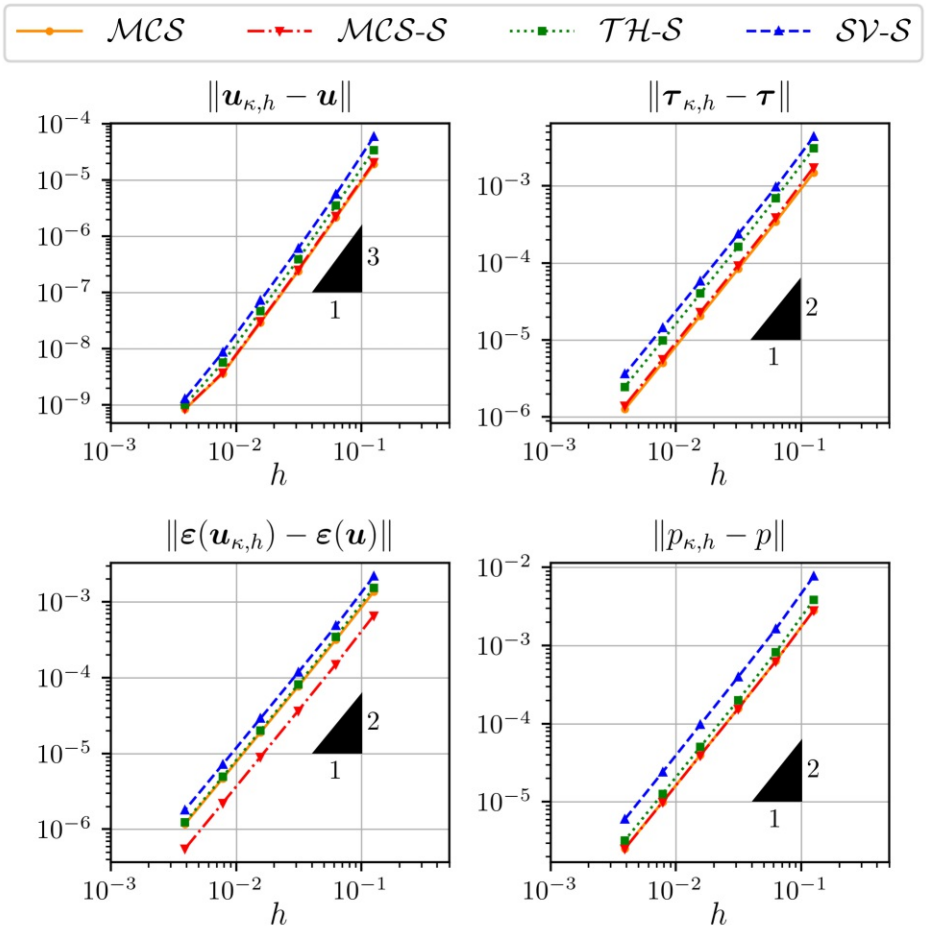

FIGURE 5.2 – L^2-errors of polynomial order $k = 2$ over mesh size h for Newtonian Stokes flow (see Table B.1). The expected convergence order from the error estimate (5.2) is represented as a slope marker

flow direction does not have to be large enough to account for the flow development. The computational domain $\Omega = (0, -1) \times (1, 1)$ used for the numerical examples together with an example of an unstructured mesh is illustrated in Figure 5.3. The above mentioned properties result in the following governing equations

$$\mathcal{G}(\boldsymbol{\tau}, \boldsymbol{\varepsilon}(\boldsymbol{u})) = 0 \qquad \text{in } \Omega, \tag{5.4a}$$
$$-\operatorname{div}(\boldsymbol{\tau}) = -\nabla p + \rho \boldsymbol{f} \qquad \text{in } \Omega, \tag{5.4b}$$
$$\operatorname{div}(\boldsymbol{u}) = 0, \qquad \text{in } \Omega, \tag{5.4c}$$
$$\boldsymbol{u} = 0 \qquad \text{on } \Gamma_{wall} \tag{5.4d}$$
$$(\cdot)(x = 1) = (\cdot)(x = 0) \qquad \text{on } \Gamma_{periodic} \tag{5.4e}$$

where $\mathcal{G}(\boldsymbol{\tau}, \boldsymbol{\varepsilon}(\boldsymbol{u}))$ is an implicit relation as mentioned in 4.4, which depending on the model can also be specified in an explicit form.
Throughout our numerical experiments we use a normalized density $\rho = 1$. The prescribed forcing term $\boldsymbol{f}$, was chosen such

$$\boldsymbol{f} = \begin{pmatrix} C \\ 0 \end{pmatrix} = \begin{pmatrix} 2 \\ 0 \end{pmatrix}$$

Die approbierte gedruckte Originalversion dieser Diplomarbeit ist an der TU Wien Bibliothek verfügbar
The approved original version of this thesis is available in print at TU Wien Bibliothek.
TU Bibliothek Your knowledge hub WIEN

(a) Computational domain $\Omega = (0,1) \times (-1,1)$ with the corresponding boundaries Γ

(b) Unstructured triangulation $\mathcal{T}_h$ of size $h = 2^{-4}$

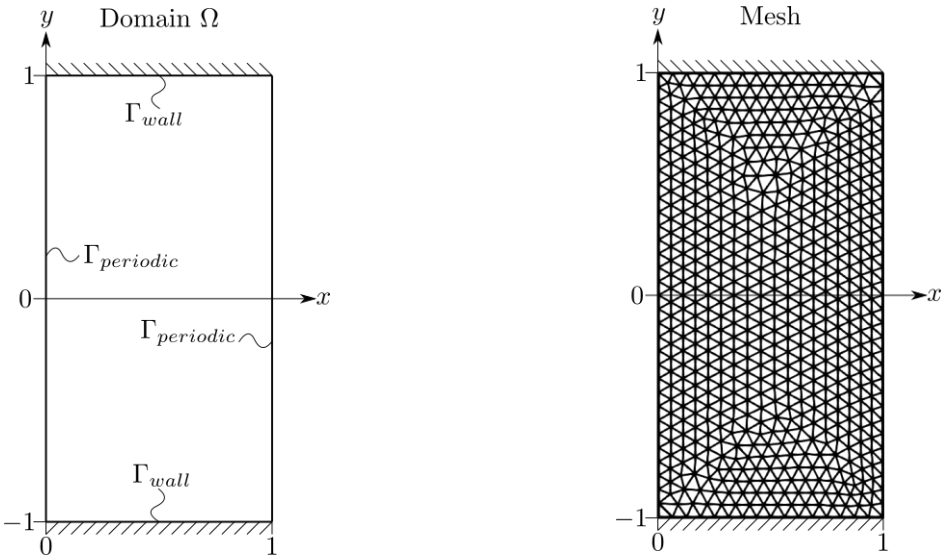

FIGURE 5.3 – Domain and illustrative mesh used for Non-Newtonian simulations

The triangulations $\mathcal{T}_h$ consists of triangles with a maximal mesh size h

$$h := \left\{2^{-3}, 2^{-4}, 2^{-5}, 2^{-6}, 2^{-7}, 2^{-8}\right\},$$

while the polynomial order of the finite elements was fixed to $k = 2$.

5.3.1 Power-law fluid

Recall the non-linear constitutive relation given by (2.7)

$$\mathcal{G}(\boldsymbol{\tau}, \boldsymbol{\varepsilon}(\boldsymbol{u})) = \boldsymbol{\tau} - 2K\dot{\gamma}^{r-2}\boldsymbol{\varepsilon}(\boldsymbol{u}) = 0 \qquad K > 0, 2 > r > 1,$$
$$\dot{\gamma} = 2|\boldsymbol{\varepsilon}(\boldsymbol{u})|$$

The consistency value K was chosen such that $K = 1$, while for the power-law index r we considered two values, namely $r = \{1.2, 1.4\}$. The existence of a weak solution for a power-law-like rheology has been proved in [DKS13]. In the paper, the authors consider the stationary *Navier-Stokes* equations and conclude that for exactly divergence-free elements the existence of a weak solution for $r > \frac{2d}{d+2}$ is given, while for discretely divergence-free elements $r > \frac{2d}{d+1}$ must hold. As this restriction comes solely from the boundedness of the convective term, we conclude that in two-dimensions for a steady *Stokes* flow (5.4) there exists a weak solution for $r > 1$. The exact solutions for a power-law-like channel flow have been derived in the Appendix A.1

$$u_x := \tfrac{r-1}{r}\left[\tfrac{C}{K}\right]^{\frac{1}{r-1}}\left(\tfrac{H}{2}\right)^{\frac{r}{r-1}}\left[1 - \left(\tfrac{2|y|}{H}\right)^{\frac{r}{r-1}}\right], \qquad u_y := 0,$$
$$\tau_{xy} := -Cy, \qquad \tau_{xx} := \tau_{yy} := 0,$$
$$\varepsilon_{xy} := -\frac{\operatorname{sgn}(y)}{2}\left(\tfrac{|Cy|}{K}\right)^{\frac{1}{r-1}}, \qquad \varepsilon_{xx} := \varepsilon_{yy} := 0,$$

Die approbierte gedruckte Originalversion dieser Diplomarbeit ist an der TU Wien Bibliothek verfügbar
The approved original version of this thesis is available in print at TU Wien Bibliothek.
TU Bibliothek Your knowledge hub WIEN

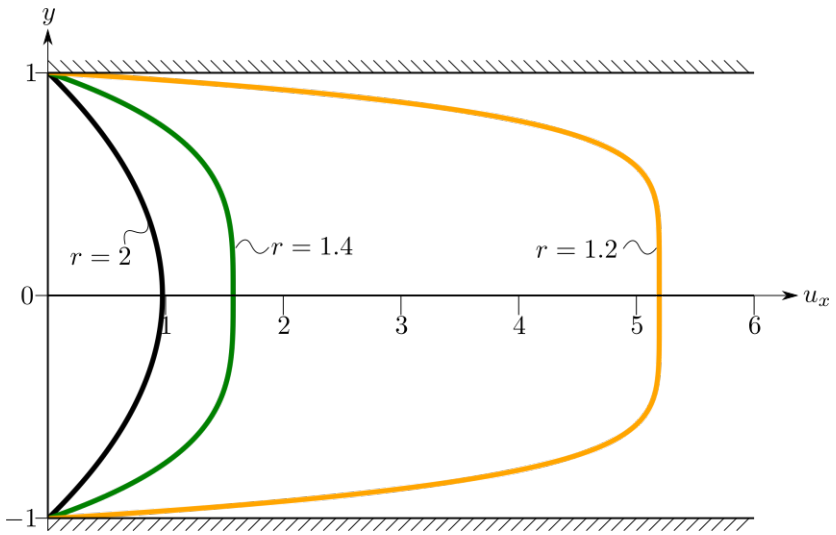

FIGURE 5.4 – Exact power-law velocity profiles u_x for some power-law exponents r. The power-law exponent $r = 2$ equals a Newtonian fluid

$$\boldsymbol{u} := \begin{pmatrix} u_x \\ 0 \end{pmatrix}, \qquad \boldsymbol{\tau} := \begin{pmatrix} \tau_{xx} & \tau_{xy} \\ \tau_{xy} & \tau_{yy} \end{pmatrix}, \qquad \boldsymbol{\varepsilon}(\boldsymbol{u}) := \begin{pmatrix} \varepsilon_{xx} & \varepsilon_{xy} \\ \varepsilon_{xy} & \varepsilon_{yy} \end{pmatrix}, \qquad p := 0.$$

Note, that for $r = 2$ we recover the Newtonian solution. In subsection 2.3.1 we discussed the scope of the power-law model and identified it as a model for pseudoplastic fluids for $r < 2$. This behaviour can be seen particularly well in Figure 5.4, where for a constant forcing $\boldsymbol{f}$ a smaller power-law exponent r results in less skin friction and therefore in a higher flow velocity u_x.

In Figure 5.5 we see the L^2-errors for a power-law exponent $r = 1.4$, obtained by solving the non-linear system with *Newton's* method. The order of convergence of the velocity error $\|\boldsymbol{u}_h - \boldsymbol{u}\|$ and the rate-of-strain tensor $\|\boldsymbol{\varepsilon}(\boldsymbol{u}_h) - \boldsymbol{\varepsilon}(\boldsymbol{u})\|$ remains unchanged in comparison to the Newtonian simulation Figure 5.2, except for the mass conserving mixed finite element ($\mathcal{MCS}$), where we lose a power of h. A possible explanation for this behaviour is the motivation why we introduced a new unknown $\boldsymbol{\varepsilon}$ for the rate-of-strain tensor in the ($\mathcal{MCS}$-$\mathcal{S}$) method in the first place. The velocity gradient $\nabla \boldsymbol{u}$ of $H(\mathrm{div}, \Omega)$-functions, which is needed for the construction of the rate-of-strain tensor $\boldsymbol{\varepsilon}(\boldsymbol{u})$, is not globally defined. However, since we explicitly need the rate-of-strain tensor $\boldsymbol{\varepsilon}(\boldsymbol{u})$ for non-Newtonian models, this may lead to this observed convergence rate loss. The error of the deviatoric stress tensor $\|\boldsymbol{\tau}_h - \boldsymbol{\tau}\|$ and the pressure $\|p_h - p\|$ seem to have an order of convergence of $\mathcal{O}\left(h^{1.4 \sim 1.5}\right)$, but we cannot draw a clear conclusion about it.

Figure 5.6 shows similar L^2-errors, but for a power-law exponent $r = 1.2$. In this setting we are dealing with a high strain rate at the walls and a almost vanishing strain rate in the center of the channel (see. Figure 5.4). To solve the arising non-linear system a fixed point method was used, as it possesses a larger radius of convergence compared to *Newton's* method. Despite this, the mass conserving mixed stress element ($\mathcal{MCS}$) did not seem to meet the convergence criterion for small mesh sizes h and is therefore not marked.

Based on the error plots, it can be said that the newly introduced ($\mathcal{MCS}$-$\mathcal{S}$) method is promising, as it achieved the best results. Only in the case of the pressure error $\|p_h - p\|$ did the augmented *Taylor-Hood* element ($\mathcal{TH}$-$\mathcal{S}$) achieve better results. A possible explanation is that the continuous approximation of the pressure is better suited

Die approbierte gedruckte Originalversion dieser Diplomarbeit ist an der TU Wien Bibliothek verfügbar
The approved original version of this thesis is available in print at TU Wien Bibliothek.
TU Bibliothek Your knowledge hub WIEN

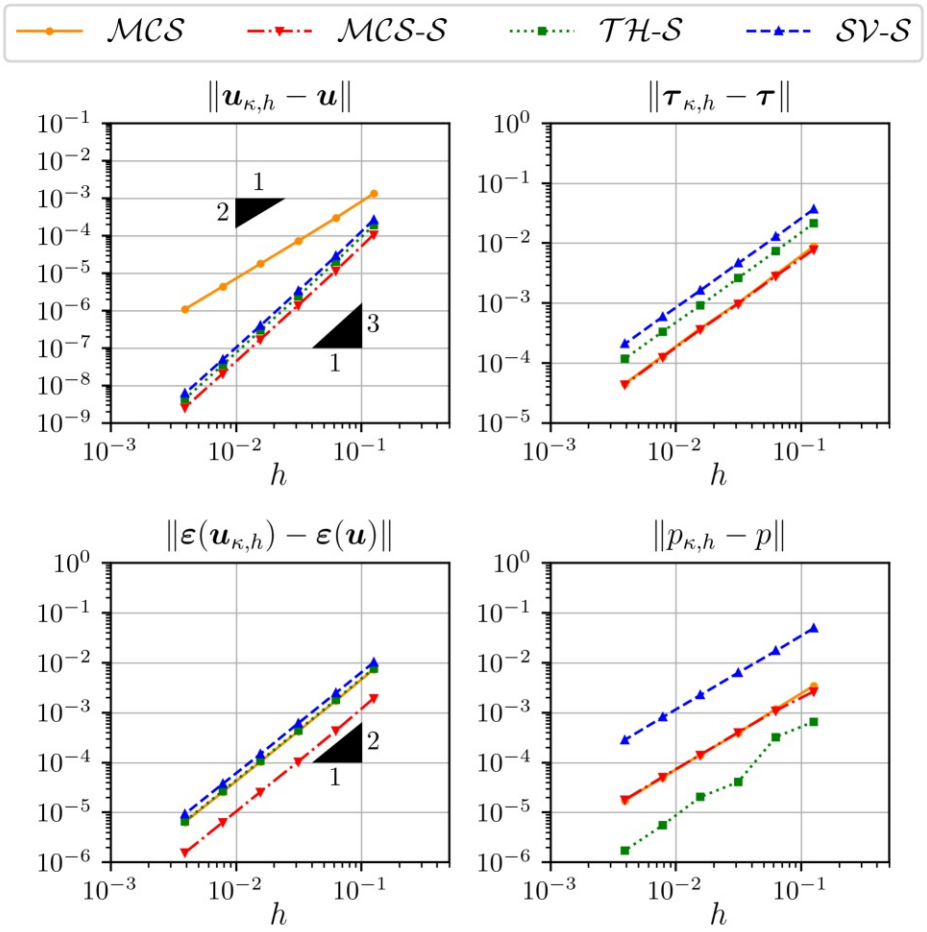

FIGURE 5.5 – L^2-errors of polynomial order $k = 2$ over mesh size h for non-Newtonian power-law channel flow with power-law exponent $r = 1.4$ (see Table B.2)

to approximate the exact constant pressure $p = 0$ in Ω.

5.3.2 Bingham fluid - explicit constitutive relation

The explicit constitutive relation for a Bingham fluid is given by (2.9)

$$\begin{cases} \boldsymbol{\tau} = 2\mu\boldsymbol{\varepsilon}(\boldsymbol{u}) + \dfrac{\tau_y}{|\boldsymbol{\varepsilon}(\boldsymbol{u})|}\boldsymbol{\varepsilon}(\boldsymbol{u}) & \text{if } |\boldsymbol{\tau}| > \tau_y, \\ \boldsymbol{\varepsilon}(\boldsymbol{u}) = \boldsymbol{0} & \text{if } |\boldsymbol{\tau}| \leq \tau_y. \end{cases}$$

In the Appendix A.2 the exact solutions $(\boldsymbol{u}, \boldsymbol{\tau}, \boldsymbol{\varepsilon}, p)$ for a two-dimensional channel flow have been derived

$$u_x := \begin{cases} \frac{C}{2\mu}\left(\frac{H^2}{4} - y^2\right) - \frac{\tau_y}{\mu}\left(y + \frac{H}{2}\right), & \text{if } -\frac{H}{2} \leq y \leq \frac{-\tau_y}{C}, \\ \frac{C}{2\mu}\left(\frac{H^2}{4} - \left(\frac{\tau_y}{C}\right)^2\right) - \frac{\tau_y}{\mu}\left(-\frac{\tau_y}{C} + \frac{H}{2}\right), & \text{if } -\frac{\tau_y}{C} \leq y \leq \frac{\tau_y}{C}, \\ \frac{C}{2\mu}\left(\frac{H^2}{4} - y^2\right) - \frac{\tau_y}{\mu}\left(-y + \frac{H}{2}\right), & \text{if } \frac{\tau_y}{C} \leq y \leq \frac{H}{2}, \end{cases}$$

Die approbierte gedruckte Originalversion dieser Diplomarbeit ist an der TU Wien Bibliothek verfügbar
The approved original version of this thesis is available in print at TU Wien Bibliothek.
TU Bibliothek Your knowledge hub WIEN

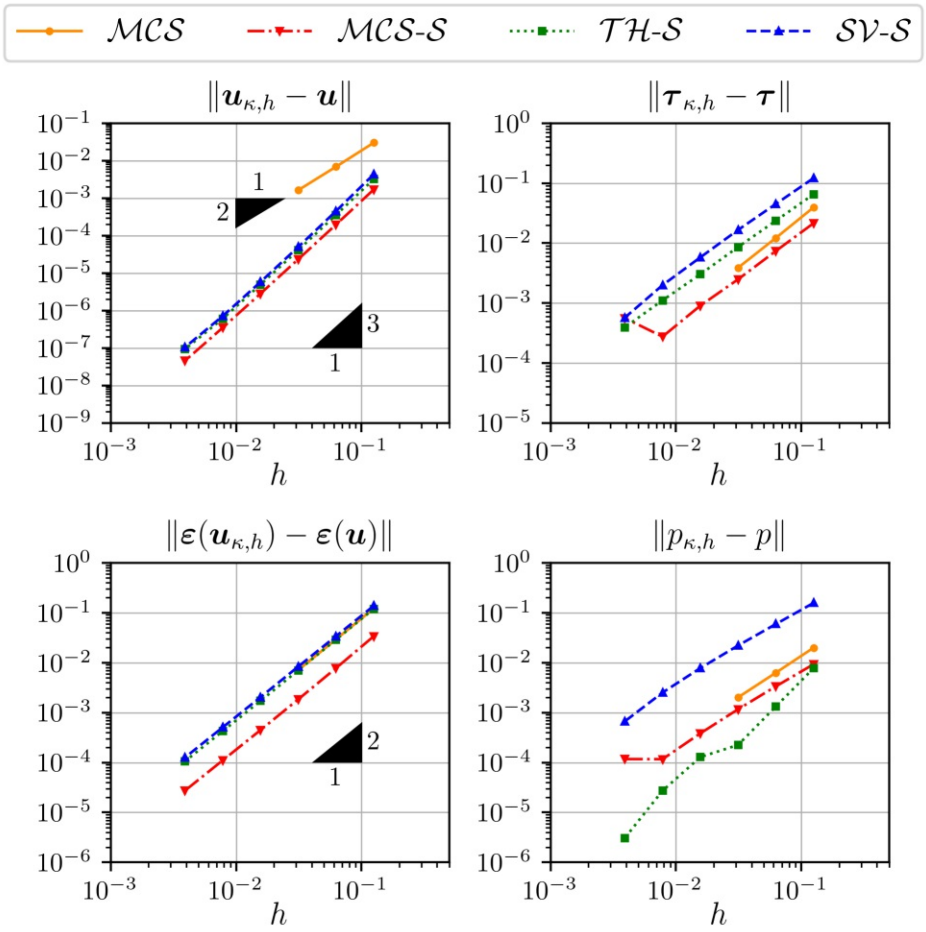

FIGURE 5.6 – L^2-errors of polynomial order $k = 2$ over mesh size h for non-Newtonian power-law channel flow with power-law exponent $r = 1.2$ (see Table B.3)

$$\varepsilon_{xy} := \frac{1}{2}\frac{\mathrm{d}u_x}{\mathrm{d}y} = \begin{cases} -\frac{C}{2\mu}y - \frac{\tau_y}{2\mu}, \\ 0, \\ -\frac{C}{2\mu}y + \frac{\tau_y}{2\mu}, \end{cases} \qquad \varepsilon_{xx} = \varepsilon_{yy} := \begin{cases} 0, & \text{if } -\frac{H}{2} \le y \le -\frac{\tau_y}{C}, \\ 0, & \text{if } -\frac{\tau_y}{C} \le y \le \frac{\tau_y}{C}, \\ 0, & \text{if } \frac{\tau_y}{C} \le y \le \frac{H}{2}, \end{cases}$$

$$\boldsymbol{u} := \begin{pmatrix} u_x \\ 0 \end{pmatrix}, \qquad \boldsymbol{\tau} := \begin{pmatrix} 0 & -Cy \\ -Cy & 0 \end{pmatrix}, \qquad \boldsymbol{\varepsilon}(\boldsymbol{u}) := \begin{pmatrix} \varepsilon_{xx} & \varepsilon_{xy} \\ \varepsilon_{xy} & \varepsilon_{yy} \end{pmatrix}, \qquad p := 0.$$

We observe (see Figure 2.2) that due to the kink at the yield point the constitutive relation is non-differentiable. Additionally, below the yield stress the development of the deviatoric stress tensor $\boldsymbol{\tau}$ is not determined. To overcome this difficulties mainly two computational methods have been elaborated [GW11, Section 4]

(I) Variational inequalities methods

(II) Regularization methods

Our focus lies on the latter. The idea is to smoothen the discontinuous constitutive relation by means of a regularisation parameter κ, such that the stress-strain rate curve becomes continuous and differentiable, hence making *Newton's* method applicable. From

Die approbierte gedruckte Originalversion dieser Diplomarbeit ist an der TU Wien Bibliothek verfügbar
The approved original version of this thesis is available in print at TU Wien Bibliothek.
TU Bibliothek Your knowledge hub WIEN

a physical perspective it can be interpreted as attributing a very high viscosity to the *unyielded* regions, such that they become very rigid in comparison to the *yielded* regions. In our numerical simulations we adapted a popular regularisation introduced in [BE80]

$$\boldsymbol{\tau}_\kappa := \left[2\mu + \frac{2\tau_y}{\sqrt{\kappa^2 + 4|\boldsymbol{\varepsilon}(\boldsymbol{u}_\kappa)|^2}}\right] \boldsymbol{\varepsilon}(\boldsymbol{u}_\kappa).$$

As $\kappa \to 0$ we hope for $(\boldsymbol{\tau}_\kappa, \boldsymbol{u}_\kappa, \boldsymbol{\varepsilon}(\boldsymbol{u}_\kappa), p_\kappa) \to (\boldsymbol{\tau}, \boldsymbol{u}, \boldsymbol{\varepsilon}(\boldsymbol{u}), p)$, although there are no general results that guarantee this convergence [GO21]. In the special case of a unidirectional pressure-driven pipe flow the convergence $\boldsymbol{u}_\kappa \to \boldsymbol{u}$ can be shown [SW17].
Nevertheless, in Figure 5.7 the impact of the regularisation parameter κ is shown by means of the regularised constitutive law and the velocity profile of a numerical simulation with yields stress $\tau_y = 1$ and dynamic viscosity $\mu = 1$.

(*a*) Regularized *Bingham* constitutive relation

(*b*) Numerical solution of a regularized *Bingham* fluid in a channel

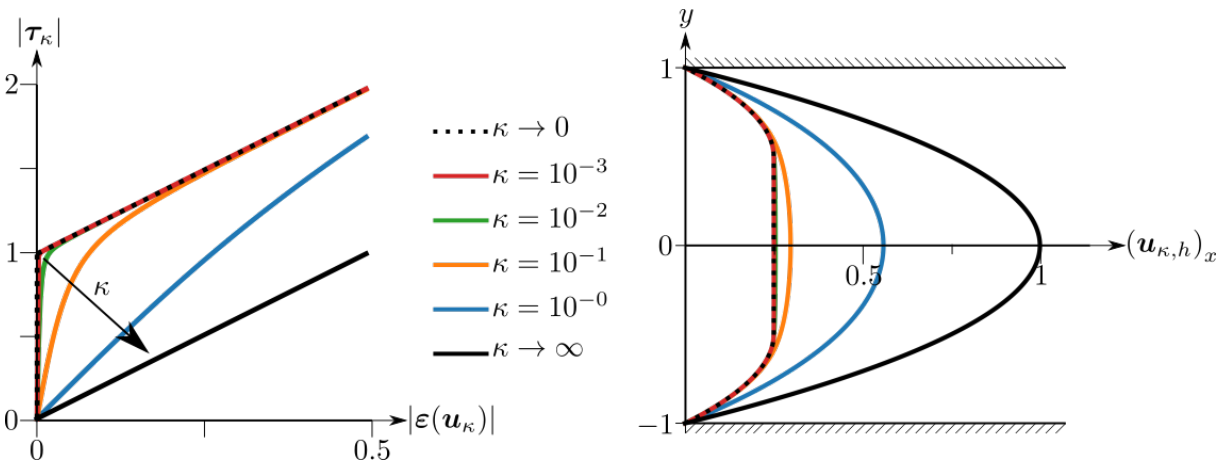

FIGURE 5.7 – Impact of a regularized *Bingham* constitutive relation with yield stress $\tau_y = 1$. $\kappa \to \infty$ denotes the Newtonian solution, while $\kappa \to 0$ indicates the exact solution

Furthermore, we turn to the numerical approximation of a *Bingham* fluid with yield stress $\tau_y = 0.2$ and normalized dynamic viscosity $\mu = 1$. The aim is to compare the L^2-errors of the finite elements ($\mathcal{MCS}$, $\mathcal{MCS}$-$\mathcal{S}$, $\mathcal{TH}$-$\mathcal{S}$, $\mathcal{SV}$-$\mathcal{S}$) and to illustrate the effect of the regularisation parameter κ on them. For this we consider following range of regularisation parameters

$$\kappa := \left\{10^0, 10^{-1}, 10^{-2}, 10^{-3}, 10^{-4}, 10^{-5}, 10^{-6}, 10^{-7}, 10^{-8}\right\},$$

where for sake of simplicity we only show the numerical results of a selection. Every case has been solved by *Newton's* method with a suitable damping parameter. In Figure 5.8 we see the obtained finite element L^2-errors for a regularisation parameter $\kappa = 10^{-4}$. Immediately, we observe a stagnation of the velocity L^2-error $\|\boldsymbol{u}_{\kappa,h} - \boldsymbol{u}\|$ for small mesh sizes h, while it is partially visible for the rate-of-strain L^2-error $\|\boldsymbol{\varepsilon}(\boldsymbol{u}_{\kappa,h}) - \boldsymbol{\varepsilon}(\boldsymbol{u})\|$. Such behaviour is caused by the regularisation parameter κ. On the other hand the deviatoric stress tensor $\|\boldsymbol{\tau}_{\kappa,h} - \boldsymbol{\tau}\|$ and the pressure $\|p_{\kappa,h} - p\|$ errors seem to convergence, but do no shows this mentioned behaviour on the considered mesh sizes h.
In Figure 5.9 we plotted on the same y-axis range as in Figure 5.8 the finite element L^2-errors for a regularisation parameter $\kappa = 10^{-8}$. As for the power-law model, the mass

TU Bibliothek Your knowledge hub WIEN
Die approbierte gedruckte Originalversion dieser Diplomarbeit ist an der TU Wien Bibliothek verfügbar
The approved original version of this thesis is available in print at TU Wien Bibliothek.

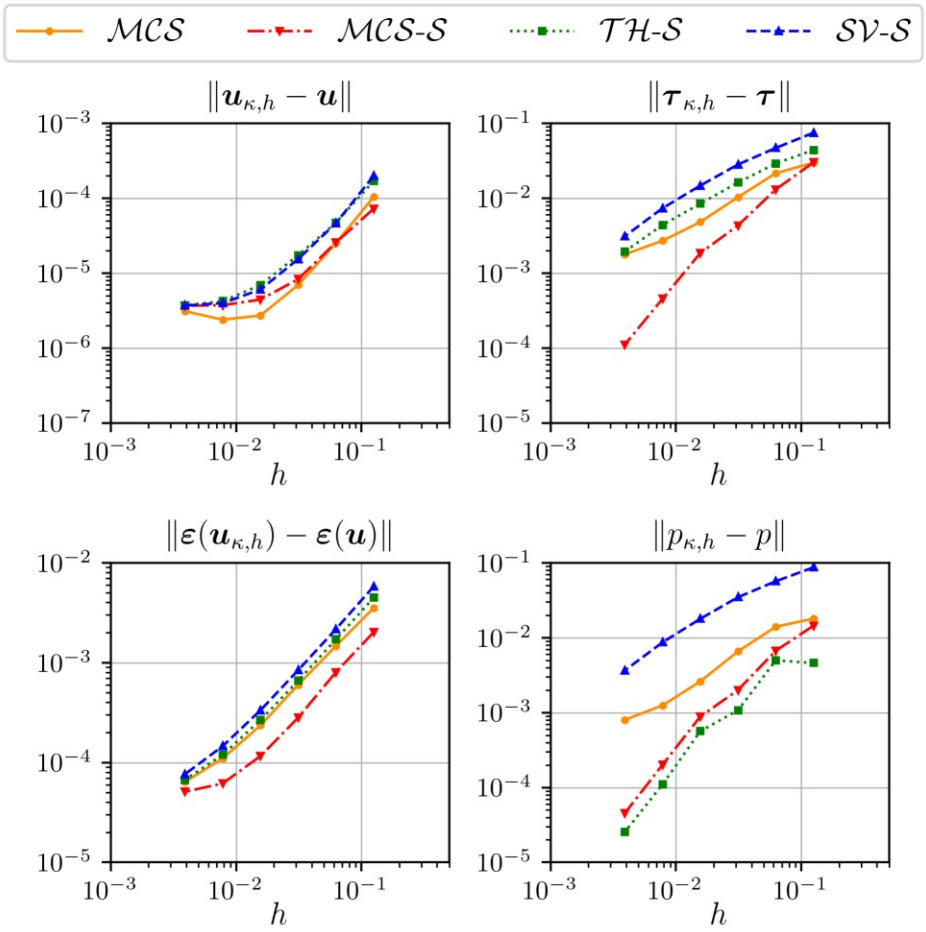

FIGURE 5.8 – L^2-errors of polynomial order $k = 2$ over mesh size h for a regularised non-Newtonian explicit constituted *Bingham*($\tau_y = 0.2$, $\kappa = 10^{-4}$) flow in a two-dimensional channel (see Table B.4)

conserving mixed finite element ($\mathcal{MCS}$) did not meet the convergence criterion for small mesh sizes h and is therefore not marked. In this case the velocity $\|\boldsymbol{u}_{\kappa,h} - \boldsymbol{u}\|$ and rate-of-strain $\|\boldsymbol{\varepsilon}(\boldsymbol{u}_{\kappa,h}) - \boldsymbol{\varepsilon}(\boldsymbol{u})\|$ L^2-errors do not stagnate, on the contrary, they seem to show some convergence order $\mathcal{O}(h^k)$. Moreover, the stress $\|\boldsymbol{\tau}_{\kappa,h} - \boldsymbol{\tau}\|$ and pressure $\|p_{\kappa,h} - p\|$ approximation seem to convergence worse, the smaller the regularisation parameter κ. This can be illustrated in Figure 5.10, where we plot the L^2-errors for a fixed mesh size $h = 2^{-6}$ over the regularisation parameter κ. By no means this behaviour has to be understood in a general sense, as it is only a cause of the specific choice of domain and boundary conditions. Namely, in a two-dimensional channel with given forcing term $\boldsymbol{f}$ and periodic boundary, the exact solution of the deviatoric stress tensor $\boldsymbol{\tau}$ and the pressure p remains unchanged, regardless of the constitutive law under consideration. This follows readily from the momentum equation (5.4b). Hence, the smaller the regularisation parameter κ the less smooth the numerical results and therefore the less accurate the approximation of the deviatoric stress tensor $\boldsymbol{\tau}_{\kappa,h}$ and the pressure $p_{\kappa,h}$.

Backed by the good L^2-finite element errors, it can again be said that the newly introduced ($\mathcal{MCS}$-$\mathcal{S}$) method is promising. As for the power-law constitutive law (see Subsection 5.3.1), only in the case of the pressure L^2-error $\|p_h - p\|$ did the stress augmented *Taylor-Hood* element ($\mathcal{TH}$-$\mathcal{S}$) achieve better results. A possible explanation is that the continuous approximation of the pressure is better suited to approximate the

Die approbierte gedruckte Originalversion dieser Diplomarbeit ist an der TU Wien Bibliothek verfügbar
The approved original version of this thesis is available in print at TU Wien Bibliothek.
TU Bibliothek Your knowledge hub WIEN

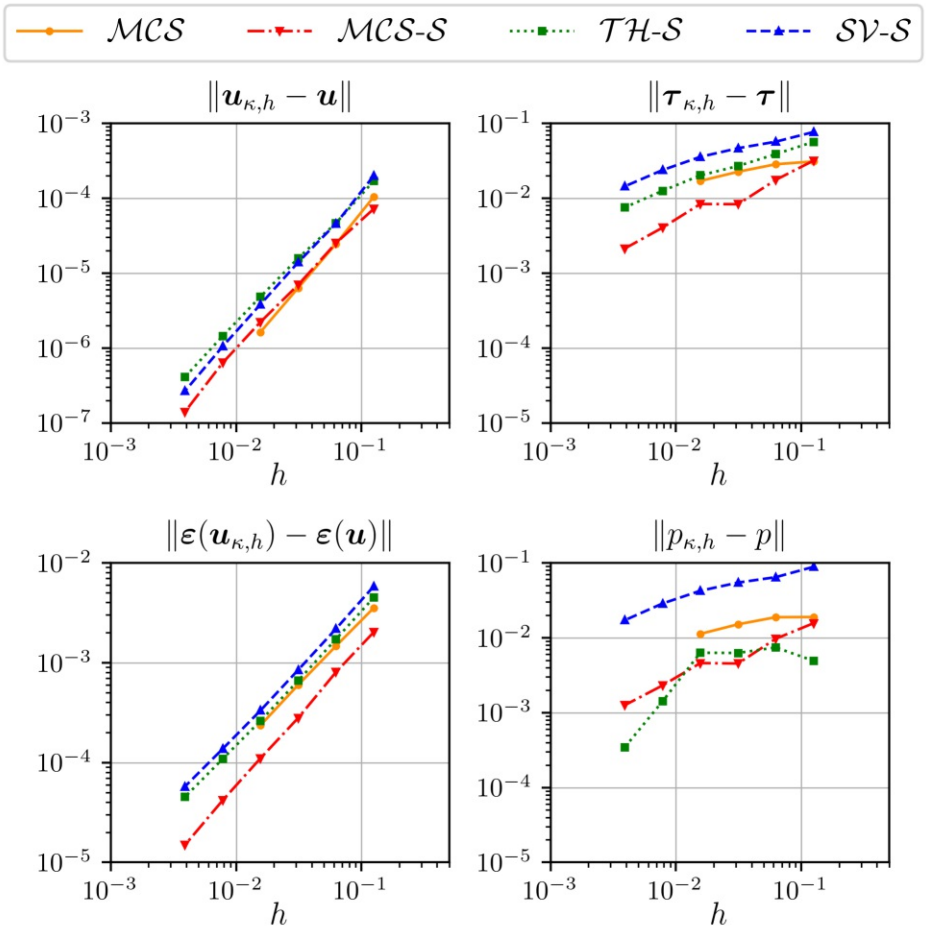

FIGURE 5.9 – L^2-errors of polynomial order $k = 2$ over mesh size h for a regularised non-Newtonian explicit constituted *Bingham*($\tau_y = 0.2$, $\kappa = 10^{-8}$) flow in a two-dimensional channel (see Table B.5)

exact constant pressure $p = 0$ in Ω.

5.3.3 Bingham fluid - implicit constitutive relation

As mentioned in Section 4.4 an important feature of the mixed finite elements ($\mathcal{TH}$-$\mathcal{S}$, $\mathcal{SV}$-$\mathcal{S}$, $\mathcal{MCS}$-$\mathcal{S}$) is the easy inclusion of an implicit constitutive relation of the form $\mathcal{G}(\boldsymbol{\tau}, \boldsymbol{\varepsilon}(\boldsymbol{u}))$, while this does not hold for the mass conserving mixed stress finite element ($\mathcal{MCS}$) and will therefore be omitted in the following. For this reason we performed some simulations of a *Bingham* fluid, where the constitutive relation is given implicitly, namely [GO21, Eq 4.b]

$$\mathcal{G}(\boldsymbol{\tau}, \boldsymbol{\varepsilon}(\boldsymbol{u})) := |\boldsymbol{\varepsilon}(\boldsymbol{u})|\boldsymbol{\tau} - (\tau_y + 2\mu|\boldsymbol{\varepsilon}(\boldsymbol{u})|)\,\boldsymbol{\varepsilon}(\boldsymbol{u}) = 0.$$

The exact solutions $(\boldsymbol{u}, \boldsymbol{\tau}, \boldsymbol{\varepsilon}, p)$ for a two-dimensional channel flow are the identical as for the explicit constitutive relation

$$u_x := \begin{cases} \frac{C}{2\mu}\left(\frac{H^2}{4} - y^2\right) - \frac{\tau_y}{\mu}\left(y + \frac{H}{2}\right), & \text{if } -\frac{H}{2} \le y \le \frac{-\tau_y}{C}, \\ \frac{C}{2\mu}\left(\frac{H^2}{4} - \left(\frac{\tau_y}{C}\right)^2\right) - \frac{\tau_y}{\mu}\left(-\frac{\tau_y}{C} + \frac{H}{2}\right), & \text{if } -\frac{\tau_y}{C} \le y \le \frac{\tau_y}{C}, \\ \frac{C}{2\mu}\left(\frac{H^2}{4} - y^2\right) - \frac{\tau_y}{\mu}\left(-y + \frac{H}{2}\right), & \text{if } \frac{\tau_y}{C} \le y \le \frac{H}{2}, \end{cases}$$

Die approbierte gedruckte Originalversion dieser Diplomarbeit ist an der TU Wien Bibliothek verfügbar
The approved original version of this thesis is available in print at TU Wien Bibliothek.
TU Bibliothek Your knowledge hub WIEN

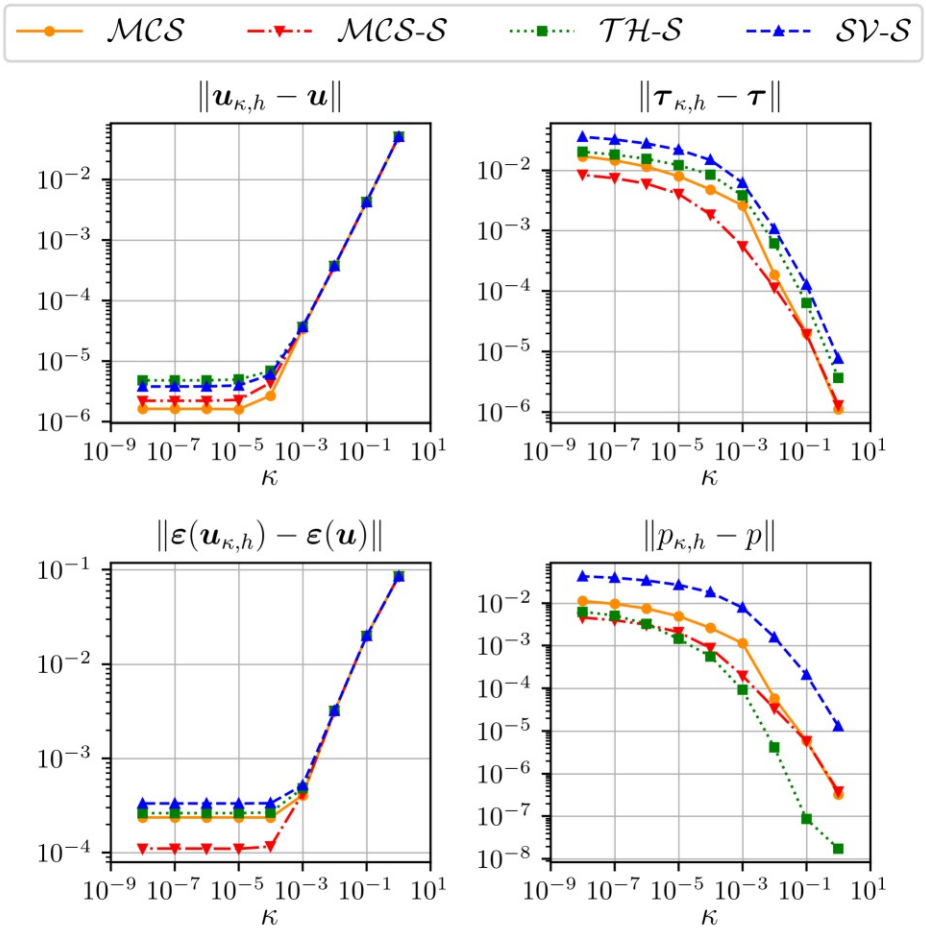

FIGURE 5.10 – L^2-errors of polynomial order $k = 2$ over regularisation parameter κ for a regularised non-Newtonian explicit constituted *Bingham*($\tau_y = 0.2$, $h = 2^{-6}$) flow in a two-dimensional channel (see Table B.6)

$$\varepsilon_{xy} := \frac{1}{2}\frac{\mathrm{d}u_x}{\mathrm{d}y} = \begin{cases} -\frac{C}{2\mu}y - \frac{\tau_y}{2\mu}, \\ 0, \\ -\frac{C}{2\mu}y + \frac{\tau_y}{2\mu}, \end{cases} \qquad \varepsilon_{xx} = \varepsilon_{yy} := \begin{cases} 0, & \text{if } -\frac{H}{2} \le y \le -\frac{\tau_y}{C}, \\ 0, & \text{if } -\frac{\tau_y}{C} \le y \le \frac{\tau_y}{C}, \\ 0, & \text{if } \frac{\tau_y}{C} \le y \le \frac{H}{2}, \end{cases}$$

$$\boldsymbol{u} := \begin{pmatrix} u_x \\ 0 \end{pmatrix}, \qquad \boldsymbol{\tau} := \begin{pmatrix} 0 & -Cy \\ -Cy & 0 \end{pmatrix}, \qquad \boldsymbol{\varepsilon}(\boldsymbol{u}) := \begin{pmatrix} \varepsilon_{xx} & \varepsilon_{xy} \\ \varepsilon_{xy} & \varepsilon_{yy} \end{pmatrix}, \qquad p := 0.$$

Furthermore, similar to the explicit case, $\mathcal{G}(\boldsymbol{\tau}, \boldsymbol{\varepsilon}(\boldsymbol{u}))$ is non differentiable, thus a certain regularisation is needed. In [GO21, Eq 6] the author makes use of a regularised implicit constitutive law of the form

$$\mathcal{G}_\kappa(\boldsymbol{\tau}, \boldsymbol{\varepsilon}(\boldsymbol{u})) := \mathcal{G}(\boldsymbol{\tau} - \kappa\boldsymbol{\varepsilon}(\boldsymbol{u}), \boldsymbol{\varepsilon}(\boldsymbol{u}) - \kappa\boldsymbol{\tau}), \qquad \kappa > 0,$$

in which κ is our previously introduced regularisation parameter. Although the regularised law $\mathcal{G}_\kappa(\boldsymbol{\tau}, \boldsymbol{\varepsilon}(\boldsymbol{u}))$ is in general non-differentiable as it inherits the smoothness of the original constitutive relation [GO21], we observed that for our test case the application of a *Newton* solver did not cause any problems. Unlike the explicit case, it was proven that as $\kappa \to 0$ the regularised solution $(\boldsymbol{\tau}_\kappa, \boldsymbol{u}_\kappa, \boldsymbol{\varepsilon}(\boldsymbol{u}_\kappa), p_\kappa)$ converges towards the exact solution $\to (\boldsymbol{\tau}, \boldsymbol{u}, \boldsymbol{\varepsilon}(\boldsymbol{u}), p)$ [GO21].

Die approbierte gedruckte Originalversion dieser Diplomarbeit ist an der TU Wien Bibliothek verfügbar
The approved original version of this thesis is available in print at TU Wien Bibliothek.
TU Bibliothek Your knowledge hub WIEN

We turn now to the performed simulations, where a normalized dynamic viscosity $\mu = 1$ is again used. In contrast to the explicit case, we fix the regularisation parameter to $\kappa = 10^{-8}$ and consider two different yield stresses

$$\tau_y := \{0.2, 1\}\,.$$

Notice that a higher yield stress leads to a greater *unyielded* region, thus one expects a bigger L^2-finite element error, since the *unyielded* regions are the source of non-differentiability of the constitutive relation.

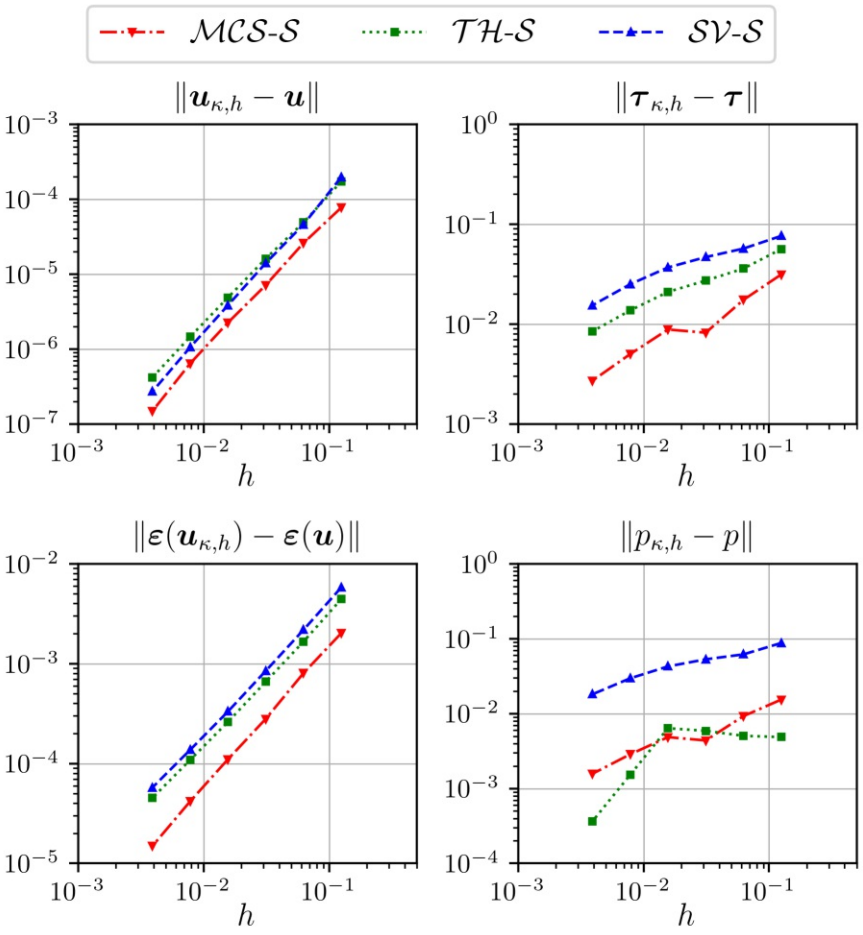

FIGURE 5.11 – L^2-errors of polynomial order $k = 2$ over mesh size h for a regularised non-Newtonian implicit constituted *Bingham*($\tau_y = 0.2$, $\kappa = 10^{-8}$) flow in a two-dimensional channel (see Table B.7)

In Figure 5.11 the finite element L^2-errors for a yield stress $\tau_y = 0.2$ are shown. They are very similar, almost identical, to the L^2-errors of the explicit constitutive law in Figure 5.9. Furthermore, in Figure 5.12 the finite element L^2-errors for a yield stress $\tau_y = 1.0$ are plotted on the same y-axis range. Unfortunately, the newly introduced ($\mathcal{MCS}$-$\mathcal{S}$) finite element does not converge at a mesh size $h = 2^{-8}$, but this is caused by the lack of an appropriate line search algorithm. In both figures the velocity $\|\boldsymbol{u}_{\kappa,h} - \boldsymbol{u}\|$ and rate-of-strain $\|\boldsymbol{\varepsilon}(\boldsymbol{u}_{\kappa,h}) - \boldsymbol{\varepsilon}(\boldsymbol{u})\|$ L^2-errors seem to show some convergence order $\mathcal{O}(h^k)$, while the pressure $\|p_{\kappa,h} - p\|$ and deviatoric stress tensor $\|\boldsymbol{\tau}_{\kappa,h} - \boldsymbol{\tau}\|$ L^2-errors seem to convergence arbitrarily. As in the other test cases, the mass conserving mixed stress-strain rate finite element ($\mathcal{MCS}$-$\mathcal{S}$) did achieve good results, if not the best.

TU Bibliothek Your knowledge hub WIEN
Die approbierte gedruckte Originalversion dieser Diplomarbeit ist an der TU Wien Bibliothek verfügbar
The approved original version of this thesis is available in print at TU Wien Bibliothek.

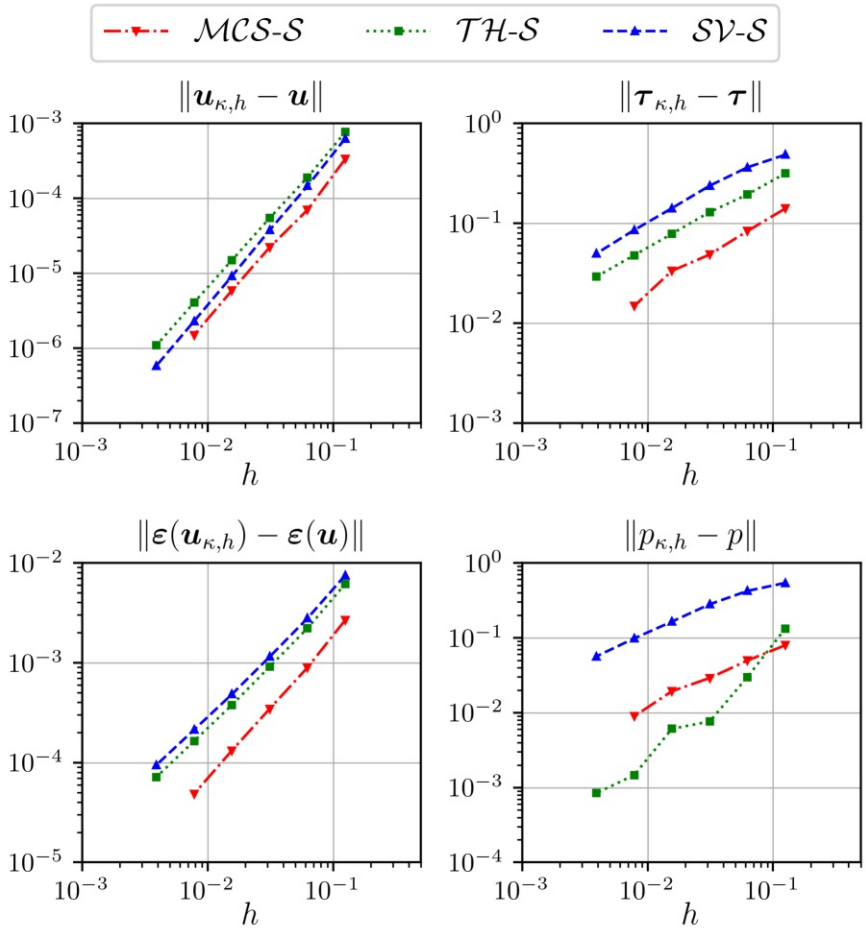

FIGURE 5.12 – L^2-errors of polynomial order $k = 2$ over mesh size h for a regularised non-Newtonian implicit constituted *Bingham*($\tau_y = 1$, $\kappa = 10^{-8}$) flow in a two-dimensional channel (see Table B.8)

5.3.4 Remarks on the ($\mathcal{MCS}$-$\mathcal{S}$) finite element

So far in this section we have shown the achieved L^2-errors of the discrete solutions relative to the exact solutions, without further commenting the solution process. This subsection is intended to reflect the observations made during the simulations.

Damping parameter

As stated, an empirically determined damping parameter d has been used together with *Newton's* method or a fixed point method. While the *Taylor-Hood* ($\mathcal{TH}$-$\mathcal{S}$) and *Scott-Vogelius* ($\mathcal{SV}$-$\mathcal{S}$) elements showed good convergence for large damping parameters $d = 1$, the mass conserving mixed methods ($\mathcal{MCS}$) and ($\mathcal{MCS}$-$\mathcal{S}$) required a damping parameter $0.1 \leq d \leq 1$. Thus, a work in progress is to combine the latter with an efficient Line Search algorithm, in order to optimise the solution process.

Degrees of freedom

At first sight one could think that the ($\mathcal{MCS}$-$\mathcal{S}$) is from a computational perspective very expensive as we approximate 5 quantitites, namely $\boldsymbol{u}_h, \boldsymbol{\tau}_h, p_h, \boldsymbol{\omega}_h, \boldsymbol{\varepsilon}_h$, which obviously increases the number of unknowns drastically. $\boldsymbol{\omega}_h$ and $\boldsymbol{\varepsilon}_h$ are local degrees of freedom,

Die approbierte gedruckte Originalversion dieser Diplomarbeit ist an der TU Wien Bibliothek verfügbar
The approved original version of this thesis is available in print at TU Wien Bibliothek.
TU Bibliothek Your knowledge hub WIEN

while $\boldsymbol{u}_h, \boldsymbol{\tau}_h$ and the lowest order degrees of freedom of p_h couple with the adjacent elements. Using a hybridization technique by introducing a new tangential velocity facet space

$$\underline{V}_h := \left\{ \underline{\boldsymbol{u}}_h \in \mathbb{P}^{k-1}(\mathcal{F}_h, \mathbb{R}^{d-1}) : (\underline{\boldsymbol{u}}_h)_n = 0 \; \forall F \in \mathcal{F}_h \right\},$$

and by using a discontinuous stress space

$$\Sigma_h^{\oplus,\mathrm{disc}} := \left\{ \boldsymbol{\tau}_h \in \mathbb{P}^k(\mathcal{T}_h, \mathbb{R}^{d\times d}) : \mathrm{tr}(\boldsymbol{\tau}_h|_T) = 0 \; \forall T \in \mathcal{T}_h, (\boldsymbol{\tau}_h)_{nt} \in \mathbb{P}^{k-1}(F, \mathbb{R}^{d-1}) \; \forall F \in \mathcal{F}_h^{\mathrm{int}} \right\},$$

we add to the discrete variational formulation VIII the terms

$$b_4(\boldsymbol{\tau}, \overline{\underline{\boldsymbol{u}}}_h) := -\sum_{F\in\mathcal{F}_h} \int_F [\![(\boldsymbol{\tau}_h)_{nt}]\!] \cdot \overline{\underline{\boldsymbol{u}}}_h \, ds,$$

$$b_4(\overline{\boldsymbol{\tau}}, \underline{\boldsymbol{u}}_h) := -\sum_{F\in\mathcal{F}_h} \int_F [\![(\overline{\boldsymbol{\tau}}_h)_{nt}]\!] \cdot \underline{\boldsymbol{u}}_h \, ds.$$

Therefore, we decoupled the stresses $\boldsymbol{\tau}_h$. The remaining coupling degrees of freedom are located in $\boldsymbol{u}_h, \underline{\boldsymbol{u}}_h$ and the lowest order of p_h. Now we can apply static condensation to the system as most of the unknowns are element local, while only a few couple. To get an idea of how many degrees of freedom we are speaking of, consider Table 5.1. While the arising

FEM	h	local	coupling
$(\mathcal{MCS})$	2^{-4}	14260	5430
	2^{-5}	55062	20669
$(\mathcal{MCS}\text{-}\mathcal{S})$	2^{-4}	21700	5430
	2^{-5}	83790	20669
$(\mathcal{TH}\text{-}\mathcal{S})$	2^{-4}	5580	2953
	2^{-5}	21546	11096
$(\mathcal{SV}\text{-}\mathcal{S})$	2^{-4}	11160	13150
	2^{-5}	43092	50532

TABLE 5.1 – Number of unknowns on unit square of polynomial order $k = 2$ for two mesh sizes h

linear system of the $(\mathcal{MCS}\text{-}\mathcal{S})$ finite element has the most unknowns, the largest part is accounted by local degrees of freedom unlike the $(\mathcal{SV}\text{-}\mathcal{S})$ finite element. As the matrix containing these unknowns is block-diagonal, it is cheaply invertible. The $(\mathcal{TH}\text{-}\mathcal{S})$ finite element definitely has the least degrees of freedom, but compared to the other methods it lacks the pointwise divergence free property (see 4.1.2).

Die approbierte gedruckte Originalversion dieser Diplomarbeit ist an der TU Wien Bibliothek verfügbar
The approved original version of this thesis is available in print at TU Wien Bibliothek.
TU Bibliothek Your knowledge hub WIEN

Die approbierte gedruckte Originalversion dieser Diplomarbeit ist an der TU Wien Bibliothek verfügbar
The approved original version of this thesis is available in print at TU Wien Bibliothek.
TU Bibliothek Your knowledge hub WIEN

6

Conclusion and Future Work

This chapter is dedicated to the summary of the thesis and to discuss open questions regarding the mass conserving mixed stress-strain rate finite element ($\mathcal{MCS}$-$\mathcal{S}$), which will be adressed in the future.

6.1 Summary

Assuming incompressible, stationary, isothermal, laminar flow we introduced in this thesis a new mixed mass conserving stress-strain rate finite element method ($\mathcal{MCS}$-$\mathcal{S}$, 4.3.2), by extending the ($\mathcal{MCS}$, 4.3.1) finite element method of the works [GLS19, GLS20] by an additional variable for the rate-of-strain tensor $\boldsymbol{\varepsilon}$. This enabled us to include an arbitrary implicit constitutive relation of the form $\mathcal{G}(\boldsymbol{\tau}, \boldsymbol{\varepsilon}) := 0$ in the discrete variational formulation, making the method suitable for the simulation of a broader range of non-Newtonian models.
In a two-dimensional Newtonian setting we proved solvability of the discrete variational formulation and the discrete LBB condition suggested the space of piecewise discontinuous symmetric trace-free matrix-valued polynomials to approximate the rate-of-strain tensor $\boldsymbol{\varepsilon}$. This seems an adequate choice, since by the conservation of mass it holds $\operatorname{tr}(\boldsymbol{\varepsilon}) = 0$ and by construction $\boldsymbol{\varepsilon} = \boldsymbol{\varepsilon}^{\mathrm{T}}$.
For the special choice of a two-dimensional channel as computational domain Ω and the non-linear constitutive relations (Power-law (2.7), *Bingham* (2.9)) we found analytic solutions, thus allowing the computation of L^2 errors. On the basis of non-Newtonian numerical experiments the achieved errors of the newly introduced mixed mass conserving stress-strain rate finite element method ($\mathcal{MCS}$-$\mathcal{S}$) have been compared to standard finite elements such as the *Taylor-Hood* ($\mathcal{TH}$-$\mathcal{S}$) and *Scott-Vogelius* ($\mathcal{SV}$-$\mathcal{S}$) element augmented with piecewise discontinuous stresses. Almost in every illustrated result the new finite element method achieved the best approximations of the velocity $\boldsymbol{u}$, rate-of-strain tensor $\boldsymbol{\varepsilon}$ and the deviatoric stress tensor $\boldsymbol{\tau}$. Only the pressure p has been approximated more accurately by the stress augmented *Taylor-Hood* ($\mathcal{TH}$-$\mathcal{S}$) element. By these results we come to the conclusion that the mass conserving mixed stress-strain rate method ($\mathcal{MCS}$-$\mathcal{S}$) is very promising, although further testing is needed.

6.2 Open Questions

- Regarding the ($\mathcal{MCS}$-$\mathcal{S}$) element, the discrete LBB condition presented in this work does not hold in a three-dimensional setting. Although it should follow similar arguments, we still need to elaborate the proof. Subsequently, numerical experiments

Die approbierte gedruckte Originalversion dieser Diplomarbeit ist an der TU Wien Bibliothek verfügbar
The approved original version of this thesis is available in print at TU Wien Bibliothek.
TU Bibliothek WIEN Your knowledge hub

in a three-dimensional computational domain Ω e.g. a pipe, are needed to draw a clearer conclusion about the new finite element method.

- Exactly divergence free and pressure robust finite elements are well suited to approximate convection dominated problems. For this reason the assessment of the new mass conserving mixed stress-strain rate finite element in an incompressible turbulent flow is potentially interesting, especially because the convective trilinear form can be reformulated as

$$\int_\Omega (\nabla \boldsymbol{u})\boldsymbol{u} \cdot \overline{\boldsymbol{u}}\, dx = \int_\Omega \boldsymbol{\varepsilon u} \cdot \overline{\boldsymbol{u}}\, dx + \int_\Omega \boldsymbol{\omega u} \cdot \overline{\boldsymbol{u}}\, dx.$$

Die approbierte gedruckte Originalversion dieser Diplomarbeit ist an der TU Wien Bibliothek verfügbar
The approved original version of this thesis is available in print at TU Wien Bibliothek.
TU Bibliothek Your knowledge hub WIEN

Appendix A Exact Solutions Non-Newtonian Periodic Channel Flow

In this chapter we will derive the exact solutions for incompressible steady Non-Newtonian laminar flows in a two-dimensional channel. Consider the two-dimensional domain Ω shown in figure Figure A.1 with the corresponding periodic boundaries $\Gamma_{periodic}$ and no-slip boundaries Γ_{wall} and the governing equations (5.4).

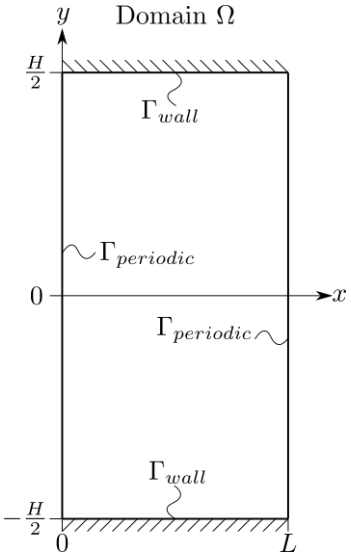

FIGURE A.1 – Two-dimensional channel with boundary designation

Mathematically, the assumptions of an incompressible steady laminar uni-directional flow can be summarised as

$$u_z = u_y = 0 \qquad \frac{\partial(\cdot)}{\partial z} = 0$$
$$\frac{\partial(\cdot)}{\partial t} = 0 \qquad \rho = \text{const}$$

Consider the flow being driven by a constant forcing term $\boldsymbol{f}$ e.g. gravity or a pressure drop.

$$\boldsymbol{f}_x = C > 0 \qquad \boldsymbol{f}_y = 0$$

The governing equations then simplify to

$$-\text{div}(\boldsymbol{\tau}) = -\nabla p + \boldsymbol{f} \qquad \text{in } \Omega,$$
$$\frac{\partial u_x}{\partial x} = 0 \qquad \text{in } \Omega,$$
$$u_x = 0 \qquad \text{on } \Gamma_{wall}$$

From the result of the continuity equation, it follows for the rate-of-strain tensor $\boldsymbol{\varepsilon}(\boldsymbol{u})$

$$\boldsymbol{\varepsilon}(\boldsymbol{u}) = \frac{1}{2}\left[\nabla \boldsymbol{u} + (\nabla \boldsymbol{u})^{\mathrm{T}}\right] = \frac{1}{2}\begin{pmatrix} 0 & \frac{\partial u_x}{\partial y} \\ \frac{\partial u_x}{\partial y} & 0 \end{pmatrix}$$

Die approbierte gedruckte Originalversion dieser Diplomarbeit ist an der TU Wien Bibliothek verfügbar
The approved original version of this thesis is available in print at TU Wien Bibliothek.
TU Bibliothek Your knowledge hub WIEN

A.1 Power-law constitutive relation

The relation between the deviatoric stress tensor $\boldsymbol{\tau}$ and $\boldsymbol{\varepsilon}(\boldsymbol{u})$ is given by equation (2.7)

$$\begin{aligned}\dot{\gamma} &= 2|\boldsymbol{\varepsilon}(\boldsymbol{u})|,\\ \boldsymbol{\tau} &= 2K\dot{\gamma}^{r-2}\boldsymbol{\varepsilon}(\boldsymbol{u})\end{aligned}$$

As the deviatoric stress tensor $\boldsymbol{\tau}$ depends explicitly on $\boldsymbol{\varepsilon}(\boldsymbol{u})$, it is easy to see that

$$\tau_{xx} = \tau_{yy} = 0$$

With the Euclidean Norm for tensors [GW11, Eq. (3.2)]

$$\begin{aligned}|\boldsymbol{\psi}| &= \sqrt{\frac{1}{2}\boldsymbol{\psi} : \boldsymbol{\psi}} && \forall \psi \in D(\Omega, \mathbb{R}^{d\times d}),\\ \boldsymbol{\psi} : \boldsymbol{\psi} &= \sum_{i=0}^{n-1}\sum_{j=0}^{m-1}\psi_{ij}^2 && \forall \psi \in D(\Omega, \mathbb{R}^{d\times d})\end{aligned}$$

we get

$$\begin{aligned}\dot{\gamma} &= \left|\frac{\partial u_x}{\partial y}\right|,\\ \boldsymbol{\tau} &= K\left(\left|\frac{\partial u_x}{\partial y}\right|\right)^{r-2}\begin{pmatrix}0 & \frac{\partial u_x}{\partial y}\\ \frac{\partial u_x}{\partial y} & 0\end{pmatrix}\end{aligned}$$

For sake of simplicity we assume

$$\frac{\partial u_x}{\partial y} \geq 0$$

hence we can omit the absolute value

$$\boldsymbol{\tau} = K\begin{pmatrix}0 & \left(\frac{\partial u_x}{\partial y}\right)^{r-1}\\ \left(\frac{\partial u_x}{\partial y}\right)^{r-1} & 0\end{pmatrix}$$

Next, we focus solely on the x-component of the momentum equation

$$-K(r-1)\left(\frac{\partial u_x}{\partial y}\right)^{r-2}\frac{\partial^2 u_x}{\partial y^2} = -\frac{\partial p}{\partial x} + C$$

As the left-hand side depends solely on y and the right-hand side solely on x it follows

$$-\frac{\partial p}{\partial x} + C = \text{const}$$

Our forcing term C is constant and arbitrary. As we applied periodic boundary conditions the only solution is that the pressure gradient in x vanishes

$$\frac{\partial p}{\partial x} = 0$$

Die approbierte gedruckte Originalversion dieser Diplomarbeit ist an der TU Wien Bibliothek verfügbar
The approved original version of this thesis is available in print at TU Wien Bibliothek.
TU Bibliothek Your knowledge hub WIEN

Since the velocity u_x depends only on y, the partial derivative is equivalent to the total derivative

$$\frac{\partial u_x}{\partial y} = \frac{\mathrm{d}u_x}{\mathrm{d}y}$$

We continue by transforming the problem in a non-linear system of first-order differential equations

$$\begin{bmatrix} \kappa \\ \kappa^{r-2}\dfrac{\mathrm{d}\kappa}{\mathrm{d}y} \end{bmatrix} = \begin{bmatrix} \dfrac{\mathrm{d}u_x}{\mathrm{d}y} \\ \dfrac{-C}{K(r-1)} \end{bmatrix}$$

With help of a separation ansatz we find a analytic solution for κ

$$\int \kappa^{r-2}\,\mathrm{d}\kappa = \int \frac{-C}{K(r-1)}\,\mathrm{d}y,$$
$$\frac{1}{(r-1)}\kappa^{r-1} = \frac{-Cy}{K(r-1)} + c_1$$

As a boundary condition we use the fact that in a channel the velocity is maximal in the center. Mathematically, this translates to

$$\left.\frac{\mathrm{d}u_x}{\mathrm{d}y}\right|_{y=0} = \kappa(y=0) = 0 = c_1$$

This result yields

$$\kappa = \frac{\mathrm{d}u_x}{\mathrm{d}y} = \left(\frac{-Cy}{K}\right)^{\frac{1}{r-1}}$$

Our initial assumption $\kappa \geq 0$, holds as long as $y \leq 0$ for $C > 0$.
By integrating further we gain an expression for the velocity u_x

$$u_x = -\frac{r-1}{r}\frac{K}{C}\left(\frac{-Cy}{K}\right)^{\frac{r}{r-1}} + c_2$$

The integration constant c_2 we determine by the no-slip boundary condition at the wall, namely

$$u_x(y=-H/2) = 0$$
$$u_x = \frac{r-1}{r}\frac{K}{C}\left[\left(\frac{CH}{2K}\right)^{\frac{r}{r-1}} - \left(\frac{-Cy}{K}\right)^{\frac{r}{r-1}}\right]$$

By a symmetry argument and the requirement $C > 0$ we can now define a velocity profile for the whole channel

$$u_x = \frac{r-1}{r}\left[\frac{C}{K}\right]^{\frac{1}{r-1}}\left(\frac{H}{2}\right)^{\frac{r}{r-1}}\left[1 - \left(\frac{2|y|}{H}\right)^{\frac{r}{r-1}}\right]$$

Die approbierte gedruckte Originalversion dieser Diplomarbeit ist an der TU Wien Bibliothek verfügbar
The approved original version of this thesis is available in print at TU Wien Bibliothek.
TU Bibliothek Your knowledge hub WIEN

The momentum equation in y-direction yields

$$\frac{\partial p}{\partial y} = f_y = 0$$

This result deduces that the pressure is only a constant. To be more precise, due to the mathematical gauging $\int_\Omega p\,dx = 0$ it follows

$$p = 0$$

In summary the exact solutions for a power-law constituted fluid are given by

$$u_x := \frac{r-1}{r}\left[\frac{C}{K}\right]^{\frac{1}{r-1}}\left(\frac{H}{2}\right)^{\frac{r}{r-1}}\left[1-\left(\frac{2|y|}{H}\right)^{\frac{r}{r-1}}\right] \qquad u_y := 0$$

$$\tau_{xy} := -Cy \qquad \tau_{xx} := \tau_{yy} := 0$$

$$\varepsilon_{xy} := -\frac{\operatorname{sgn}(y)}{2}\left(\frac{|Cy|}{K}\right)^{\frac{1}{r-1}} \qquad \varepsilon_{xx} := \varepsilon_{yy} := 0$$

$$\boldsymbol{u} := \begin{pmatrix} u_x \\ u_y \end{pmatrix} \qquad \boldsymbol{\tau} := \begin{pmatrix} \tau_{xx} & \tau_{xy} \\ \tau_{xy} & \tau_{yy} \end{pmatrix} \qquad \boldsymbol{\varepsilon}(\boldsymbol{u}) := \begin{pmatrix} \varepsilon_{xx} & \varepsilon_{xy} \\ \varepsilon_{xy} & \varepsilon_{yy} \end{pmatrix} \qquad p := 0$$

Note, that for a power-law exponent $r = 2$ we recover the Newtonian solution

A.2 Bingham constitutive relation

For a Bingham fluid the constitutive relation is given by equation (2.9)

$$\begin{cases} \boldsymbol{\tau} = 2\mu\boldsymbol{\varepsilon}(\boldsymbol{u}) + \dfrac{\tau_y}{|\boldsymbol{\varepsilon}(\boldsymbol{u})|}\boldsymbol{\varepsilon}(\boldsymbol{u}) & \text{if } |\boldsymbol{\tau}| > \tau_y, \\ \boldsymbol{\varepsilon}(\boldsymbol{u}) = \boldsymbol{0} & \text{if } |\boldsymbol{\tau}| \le \tau_y \end{cases}$$

Similarly to the power-law model, we have the explicit dependency of the deviatoric stress tensor $\boldsymbol{\tau}$ on $\boldsymbol{\varepsilon}(\boldsymbol{u})$. Hence it holds

$$\tau_{xx} = \tau_{yy} = 0$$

and due to the momentum equation it follows

$$\tau_{xy} = -Cy$$

The considerations done in the previous section regarding the pressure p hold also for the Bingham model. Hence

$$p = 0$$

Next we determine the threshold value below which rigid body translation occurs

$$|\boldsymbol{\tau}| = |Cy| = \tau_y$$

Die approbierte gedruckte Originalversion dieser Diplomarbeit ist an der TU Wien Bibliothek verfügbar
The approved original version of this thesis is available in print at TU Wien Bibliothek.
TU Bibliothek Your knowledge hub WIEN

Assume

$$|Cy| > \tau_y \qquad \text{and} \qquad \frac{\mathrm{d}u_x}{\mathrm{d}y} \geq 0$$

such that the fluid is in motion and the velocity gradient is positive. Then the constitutive relation becomes in one component

$$-Cy = \mu \frac{\mathrm{d}u_x}{\mathrm{d}y} + \tau_y$$

By integrating we find an expression for the velocity u_x

$$u_x = -\frac{Cy^2}{2\mu} - \tau_y y + c_2$$

The requirement

$$\frac{\mathrm{d}u_x}{\mathrm{d}y} = -\frac{Cy}{\mu} - \frac{\tau_y}{\mu} > 0$$

is only fulfilled (for given $C > 0$) if

$$y < -\frac{\tau_y}{C}$$

This implies for the spatial coordinate y

$$-\frac{H}{2} < y < -\frac{\tau_y}{C}$$

whereby the lower limit results from the boundedness of the geometry. By above considerations we apply a no-slip boundary condition on the lower wall $y = -H/2$

$$u_x(y = -\frac{H}{2}) = -\frac{CH^2}{8\mu} + \frac{\tau_y H}{2\mu} + c_2$$
$$c_2 = -\frac{\tau_y H}{2\mu} + \frac{CH^2}{8\mu}$$

Hence the velocity field in the interval $-H/2 < y < -\tau_y/C$ is given by

$$u_x = \frac{C}{2\mu}\left(\frac{H^2}{4} - y^2\right) - \frac{\tau_y}{\mu}\left(y + \frac{H}{2}\right)$$

If we further consider the remaining options, namely

$$|Cy| > \tau_y \qquad \text{and} \qquad \frac{\mathrm{d}u_x}{\mathrm{d}y} \leq 0,$$
$$|Cy| \leq \tau_y \qquad \text{and} \qquad \frac{\mathrm{d}u_x}{\mathrm{d}y} = 0$$

and the continuity of the velocity, we obtain an expression for the entire canal

$$u_x := \begin{cases} \frac{C}{2\mu}\left(\frac{H^2}{4} - y^2\right) - \frac{\tau_y}{\mu}\left(y + \frac{H}{2}\right), & \text{if } -\frac{H}{2} \leq y \leq \frac{-\tau_y}{C}, \\ \frac{C}{2\mu}\left(\frac{H^2}{4} - \left(\frac{\tau_y}{C}\right)^2\right) - \frac{\tau_y}{\mu}\left(-\frac{\tau_y}{C} + \frac{H}{2}\right), & \text{if } -\frac{\tau_y}{C} \leq y \leq \frac{\tau_y}{C}, \\ \frac{C}{2\mu}\left(\frac{H^2}{4} - y^2\right) - \frac{\tau_y}{\mu}\left(-y + \frac{H}{2}\right), & \text{if } \frac{\tau_y}{C} \leq y \leq \frac{H}{2}. \end{cases}$$

Die approbierte gedruckte Originalversion dieser Diplomarbeit ist an der TU Wien Bibliothek verfügbar
The approved original version of this thesis is available in print at TU Wien Bibliothek.
TU Bibliothek Your knowledge hub WIEN

Respectively, the rate-of-strain tensor $\boldsymbol{\varepsilon}$ is

$$\varepsilon_{xy} := \frac{1}{2}\frac{\mathrm{d}u_x}{\mathrm{d}y} = \begin{cases} -\frac{C}{2\mu}y - \frac{\tau_y}{2\mu}, \\ 0, \\ -\frac{C}{2\mu}y + \frac{\tau_y}{2\mu}, \end{cases} \qquad \varepsilon_{xx} = \varepsilon_{yy} := \begin{cases} 0, & \text{if } -\frac{H}{2} \leq y \leq -\frac{\tau_y}{C}, \\ 0, & \text{if } -\frac{\tau_y}{C} \leq y \leq \frac{\tau_y}{C}, \\ 0, & \text{if } \frac{\tau_y}{C} \leq y \leq \frac{H}{2}. \end{cases}$$

Finally, the exact solutions can be listed

$$\boldsymbol{u} := \begin{pmatrix} u_x \\ u_y \end{pmatrix} \qquad \boldsymbol{\tau} := \begin{pmatrix} \tau_{xx} & \tau_{xy} \\ \tau_{xy} & \tau_{yy} \end{pmatrix} \qquad \boldsymbol{\varepsilon} := \begin{pmatrix} \varepsilon_{xx} & \varepsilon_{xy} \\ \varepsilon_{xy} & \varepsilon_{yy} \end{pmatrix} \qquad p := 0$$

Also in this case, if τ_y equals zero, we obtain the Newtonian solution.

Die approbierte gedruckte Originalversion dieser Diplomarbeit ist an der TU Wien Bibliothek verfügbar
The approved original version of this thesis is available in print at TU Wien Bibliothek.
TU Bibliothek Your knowledge hub WIEN

Appendix B Non-Newtonian Numerical Experiments - Values

In this chapter we list explicitly the finite element errors achieved in Chapter 5.

FEM	h	$\|\boldsymbol{u}_h - \boldsymbol{u}\|$	$\|\boldsymbol{\tau}_h - \boldsymbol{\tau}\|$	$\|\boldsymbol{\varepsilon}(\boldsymbol{u}_h) - \boldsymbol{\varepsilon}(\boldsymbol{u})\|$	$\|p_h - p\|$
$(\mathcal{MCS})$	2^{-3}	$1.90213 \cdot 10^{-5}$	$1.47863 \cdot 10^{-3}$	$1.35104 \cdot 10^{-3}$	$2.81869 \cdot 10^{-3}$
	2^{-4}	$2.15127 \cdot 10^{-6}$	$3.43256 \cdot 10^{-4}$	$3.16204 \cdot 10^{-4}$	$6.32529 \cdot 10^{-4}$
	2^{-5}	$2.41273 \cdot 10^{-7}$	$8.31689 \cdot 10^{-5}$	$7.63686 \cdot 10^{-5}$	$1.55417 \cdot 10^{-4}$
	2^{-6}	$2.92356 \cdot 10^{-8}$	$2.04546 \cdot 10^{-5}$	$1.89154 \cdot 10^{-5}$	$3.95733 \cdot 10^{-5}$
	2^{-7}	$3.61569 \cdot 10^{-9}$	$5.04209 \cdot 10^{-6}$	$4.67663 \cdot 10^{-6}$	$9.98644 \cdot 10^{-6}$
	2^{-8}	$8.42376 \cdot 10^{-10}$	$1.25975 \cdot 10^{-6}$	$1.17053 \cdot 10^{-6}$	$2.52605 \cdot 10^{-6}$
$(\mathcal{MCS}\text{-}\mathcal{S})$	2^{-3}	$2.05517 \cdot 10^{-5}$	$1.73757 \cdot 10^{-3}$	$6.57805 \cdot 10^{-4}$	$2.79707 \cdot 10^{-3}$
	2^{-4}	$2.28454 \cdot 10^{-6}$	$3.86764 \cdot 10^{-4}$	$1.50323 \cdot 10^{-4}$	$6.27411 \cdot 10^{-4}$
	2^{-5}	$2.53838 \cdot 10^{-7}$	$9.29537 \cdot 10^{-5}$	$3.65137 \cdot 10^{-5}$	$1.54262 \cdot 10^{-4}$
	2^{-6}	$3.06172 \cdot 10^{-8}$	$2.28053 \cdot 10^{-5}$	$8.98559 \cdot 10^{-6}$	$3.93139 \cdot 10^{-5}$
	2^{-7}	$3.77060 \cdot 10^{-9}$	$5.61245 \cdot 10^{-6}$	$2.21459 \cdot 10^{-6}$	$9.92531 \cdot 10^{-6}$
	2^{-8}	$8.57683 \cdot 10^{-10}$	$1.40140 \cdot 10^{-6}$	$5.53090 \cdot 10^{-7}$	$2.51103 \cdot 10^{-6}$
$(\mathcal{TH}\text{-}\mathcal{S})$	2^{-3}	$3.36631 \cdot 10^{-5}$	$3.05175 \cdot 10^{-3}$	$1.52588 \cdot 10^{-3}$	$3.80765 \cdot 10^{-3}$
	2^{-4}	$3.54925 \cdot 10^{-6}$	$6.89170 \cdot 10^{-4}$	$3.44585 \cdot 10^{-4}$	$8.19761 \cdot 10^{-4}$
	2^{-5}	$3.87950 \cdot 10^{-7}$	$1.62644 \cdot 10^{-4}$	$8.13221 \cdot 10^{-5}$	$1.98395 \cdot 10^{-4}$
	2^{-6}	$4.66884 \cdot 10^{-8}$	$3.99332 \cdot 10^{-5}$	$1.99666 \cdot 10^{-5}$	$5.03268 \cdot 10^{-5}$
	2^{-7}	$5.67935 \cdot 10^{-9}$	$9.84458 \cdot 10^{-6}$	$4.92229 \cdot 10^{-6}$	$1.26780 \cdot 10^{-5}$
	2^{-8}	$1.00215 \cdot 10^{-9}$	$2.46123 \cdot 10^{-6}$	$1.23062 \cdot 10^{-6}$	$3.20576 \cdot 10^{-6}$
$(\mathcal{SV}\text{-}\mathcal{S})$	2^{-3}	$5.85754 \cdot 10^{-5}$	$4.31916 \cdot 10^{-3}$	$2.15958 \cdot 10^{-3}$	$7.65096 \cdot 10^{-3}$
	2^{-4}	$5.58276 \cdot 10^{-6}$	$9.59959 \cdot 10^{-4}$	$4.79979 \cdot 10^{-4}$	$1.62506 \cdot 10^{-3}$
	2^{-5}	$6.06796 \cdot 10^{-7}$	$2.34000 \cdot 10^{-4}$	$1.17000 \cdot 10^{-4}$	$3.93745 \cdot 10^{-4}$
	2^{-6}	$7.16205 \cdot 10^{-8}$	$5.78887 \cdot 10^{-5}$	$2.89443 \cdot 10^{-5}$	$9.70207 \cdot 10^{-5}$
	2^{-7}	$8.64926 \cdot 10^{-9}$	$1.43216 \cdot 10^{-5}$	$7.16082 \cdot 10^{-6}$	$2.39544 \cdot 10^{-5}$
	2^{-8}	$1.28866 \cdot 10^{-9}$	$3.58030 \cdot 10^{-6}$	$1.79015 \cdot 10^{-6}$	$5.96998 \cdot 10^{-6}$

TABLE B.1 – L^2-errors of polynomial order $k = 2$ over mesh size h for Newtonian Stokes flow (Figure 5.2)

Die approbierte gedruckte Originalversion dieser Diplomarbeit ist an der TU Wien Bibliothek verfügbar
The approved original version of this thesis is available in print at TU Wien Bibliothek.
TU Bibliothek Your knowledge hub WIEN

FEM	h	$\|\boldsymbol{u}_h - \boldsymbol{u}\|$	$\|\boldsymbol{\tau}_h - \boldsymbol{\tau}\|$	$\|\boldsymbol{\varepsilon}(\boldsymbol{u}_h) - \boldsymbol{\varepsilon}(\boldsymbol{u})\|$	$\|p_h - p\|$
$(\mathcal{MCS})$	2^{-3}	$1.32038 \cdot 10^{-3}$	$8.78333 \cdot 10^{-3}$	$7.35639 \cdot 10^{-3}$	$3.42657 \cdot 10^{-3}$
	2^{-4}	$2.97984 \cdot 10^{-4}$	$2.98392 \cdot 10^{-3}$	$1.72910 \cdot 10^{-3}$	$1.17525 \cdot 10^{-3}$
	2^{-5}	$7.18709 \cdot 10^{-5}$	$1.00163 \cdot 10^{-3}$	$4.21934 \cdot 10^{-4}$	$3.88623 \cdot 10^{-4}$
	2^{-6}	$1.76700 \cdot 10^{-5}$	$3.76282 \cdot 10^{-4}$	$1.03681 \cdot 10^{-4}$	$1.42514 \cdot 10^{-4}$
	2^{-7}	$4.37474 \cdot 10^{-6}$	$1.29909 \cdot 10^{-4}$	$2.57607 \cdot 10^{-5}$	$4.96986 \cdot 10^{-5}$
	2^{-8}	$1.08351 \cdot 10^{-6}$	$4.50095 \cdot 10^{-5}$	$6.41693 \cdot 10^{-6}$	$1.73380 \cdot 10^{-5}$
$(\mathcal{MCS}\text{-}\mathcal{S})$	2^{-3}	$1.06067 \cdot 10^{-4}$	$7.74937 \cdot 10^{-3}$	$1.93248 \cdot 10^{-3}$	$2.63806 \cdot 10^{-3}$
	2^{-4}	$1.16177 \cdot 10^{-5}$	$2.81634 \cdot 10^{-3}$	$4.34245 \cdot 10^{-4}$	$1.09265 \cdot 10^{-3}$
	2^{-5}	$1.38090 \cdot 10^{-6}$	$9.71699 \cdot 10^{-4}$	$1.04248 \cdot 10^{-4}$	$4.00706 \cdot 10^{-4}$
	2^{-6}	$1.69745 \cdot 10^{-7}$	$3.60422 \cdot 10^{-4}$	$2.58033 \cdot 10^{-5}$	$1.42302 \cdot 10^{-4}$
	2^{-7}	$2.06756 \cdot 10^{-8}$	$1.25053 \cdot 10^{-4}$	$6.33382 \cdot 10^{-6}$	$5.12562 \cdot 10^{-5}$
	2^{-8}	$2.55423 \cdot 10^{-9}$	$4.34045 \cdot 10^{-5}$	$1.56365 \cdot 10^{-6}$	$1.79564 \cdot 10^{-5}$
$(\mathcal{TH}\text{-}\mathcal{S})$	2^{-3}	$1.89834 \cdot 10^{-4}$	$2.12691 \cdot 10^{-2}$	$7.68582 \cdot 10^{-3}$	$6.56656 \cdot 10^{-4}$
	2^{-4}	$2.03469 \cdot 10^{-5}$	$7.33263 \cdot 10^{-3}$	$1.81097 \cdot 10^{-3}$	$3.22760 \cdot 10^{-4}$
	2^{-5}	$2.38638 \cdot 10^{-6}$	$2.60270 \cdot 10^{-3}$	$4.41452 \cdot 10^{-4}$	$4.04835 \cdot 10^{-5}$
	2^{-6}	$2.91059 \cdot 10^{-7}$	$9.09193 \cdot 10^{-4}$	$1.08225 \cdot 10^{-4}$	$2.04025 \cdot 10^{-5}$
	2^{-7}	$3.54040 \cdot 10^{-8}$	$3.31790 \cdot 10^{-4}$	$2.69215 \cdot 10^{-5}$	$5.50049 \cdot 10^{-6}$
	2^{-8}	$4.37435 \cdot 10^{-9}$	$1.17407 \cdot 10^{-4}$	$6.69711 \cdot 10^{-6}$	$1.72743 \cdot 10^{-6}$
$(\mathcal{SV}\text{-}\mathcal{S})$	2^{-3}	$2.64247 \cdot 10^{-4}$	$3.65985 \cdot 10^{-2}$	$1.01084 \cdot 10^{-2}$	$4.87222 \cdot 10^{-2}$
	2^{-4}	$2.84369 \cdot 10^{-5}$	$1.27300 \cdot 10^{-2}$	$2.47372 \cdot 10^{-3}$	$1.70931 \cdot 10^{-2}$
	2^{-5}	$3.31960 \cdot 10^{-6}$	$4.59772 \cdot 10^{-3}$	$6.09543 \cdot 10^{-4}$	$6.24696 \cdot 10^{-3}$
	2^{-6}	$3.94280 \cdot 10^{-7}$	$1.61911 \cdot 10^{-3}$	$1.48050 \cdot 10^{-4}$	$2.23650 \cdot 10^{-3}$
	2^{-7}	$4.89438 \cdot 10^{-8}$	$5.86971 \cdot 10^{-4}$	$3.73691 \cdot 10^{-5}$	$8.04799 \cdot 10^{-4}$
	2^{-8}	$6.09140 \cdot 10^{-9}$	$2.07296 \cdot 10^{-4}$	$9.30756 \cdot 10^{-6}$	$2.83111 \cdot 10^{-4}$

TABLE B.2 – L^2-errors of polynomial order $k = 2$ over mesh size h for non-Newtonian power-law channel flow with power-law exponent $r = 1.4$ (Figure 5.5)

Die approbierte gedruckte Originalversion dieser Diplomarbeit ist an der TU Wien Bibliothek verfügbar
The approved original version of this thesis is available in print at TU Wien Bibliothek.
TU Bibliothek Your knowledge hub WIEN

FEM	h	$\|\boldsymbol{u}_h - \boldsymbol{u}\|$	$\|\boldsymbol{\tau}_h - \boldsymbol{\tau}\|$	$\|\boldsymbol{\varepsilon}(\boldsymbol{u}_h) - \boldsymbol{\varepsilon}(\boldsymbol{u})\|$	$\|p_h - p\|$
$(\mathcal{MCS})$	2^{-3}	$3.01320 \cdot 10^{-2}$	$3.93966 \cdot 10^{-2}$	$1.21350 \cdot 10^{-1}$	$1.98483 \cdot 10^{-2}$
	2^{-4}	$6.88177 \cdot 10^{-3}$	$1.21660 \cdot 10^{-2}$	$2.92039 \cdot 10^{-2}$	$6.26465 \cdot 10^{-3}$
	2^{-5}	$1.63061 \cdot 10^{-3}$	$3.86796 \cdot 10^{-3}$	$7.10518 \cdot 10^{-3}$	$2.01256 \cdot 10^{-3}$
$(\mathcal{MCS}\text{-}\mathcal{S})$	2^{-3}	$1.69587 \cdot 10^{-3}$	$2.14399 \cdot 10^{-2}$	$3.36952 \cdot 10^{-2}$	$9.27461 \cdot 10^{-3}$
	2^{-4}	$1.96057 \cdot 10^{-4}$	$7.36999 \cdot 10^{-3}$	$7.74493 \cdot 10^{-3}$	$3.34386 \cdot 10^{-3}$
	2^{-5}	$2.32720 \cdot 10^{-5}$	$2.48338 \cdot 10^{-3}$	$1.83848 \cdot 10^{-3}$	$1.16450 \cdot 10^{-3}$
	2^{-6}	$2.81653 \cdot 10^{-6}$	$9.01096 \cdot 10^{-4}$	$4.44931 \cdot 10^{-4}$	$3.82739 \cdot 10^{-4}$
	2^{-7}	$3.47474 \cdot 10^{-7}$	$2.74958 \cdot 10^{-4}$	$1.10317 \cdot 10^{-4}$	$1.16630 \cdot 10^{-4}$
	2^{-8}	$4.53980 \cdot 10^{-8}$	$5.59742 \cdot 10^{-4}$	$2.73158 \cdot 10^{-5}$	$1.17180 \cdot 10^{-4}$
$(\mathcal{TH}\text{-}\mathcal{S})$	2^{-3}	$3.19885 \cdot 10^{-3}$	$6.52286 \cdot 10^{-2}$	$1.19210 \cdot 10^{-1}$	$7.72547 \cdot 10^{-3}$
	2^{-4}	$3.54147 \cdot 10^{-4}$	$2.35633 \cdot 10^{-2}$	$2.87678 \cdot 10^{-2}$	$1.31912 \cdot 10^{-3}$
	2^{-5}	$4.10050 \cdot 10^{-5}$	$8.59679 \cdot 10^{-3}$	$6.99370 \cdot 10^{-3}$	$2.24580 \cdot 10^{-4}$
	2^{-6}	$4.90107 \cdot 10^{-6}$	$3.01286 \cdot 10^{-3}$	$1.70929 \cdot 10^{-3}$	$1.28345 \cdot 10^{-4}$
	2^{-7}	$6.04137 \cdot 10^{-7}$	$1.10795 \cdot 10^{-3}$	$4.24368 \cdot 10^{-4}$	$2.71917 \cdot 10^{-5}$
	2^{-8}	$9.26531 \cdot 10^{-8}$	$3.92443 \cdot 10^{-4}$	$1.05588 \cdot 10^{-4}$	$3.07830 \cdot 10^{-6}$
$(\mathcal{SV}\text{-}\mathcal{S})$	2^{-3}	$4.32434 \cdot 10^{-3}$	$1.21405 \cdot 10^{-1}$	$1.37237 \cdot 10^{-1}$	$1.56732 \cdot 10^{-1}$
	2^{-4}	$4.49538 \cdot 10^{-4}$	$4.49340 \cdot 10^{-2}$	$3.38076 \cdot 10^{-2}$	$5.90568 \cdot 10^{-2}$
	2^{-5}	$4.96667 \cdot 10^{-5}$	$1.65641 \cdot 10^{-2}$	$8.32623 \cdot 10^{-3}$	$2.19770 \cdot 10^{-2}$
	2^{-6}	$5.77596 \cdot 10^{-6}$	$5.77156 \cdot 10^{-3}$	$2.02830 \cdot 10^{-3}$	$7.75360 \cdot 10^{-3}$
	2^{-7}	$7.09904 \cdot 10^{-7}$	$1.98614 \cdot 10^{-3}$	$5.06334 \cdot 10^{-4}$	$2.51397 \cdot 10^{-3}$
	2^{-8}	$1.04256 \cdot 10^{-7}$	$5.69274 \cdot 10^{-4}$	$1.25783 \cdot 10^{-4}$	$6.66623 \cdot 10^{-4}$

TABLE B.3 – L^2-errors of polynomial order $k = 2$ over mesh size h for non-Newtonian power-law channel flow with power-law exponent $r = 1.2$ (Figure 5.6)

Die approbierte gedruckte Originalversion dieser Diplomarbeit ist an der TU Wien Bibliothek verfügbar
The approved original version of this thesis is available in print at TU Wien Bibliothek.
TU Bibliothek Your knowledge hub WIEN

FEM	h	$\|\boldsymbol{u}_{\kappa,h} - \boldsymbol{u}\|$	$\|\boldsymbol{\tau}_{\kappa,h} - \boldsymbol{\tau}\|$	$\|\boldsymbol{\varepsilon}(\boldsymbol{u}_{\kappa,h}) - \boldsymbol{\varepsilon}(\boldsymbol{u})\|$	$\|p_{\kappa,h} - p\|$
$(\mathcal{MCS})$	2^{-3}	$1.03965 \cdot 10^{-4}$	$2.97336 \cdot 10^{-2}$	$3.52807 \cdot 10^{-3}$	$1.79785 \cdot 10^{-2}$
	2^{-4}	$2.51485 \cdot 10^{-5}$	$2.15065 \cdot 10^{-2}$	$1.46755 \cdot 10^{-3}$	$1.39818 \cdot 10^{-2}$
	2^{-5}	$6.94404 \cdot 10^{-6}$	$1.03089 \cdot 10^{-2}$	$6.00139 \cdot 10^{-4}$	$6.55596 \cdot 10^{-3}$
	2^{-6}	$2.70773 \cdot 10^{-6}$	$4.80009 \cdot 10^{-3}$	$2.34934 \cdot 10^{-4}$	$2.60950 \cdot 10^{-3}$
	2^{-7}	$2.38510 \cdot 10^{-6}$	$2.69988 \cdot 10^{-3}$	$1.10110 \cdot 10^{-4}$	$1.24398 \cdot 10^{-3}$
	2^{-8}	$3.09216 \cdot 10^{-6}$	$1.77793 \cdot 10^{-3}$	$6.38316 \cdot 10^{-5}$	$7.99341 \cdot 10^{-4}$
$(\mathcal{MCS}\text{-}\mathcal{S})$	2^{-3}	$7.21995 \cdot 10^{-5}$	$3.00154 \cdot 10^{-2}$	$2.01677 \cdot 10^{-3}$	$1.44420 \cdot 10^{-2}$
	2^{-4}	$2.56162 \cdot 10^{-5}$	$1.30852 \cdot 10^{-2}$	$8.02172 \cdot 10^{-4}$	$6.69159 \cdot 10^{-3}$
	2^{-5}	$8.29655 \cdot 10^{-6}$	$4.31829 \cdot 10^{-3}$	$2.81455 \cdot 10^{-4}$	$2.00257 \cdot 10^{-3}$
	2^{-6}	$4.42891 \cdot 10^{-6}$	$1.84766 \cdot 10^{-3}$	$1.15777 \cdot 10^{-4}$	$8.84100 \cdot 10^{-4}$
	2^{-7}	$3.72493 \cdot 10^{-6}$	$4.53010 \cdot 10^{-4}$	$6.17368 \cdot 10^{-5}$	$2.01024 \cdot 10^{-4}$
	2^{-8}	$3.65588 \cdot 10^{-6}$	$1.10583 \cdot 10^{-4}$	$5.09433 \cdot 10^{-5}$	$4.53148 \cdot 10^{-5}$
$(\mathcal{TH}\text{-}\mathcal{S})$	2^{-3}	$1.69424 \cdot 10^{-4}$	$4.39252 \cdot 10^{-2}$	$4.46945 \cdot 10^{-3}$	$4.58327 \cdot 10^{-3}$
	2^{-4}	$4.70873 \cdot 10^{-5}$	$2.89980 \cdot 10^{-2}$	$1.71281 \cdot 10^{-3}$	$4.98736 \cdot 10^{-3}$
	2^{-5}	$1.72887 \cdot 10^{-5}$	$1.61828 \cdot 10^{-2}$	$6.59220 \cdot 10^{-4}$	$1.07445 \cdot 10^{-3}$
	2^{-6}	$6.92208 \cdot 10^{-6}$	$8.44059 \cdot 10^{-3}$	$2.65969 \cdot 10^{-4}$	$5.63551 \cdot 10^{-4}$
	2^{-7}	$4.20673 \cdot 10^{-6}$	$4.38346 \cdot 10^{-3}$	$1.19713 \cdot 10^{-4}$	$1.09933 \cdot 10^{-4}$
	2^{-8}	$3.70530 \cdot 10^{-6}$	$1.93670 \cdot 10^{-3}$	$6.71325 \cdot 10^{-5}$	$2.53970 \cdot 10^{-5}$
$(\mathcal{SV}\text{-}\mathcal{S})$	2^{-3}	$1.98590 \cdot 10^{-4}$	$7.47575 \cdot 10^{-2}$	$5.79693 \cdot 10^{-3}$	$8.68304 \cdot 10^{-2}$
	2^{-4}	$4.63793 \cdot 10^{-5}$	$4.67935 \cdot 10^{-2}$	$2.16875 \cdot 10^{-3}$	$5.66539 \cdot 10^{-2}$
	2^{-5}	$1.53832 \cdot 10^{-5}$	$2.81496 \cdot 10^{-2}$	$8.40561 \cdot 10^{-4}$	$3.46833 \cdot 10^{-2}$
	2^{-6}	$6.01982 \cdot 10^{-6}$	$1.47216 \cdot 10^{-2}$	$3.33347 \cdot 10^{-4}$	$1.78533 \cdot 10^{-2}$
	2^{-7}	$3.97675 \cdot 10^{-6}$	$7.33488 \cdot 10^{-3}$	$1.45814 \cdot 10^{-4}$	$8.65522 \cdot 10^{-3}$
	2^{-8}	$3.67866 \cdot 10^{-6}$	$3.09925 \cdot 10^{-3}$	$7.63385 \cdot 10^{-5}$	$3.65096 \cdot 10^{-3}$

TABLE B.4 – L^2-errors of polynomial order $k = 2$ over mesh size h for a regularised non-Newtonian explicit constituted *Bingham*($\tau_y = 0.2$, $\kappa = 10^{-4}$) flow in a two-dimensional channel (Figure 5.8)

Die approbierte gedruckte Originalversion dieser Diplomarbeit ist an der TU Wien Bibliothek verfügbar
The approved original version of this thesis is available in print at TU Wien Bibliothek.
TU Bibliothek Your knowledge hub WIEN

FEM	h	$\|\boldsymbol{u}_{\kappa,h} - \boldsymbol{u}\|$	$\|\boldsymbol{\tau}_{\kappa,h} - \boldsymbol{\tau}\|$	$\|\boldsymbol{\varepsilon}(\boldsymbol{u}_{\kappa,h}) - \boldsymbol{\varepsilon}(\boldsymbol{u})\|$	$\|p_{\kappa,h} - p\|$
$(\mathcal{MCS})$	2^{-3}	$1.04045 \cdot 10^{-4}$	$3.09136 \cdot 10^{-2}$	$3.52788 \cdot 10^{-3}$	$1.88613 \cdot 10^{-2}$
	2^{-4}	$2.45207 \cdot 10^{-5}$	$2.83537 \cdot 10^{-2}$	$1.46602 \cdot 10^{-3}$	$1.87629 \cdot 10^{-2}$
	2^{-5}	$6.33948 \cdot 10^{-6}$	$2.25067 \cdot 10^{-2}$	$5.98688 \cdot 10^{-4}$	$1.50863 \cdot 10^{-2}$
	2^{-6}	$1.63015 \cdot 10^{-6}$	$1.69685 \cdot 10^{-2}$	$2.35576 \cdot 10^{-4}$	$1.12317 \cdot 10^{-2}$
$(\mathcal{MCS}\text{-}\mathcal{S})$	2^{-3}	$7.18251 \cdot 10^{-5}$	$3.16937 \cdot 10^{-2}$	$2.01689 \cdot 10^{-3}$	$1.55931 \cdot 10^{-2}$
	2^{-4}	$2.51097 \cdot 10^{-5}$	$1.75483 \cdot 10^{-2}$	$8.02717 \cdot 10^{-4}$	$9.67964 \cdot 10^{-3}$
	2^{-5}	$6.97184 \cdot 10^{-6}$	$8.30269 \cdot 10^{-3}$	$2.79536 \cdot 10^{-4}$	$4.51718 \cdot 10^{-3}$
	2^{-6}	$2.21923 \cdot 10^{-6}$	$8.34415 \cdot 10^{-3}$	$1.10141 \cdot 10^{-4}$	$4.57656 \cdot 10^{-3}$
	2^{-7}	$6.34195 \cdot 10^{-7}$	$4.03561 \cdot 10^{-3}$	$4.18414 \cdot 10^{-5}$	$2.30229 \cdot 10^{-3}$
	2^{-8}	$1.40470 \cdot 10^{-7}$	$2.12781 \cdot 10^{-3}$	$1.49231 \cdot 10^{-5}$	$1.25554 \cdot 10^{-3}$
$(\mathcal{TH}\text{-}\mathcal{S})$	2^{-3}	$1.69267 \cdot 10^{-4}$	$5.64582 \cdot 10^{-2}$	$4.47526 \cdot 10^{-3}$	$4.91162 \cdot 10^{-3}$
	2^{-4}	$4.64150 \cdot 10^{-5}$	$3.86842 \cdot 10^{-2}$	$1.71799 \cdot 10^{-3}$	$7.40322 \cdot 10^{-3}$
	2^{-5}	$1.58371 \cdot 10^{-5}$	$2.68549 \cdot 10^{-2}$	$6.59257 \cdot 10^{-4}$	$6.24854 \cdot 10^{-3}$
	2^{-6}	$4.82117 \cdot 10^{-6}$	$2.01189 \cdot 10^{-2}$	$2.61454 \cdot 10^{-4}$	$6.28860 \cdot 10^{-3}$
	2^{-7}	$1.44453 \cdot 10^{-6}$	$1.25254 \cdot 10^{-2}$	$1.08699 \cdot 10^{-4}$	$1.41318 \cdot 10^{-3}$
	2^{-8}	$4.09675 \cdot 10^{-7}$	$7.51298 \cdot 10^{-3}$	$4.51997 \cdot 10^{-5}$	$3.44866 \cdot 10^{-4}$
$(\mathcal{SV}\text{-}\mathcal{S})$	2^{-3}	$1.98617 \cdot 10^{-4}$	$7.63745 \cdot 10^{-2}$	$5.80703 \cdot 10^{-3}$	$8.82920 \cdot 10^{-2}$
	2^{-4}	$4.57339 \cdot 10^{-5}$	$5.67136 \cdot 10^{-2}$	$2.17912 \cdot 10^{-3}$	$6.42430 \cdot 10^{-2}$
	2^{-5}	$1.39207 \cdot 10^{-5}$	$4.64221 \cdot 10^{-2}$	$8.45434 \cdot 10^{-4}$	$5.43506 \cdot 10^{-2}$
	2^{-6}	$3.81609 \cdot 10^{-6}$	$3.55602 \cdot 10^{-2}$	$3.31603 \cdot 10^{-4}$	$4.22490 \cdot 10^{-2}$
	2^{-7}	$1.04857 \cdot 10^{-6}$	$2.37087 \cdot 10^{-2}$	$1.37080 \cdot 10^{-4}$	$2.85799 \cdot 10^{-2}$
	2^{-8}	$2.65935 \cdot 10^{-7}$	$1.43772 \cdot 10^{-2}$	$5.74848 \cdot 10^{-5}$	$1.71005 \cdot 10^{-2}$

TABLE B.5 – L^2-errors of polynomial order $k = 2$ over mesh size h for a regularised non-Newtonian explicit constituted *Bingham*($\tau_y = 0.2$, $\kappa = 10^{-8}$) flow in a two-dimensional channel (Figure 5.9)

Die approbierte gedruckte Originalversion dieser Diplomarbeit ist an der TU Wien Bibliothek verfügbar
The approved original version of this thesis is available in print at TU Wien Bibliothek.
TU Bibliothek Your knowledge hub WIEN

FEM	h	$\|\boldsymbol{u}_{\kappa,h} - \boldsymbol{u}\|$	$\|\boldsymbol{\tau}_{\kappa,h} - \boldsymbol{\tau}\|$	$\|\boldsymbol{\varepsilon}(\boldsymbol{u}_{\kappa,h}) - \boldsymbol{\varepsilon}(\boldsymbol{u})\|$	$\|p_{\kappa,h} - p\|$
$(\mathcal{MCS})$	10^{0}	$5.05825 \cdot 10^{-2}$	$1.11573 \cdot 10^{-6}$	$8.51713 \cdot 10^{-2}$	$3.28702 \cdot 10^{-7}$
	10^{-1}	$4.27329 \cdot 10^{-3}$	$2.00169 \cdot 10^{-5}$	$1.98249 \cdot 10^{-2}$	$5.96624 \cdot 10^{-6}$
	10^{-2}	$3.72516 \cdot 10^{-4}$	$1.87703 \cdot 10^{-4}$	$3.16264 \cdot 10^{-3}$	$5.83602 \cdot 10^{-5}$
	10^{-3}	$3.41941 \cdot 10^{-5}$	$2.61715 \cdot 10^{-3}$	$4.05656 \cdot 10^{-4}$	$1.14634 \cdot 10^{-3}$
	10^{-4}	$2.70773 \cdot 10^{-6}$	$4.80009 \cdot 10^{-3}$	$2.34934 \cdot 10^{-4}$	$2.60950 \cdot 10^{-3}$
	10^{-5}	$1.60753 \cdot 10^{-6}$	$7.93879 \cdot 10^{-3}$	$2.35653 \cdot 10^{-4}$	$4.93492 \cdot 10^{-3}$
	10^{-6}	$1.62827 \cdot 10^{-6}$	$1.14848 \cdot 10^{-2}$	$2.35594 \cdot 10^{-4}$	$7.44179 \cdot 10^{-3}$
	10^{-7}	$1.63004 \cdot 10^{-6}$	$1.45549 \cdot 10^{-2}$	$2.35578 \cdot 10^{-4}$	$9.56404 \cdot 10^{-3}$
	10^{-8}	$1.63015 \cdot 10^{-6}$	$1.69685 \cdot 10^{-2}$	$2.35576 \cdot 10^{-4}$	$1.12317 \cdot 10^{-2}$
$(\mathcal{MCS}\text{-}\mathcal{S})$	10^{0}	$5.05825 \cdot 10^{-2}$	$1.29512 \cdot 10^{-6}$	$8.51717 \cdot 10^{-2}$	$3.80847 \cdot 10^{-7}$
	10^{-1}	$4.27358 \cdot 10^{-3}$	$1.93471 \cdot 10^{-5}$	$1.98289 \cdot 10^{-2}$	$5.73817 \cdot 10^{-6}$
	10^{-2}	$3.73581 \cdot 10^{-4}$	$1.14842 \cdot 10^{-4}$	$3.17414 \cdot 10^{-3}$	$3.36135 \cdot 10^{-5}$
	10^{-3}	$3.66585 \cdot 10^{-5}$	$5.54249 \cdot 10^{-4}$	$4.22521 \cdot 10^{-4}$	$1.99049 \cdot 10^{-4}$
	10^{-4}	$4.42891 \cdot 10^{-6}$	$1.84766 \cdot 10^{-3}$	$1.15777 \cdot 10^{-4}$	$8.84100 \cdot 10^{-4}$
	10^{-5}	$2.29086 \cdot 10^{-6}$	$4.06726 \cdot 10^{-3}$	$1.09558 \cdot 10^{-4}$	$2.08368 \cdot 10^{-3}$
	10^{-6}	$2.22030 \cdot 10^{-6}$	$5.99281 \cdot 10^{-3}$	$1.10031 \cdot 10^{-4}$	$3.12141 \cdot 10^{-3}$
	10^{-7}	$2.21963 \cdot 10^{-6}$	$7.37163 \cdot 10^{-3}$	$1.10134 \cdot 10^{-4}$	$3.95559 \cdot 10^{-3}$
	10^{-8}	$2.21923 \cdot 10^{-6}$	$8.34415 \cdot 10^{-3}$	$1.10141 \cdot 10^{-4}$	$4.57656 \cdot 10^{-3}$
$(\mathcal{TH}\text{-}\mathcal{S})$	10^{0}	$5.05825 \cdot 10^{-2}$	$3.64600 \cdot 10^{-6}$	$8.51717 \cdot 10^{-2}$	$1.73079 \cdot 10^{-8}$
	10^{-1}	$4.27358 \cdot 10^{-3}$	$6.36696 \cdot 10^{-5}$	$1.98290 \cdot 10^{-2}$	$8.61349 \cdot 10^{-8}$
	10^{-2}	$3.73587 \cdot 10^{-4}$	$6.13594 \cdot 10^{-4}$	$3.17618 \cdot 10^{-3}$	$4.08002 \cdot 10^{-6}$
	10^{-3}	$3.69613 \cdot 10^{-5}$	$3.82025 \cdot 10^{-3}$	$4.80570 \cdot 10^{-4}$	$9.20393 \cdot 10^{-5}$
	10^{-4}	$6.92208 \cdot 10^{-6}$	$8.44059 \cdot 10^{-3}$	$2.65969 \cdot 10^{-4}$	$5.63551 \cdot 10^{-4}$
	10^{-5}	$4.97680 \cdot 10^{-6}$	$1.21169 \cdot 10^{-2}$	$2.61645 \cdot 10^{-4}$	$1.44433 \cdot 10^{-3}$
	10^{-6}	$4.83367 \cdot 10^{-6}$	$1.53744 \cdot 10^{-2}$	$2.61476 \cdot 10^{-4}$	$3.26170 \cdot 10^{-3}$
	10^{-7}	$4.82204 \cdot 10^{-6}$	$1.81113 \cdot 10^{-2}$	$2.61454 \cdot 10^{-4}$	$5.10613 \cdot 10^{-3}$
	10^{-8}	$4.82117 \cdot 10^{-6}$	$2.01189 \cdot 10^{-2}$	$2.61454 \cdot 10^{-4}$	$6.28860 \cdot 10^{-3}$
$(\mathcal{SV}\text{-}\mathcal{S})$	10^{0}	$5.05825 \cdot 10^{-2}$	$7.67495 \cdot 10^{-6}$	$8.51718 \cdot 10^{-2}$	$1.27892 \cdot 10^{-5}$
	10^{-1}	$4.27358 \cdot 10^{-3}$	$1.26987 \cdot 10^{-4}$	$1.98291 \cdot 10^{-2}$	$2.09251 \cdot 10^{-4}$
	10^{-2}	$3.73571 \cdot 10^{-4}$	$1.07208 \cdot 10^{-3}$	$3.17912 \cdot 10^{-3}$	$1.57265 \cdot 10^{-3}$
	10^{-3}	$3.67914 \cdot 10^{-5}$	$6.20311 \cdot 10^{-3}$	$5.18295 \cdot 10^{-4}$	$7.77608 \cdot 10^{-3}$
	10^{-4}	$6.01982 \cdot 10^{-6}$	$1.47216 \cdot 10^{-2}$	$3.33347 \cdot 10^{-4}$	$1.78533 \cdot 10^{-2}$
	10^{-5}	$3.97328 \cdot 10^{-6}$	$2.18379 \cdot 10^{-2}$	$3.31365 \cdot 10^{-4}$	$2.66791 \cdot 10^{-2}$
	10^{-6}	$3.82938 \cdot 10^{-6}$	$2.75893 \cdot 10^{-2}$	$3.31585 \cdot 10^{-4}$	$3.38315 \cdot 10^{-2}$
	10^{-7}	$3.81713 \cdot 10^{-6}$	$3.21911 \cdot 10^{-2}$	$3.31602 \cdot 10^{-4}$	$3.93097 \cdot 10^{-2}$
	10^{-8}	$3.81609 \cdot 10^{-6}$	$3.55602 \cdot 10^{-2}$	$3.31603 \cdot 10^{-4}$	$4.22490 \cdot 10^{-2}$

TABLE B.6 – L^2-errors of polynomial order $k = 2$ over regularisation parameter κ for a regularised non-Newtonian explicit constituted *Bingham*($\tau_y = 0.2$, $h = 2^{-6}$) flow in a two-dimensional channel (Figure 5.10)

Die approbierte gedruckte Originalversion dieser Diplomarbeit ist an der TU Wien Bibliothek verfügbar
The approved original version of this thesis is available in print at TU Wien Bibliothek.
TU Bibliothek Your knowledge hub WIEN

FEM	h	$\|\boldsymbol{u}_{\kappa,h} - \boldsymbol{u}\|$	$\|\boldsymbol{\tau}_{\kappa,h} - \boldsymbol{\tau}\|$	$\|\boldsymbol{\varepsilon}(\boldsymbol{u}_{\kappa,h}) - \boldsymbol{\varepsilon}(\boldsymbol{u})\|$	$\|p_{\kappa,h} - p\|$
$(\mathcal{MCS}\text{-}\mathcal{S})$	2^{-3}	$7.70449 \cdot 10^{-5}$	$3.13312 \cdot 10^{-2}$	$2.01678 \cdot 10^{-3}$	$1.53594 \cdot 10^{-2}$
	2^{-4}	$2.59232 \cdot 10^{-5}$	$1.74398 \cdot 10^{-2}$	$8.02592 \cdot 10^{-4}$	$9.25422 \cdot 10^{-3}$
	2^{-5}	$7.09990 \cdot 10^{-6}$	$8.18488 \cdot 10^{-3}$	$2.79639 \cdot 10^{-4}$	$4.37628 \cdot 10^{-3}$
	2^{-6}	$2.24721 \cdot 10^{-6}$	$8.80460 \cdot 10^{-3}$	$1.10209 \cdot 10^{-4}$	$4.84483 \cdot 10^{-3}$
	2^{-7}	$6.40323 \cdot 10^{-7}$	$4.99472 \cdot 10^{-3}$	$4.18128 \cdot 10^{-5}$	$2.85696 \cdot 10^{-3}$
	2^{-8}	$1.48181 \cdot 10^{-7}$	$2.70449 \cdot 10^{-3}$	$1.49251 \cdot 10^{-5}$	$1.57089 \cdot 10^{-3}$
$(\mathcal{TH}\text{-}\mathcal{S})$	2^{-3}	$1.71452 \cdot 10^{-4}$	$5.62779 \cdot 10^{-2}$	$4.42286 \cdot 10^{-3}$	$4.86206 \cdot 10^{-3}$
	2^{-4}	$4.88253 \cdot 10^{-5}$	$3.58780 \cdot 10^{-2}$	$1.66080 \cdot 10^{-3}$	$5.04102 \cdot 10^{-3}$
	2^{-5}	$1.60294 \cdot 10^{-5}$	$2.71977 \cdot 10^{-2}$	$6.57556 \cdot 10^{-4}$	$5.88371 \cdot 10^{-3}$
	2^{-6}	$4.85453 \cdot 10^{-6}$	$2.09468 \cdot 10^{-2}$	$2.61092 \cdot 10^{-4}$	$6.37322 \cdot 10^{-3}$
	2^{-7}	$1.45460 \cdot 10^{-6}$	$1.36698 \cdot 10^{-2}$	$1.08621 \cdot 10^{-4}$	$1.52218 \cdot 10^{-3}$
	2^{-8}	$4.16820 \cdot 10^{-7}$	$8.43207 \cdot 10^{-3}$	$4.51821 \cdot 10^{-5}$	$3.64562 \cdot 10^{-4}$
$(\mathcal{SV}\text{-}\mathcal{S})$	2^{-3}	$1.96694 \cdot 10^{-4}$	$7.61350 \cdot 10^{-2}$	$5.78832 \cdot 10^{-3}$	$8.75403 \cdot 10^{-2}$
	2^{-4}	$4.57451 \cdot 10^{-5}$	$5.69211 \cdot 10^{-2}$	$2.17593 \cdot 10^{-3}$	$6.17108 \cdot 10^{-2}$
	2^{-5}	$1.39819 \cdot 10^{-5}$	$4.67325 \cdot 10^{-2}$	$8.44727 \cdot 10^{-4}$	$5.29879 \cdot 10^{-2}$
	2^{-6}	$3.82707 \cdot 10^{-6}$	$3.68067 \cdot 10^{-2}$	$3.31437 \cdot 10^{-4}$	$4.26010 \cdot 10^{-2}$
	2^{-7}	$1.05324 \cdot 10^{-6}$	$2.49938 \cdot 10^{-2}$	$1.37039 \cdot 10^{-4}$	$2.95598 \cdot 10^{-2}$
	2^{-8}	$2.70084 \cdot 10^{-7}$	$1.53739 \cdot 10^{-2}$	$5.74751 \cdot 10^{-5}$	$1.80839 \cdot 10^{-2}$

TABLE B.7 – L^2-errors of polynomial order $k = 2$ over mesh size h for a regularised non-Newtonian implicit constituted *Bingham*($\tau_y = 0.2$, $\kappa = 10^{-8}$) flow in a two-dimensional channel (Figure 5.11)

FEM	h	$\|\boldsymbol{u}_{\kappa,h} - \boldsymbol{u}\|$	$\|\boldsymbol{\tau}_{\kappa,h} - \boldsymbol{\tau}\|$	$\|\boldsymbol{\varepsilon}(\boldsymbol{u}_{\kappa,h}) - \boldsymbol{\varepsilon}(\boldsymbol{u})\|$	$\|p_{\kappa,h} - p\|$
$(\mathcal{MCS}\text{-}\mathcal{S})$	2^{-3}	$3.32707 \cdot 10^{-4}$	$1.39853 \cdot 10^{-1}$	$2.66704 \cdot 10^{-3}$	$7.92078 \cdot 10^{-2}$
	2^{-4}	$6.95563 \cdot 10^{-5}$	$8.32659 \cdot 10^{-2}$	$8.92861 \cdot 10^{-4}$	$4.95861 \cdot 10^{-2}$
	2^{-5}	$2.20447 \cdot 10^{-5}$	$4.84625 \cdot 10^{-2}$	$3.45441 \cdot 10^{-4}$	$2.89463 \cdot 10^{-2}$
	2^{-6}	$5.86629 \cdot 10^{-6}$	$3.32692 \cdot 10^{-2}$	$1.31949 \cdot 10^{-4}$	$1.92931 \cdot 10^{-2}$
	2^{-7}	$1.49213 \cdot 10^{-6}$	$1.47931 \cdot 10^{-2}$	$4.86311 \cdot 10^{-5}$	$8.90156 \cdot 10^{-3}$
$(\mathcal{TH}\text{-}\mathcal{S})$	2^{-3}	$7.59530 \cdot 10^{-4}$	$3.14475 \cdot 10^{-1}$	$6.14143 \cdot 10^{-3}$	$1.31983 \cdot 10^{-1}$
	2^{-4}	$1.88834 \cdot 10^{-4}$	$1.93477 \cdot 10^{-1}$	$2.20445 \cdot 10^{-3}$	$2.98604 \cdot 10^{-2}$
	2^{-5}	$5.42623 \cdot 10^{-5}$	$1.29146 \cdot 10^{-1}$	$9.11221 \cdot 10^{-4}$	$7.60756 \cdot 10^{-3}$
	2^{-6}	$1.48671 \cdot 10^{-5}$	$7.80893 \cdot 10^{-2}$	$3.76903 \cdot 10^{-4}$	$6.07447 \cdot 10^{-3}$
	2^{-7}	$4.05607 \cdot 10^{-6}$	$4.77153 \cdot 10^{-2}$	$1.64207 \cdot 10^{-4}$	$1.46491 \cdot 10^{-3}$
	2^{-8}	$1.08358 \cdot 10^{-6}$	$2.90648 \cdot 10^{-2}$	$7.15956 \cdot 10^{-5}$	$8.41194 \cdot 10^{-4}$
$(\mathcal{SV}\text{-}\mathcal{S})$	2^{-3}	$6.24381 \cdot 10^{-4}$	$4.83952 \cdot 10^{-1}$	$7.49686 \cdot 10^{-3}$	$5.38078 \cdot 10^{-1}$
	2^{-4}	$1.45303 \cdot 10^{-4}$	$3.61695 \cdot 10^{-1}$	$2.77747 \cdot 10^{-3}$	$4.20842 \cdot 10^{-1}$
	2^{-5}	$3.74981 \cdot 10^{-5}$	$2.37107 \cdot 10^{-1}$	$1.14610 \cdot 10^{-3}$	$2.79024 \cdot 10^{-1}$
	2^{-6}	$9.09721 \cdot 10^{-6}$	$1.41064 \cdot 10^{-1}$	$4.82299 \cdot 10^{-4}$	$1.63948 \cdot 10^{-1}$
	2^{-7}	$2.28601 \cdot 10^{-6}$	$8.51863 \cdot 10^{-2}$	$2.13317 \cdot 10^{-4}$	$9.77697 \cdot 10^{-2}$
	2^{-8}	$5.78815 \cdot 10^{-7}$	$4.95745 \cdot 10^{-2}$	$9.45073 \cdot 10^{-5}$	$5.63007 \cdot 10^{-2}$

TABLE B.8 – L^2-errors of polynomial order $k = 2$ over mesh size h for a regularised non-Newtonian implicit constituted *Bingham*($\tau_y = 1$, $\kappa = 10^{-8}$) flow in a two-dimensional channel (Figure 5.12)

Die approbierte gedruckte Originalversion dieser Diplomarbeit ist an der TU Wien Bibliothek verfügbar
The approved original version of this thesis is available in print at TU Wien Bibliothek.
TU Bibliothek Your knowledge hub WIEN

Die approbierte gedruckte Originalversion dieser Diplomarbeit ist an der TU Wien Bibliothek verfügbar
The approved original version of this thesis is available in print at TU Wien Bibliothek.

Bibliography

[AMS+04] S. S. Antman, J. E. Marsden, L. Sirovich, A. Ern, and J. Guermond. *Theory and Practice of Finite Elements*, volume 159. Springer New York, New York, NY, 2004.

[And17] J. D. Anderson. *Fundamentals of Aerodynamics*. McGraw-Hill series in Aeronautical and Aerospace Engineering. McGraw-Hill Education, New York, NY, sixth edition edition, 2017.

[Bar89a] Chapter 2 - viscosity. In H.A. Barnes, J.F. Hutton, and K. Walters, editors, *An Introduction to Rheology*, volume 3 of *Rheology Series*, pages 11–35. Elsevier, 1989.

[Bar89b] Chapter 7 - rheology of suspensions. In H.A. Barnes, J.F. Hutton, and K. Walters, editors, *An Introduction to Rheology*, volume 3 of *Rheology Series*, pages 115–139. Elsevier, 1989.

[Bar00] H.A. Barnes. *A Handbook of Elementary Rheology*. Raymond F. Boyer Library Collection. University of Wales, Institute of Non-Newtonian Fluid Mechanics, 2000.

[Bat00] G. K. Batchelor. *An Introduction to Fluid Dynamics*. Cambridge Mathematical Library. Cambridge University Press, 2000.

[BBF13] D. Boffi, F. Brezzi, and M. Fortin. *Mixed Finite Element Methods and Applications*, volume 44 of *Springer Series in Computational Mathematics*. Springer Berlin Heidelberg, Berlin, Heidelberg, 2013.

[BE80] M. Bercovier and M. Engelman. A finite-element method for incompressible non-newtonian flows. *Journal of Computational Physics*, 36(3):313–326, 1980.

[BKST15] P. R. Brune, M. G. Knepley, B. F. Smith, and X. Tu. Composing scalable nonlinear algebraic solvers. *SIAM Review*, 57(4):535–565, Jan 2015.

[Bre74] F. Brezzi. On the existence, uniqueness and approximation of saddle-point problems arising from lagrangian multipliers. *ESAIM: Mathematical Modelling and Numerical Analysis - Modélisation Mathématique et Analyse Numérique*, 8(R2):129–151, 1974.

[CDD+76] S. S. Chern, J. L. Doob, J. Douglas, A. Grothendieck, E. Heinz, F. Hirzebruch, E. Hopf, S. Mac Lane, W. Magnus, M. M. Postnikov, F. K. Schmidt, W. Schmidt, D. S. Scott, K. Stein, J. Tits, B. L. van der Waerden, B. Eckmann, J. K. Moser, G. Duvaut, and J. L. Lions. *Inequalities in Mechanics and Physics*, volume 219 of *Grundlehren der mathematischen Wissenschaften, A Series of Comprehensive Studies in Mathematics*. Springer Berlin Heidelberg, Berlin, Heidelberg, 1976.

Die approbierte gedruckte Originalversion dieser Diplomarbeit ist an der TU Wien Bibliothek verfügbar
The approved original version of this thesis is available in print at TU Wien Bibliothek.
TU Bibliothek Your knowledge hub WIEN

[CR08] R.P. Chhabra and J.F. Richardson. Chapter 1 - non-newtonian fluid behaviour. In R.P. Chhabra and J.F. Richardson, editors, *Non-Newtonian Flow and Applied Rheology (Second Edition)*, pages 1–55. Butterworth-Heinemann, Oxford, second edition edition, 2008.

[DKS13] L. Diening, C. Kreuzer, and E. Süli. Finite element approximation of steady flows of incompressible fluids with implicit power-law-like rheology, 2013.

[FP89] M. Fortin and R. Pierre. On the convergence of the mixed method of crochet and marchal for viscoelastic flows. *Computer Methods in Applied Mechanics and Engineering*, 73(3):341–350, 1989.

[GLS19] J. Gopalakrishnan, P. L. Lederer, and J. Schöberl. A mass conserving mixed stress formulation for the Stokes equations. *IMA Journal of Numerical Analysis*, 40(3):1838–1874, 05 2019.

[GLS20] J. Gopalakrishnan, P. L. Lederer, and J. Schöberl. A mass conserving mixed stress formulation for stokes flow with weakly imposed stress symmetry. *SIAM Journal on Numerical Analysis*, 58(1):706–732, 2020.

[GO20] P. A. Gazca Orozco. *Numerical analysis of implicitly constituted incompressible fluids: mixed formulations*. PhD thesis, University of Oxford, 2020.

[GO21] P. A. Gazca Orozco. A semismooth newton method for implicitly constituted non-newtonian fluids and its application to the numerical approximation of bingham flow, 2021.

[GSMS20] P. Gangl, K. Sturm, M.Neunteufel, and J. Schöberl. Fully and semi-automated shape differentiation in ngsolve, 2020.

[GW11] Roland Glowinski and Anthony Wachs. On the numerical simulation of viscoplastic fluid flow. In R. Glowinski and J. Xu, editors, *Numerical Methods for Non-Newtonian Fluids*, volume 16 of *Handbook of Numerical Analysis*, pages 483–717. Elsevier, 2011.

[Her16] H. Herwig. *Strömungsmechanik: Einführung in die Physik von technischen Strömungen*. Springer Fachmedien Wiesbaden, Wiesbaden, 2., überarbeitete und erweiterte auflage edition, 2016.

[HMST17] J. Hron, J. Málek, J. Stebel, and K. Touška. A novel view on computations of steady flows of bingham fluids using implicit constitutive relations. *Journal of Non-Newtonian Fluid Mechanics*, 2017.

[Led19] P. L. Lederer. *A Mass conserving mixed stress formulation for incompressible flows*. PhD thesis, Vienna University of Technology, 2019.

[LS16] P. L. Lederer and J. Schöberl. Polynomial robust stability analysis for $h(\mathrm{div})$-conforming finite elements for the stokes equations, 2016.

[Pop12] S. B. Pope. *Turbulent Flows*. Cambridge University Press, 2012.

[Raj03] K. R. Rajagopal. On implicit constitutive theories. *Applications of Mathematics*, 48(4):279–319, 2003.

Die approbierte gedruckte Originalversion dieser Diplomarbeit ist an der TU Wien Bibliothek verfügbar
The approved original version of this thesis is available in print at TU Wien Bibliothek.
TU Bibliothek Your knowledge hub WIEN

[Raj06] K. R. Rajagopal. On implicit constitutive theories for fluids. *Journal of Fluid Mechanics*, 550:243–249, 2006.

[Raj15] K. R. Rajagopal. Remarks on the notion of "pressure". *International Journal of Non-Linear Mechanics*, 71:165–172, 2015.

[Sch97] J. Schöberl. Netgen an advancing front 2d/3d-mesh generator based on abstract rules. *Computing and Visualization in Science*, 1(1):41–52, 1997.

[Sch14] J. Schöberl. C++11 implementation of finite elements in ngsolve. 2014.

[SG04] O. Schenk and K. Gärtner. Solving unsymmetric sparse systems of linear equations with paradiso. *Future Generation Computer Systems*, 20:475–487, 04 2004.

[Ste15] R. Stenberg. Weakly symmetric mixed finite elements for linear elasticity. *Lecture Notes in Computational Science and Engineering*, 103:3–18, 01 2015.

[SV85] L. R. Scott and M. Vogelius. Norm estimates for a maximal right inverse of the divergence operator in spaces of piecewise polynomials. *ESAIM: Mathematical Modelling and Numerical Analysis*, 19(1):111–143, 1985.

[SW17] P. Saramito and A. Wachs. Progress in numerical simulation of yield stress fluid flows. *Rheologica Acta*, 56:211–230, 2017.

[TH73] C. Taylor and P. Hood. A numerical solution of the navier-stokes equations using the finite element technique. *Computers & Fluids*, 1(1):73–100, 1973.

[Was75] K. Washizu. *Variational methods in elasticity and plasticity*, volume 3. Pergamon press Oxford, 1975.

Die approbierte gedruckte Originalversion dieser Diplomarbeit ist an der TU Wien Bibliothek verfügbar
The approved original version of this thesis is available in print at TU Wien Bibliothek.
TU Bibliothek Your knowledge hub WIEN

Die approbierte gedruckte Originalversion dieser Diplomarbeit ist an der TU Wien Bibliothek verfügbar
The approved original version of this thesis is available in print at TU Wien Bibliothek.